IMPACT OF CARBON BLACK PARTICLE SIZE ON METALLIC WEAR USING FOUR-BALL WEAR TESTER

WARAWUT AMORNPRAPA

A THESIS REPORT SUBMITTED IN PARTIAL FULFILLMENT
OF THE REQUIREMENTS FOR THE DEGREE OF
MASTER OF ENGINEERING IN AUTOMOTIVE ENGINEERING
INTERNATIONAL COLLEGE
KING MONGKUT'S INSTITUTE OF TECHNOLOGY LADKRABANG
ACADEMIC YEAR 2017
KMITL-2017-IC-M-004-004

IMPACT OF CARBON BLACK PARTICLE SIZE ON METALLIC WEAR USING FOUR-BALL WEAR TESTER

WARAWUT AMORNPRAPA

A THESIS REPORT SUBMITTED IN PARTIAL FULFILLMENT
OF THE REQUIREMENTS FOR THE DEGREE OF
MASTER OF ENGINEERING IN AUTOMOTIVE ENGINEERING
INTERNATIONAL COLLEGE
KING MONGKUT'S INSTITUTE OF TECHNOLOGY LADKRABANG
ACADEMIC YEAR 2017
KMITL-2017-IC-M-004-004

THESIS TITLE	Impact of carbon black particle size on metallic wear using four-ball wear tester
STUDENT NAME	Mr. Warawut Amornprapa
STUDENT ID	58610006
DEGREE	Master of Engineering
PROGRAME	Automotive Engineering
ADVISOR	Asst.Prof. Dr. Preechar Karin
CO-ADVISOR	Dr. Kobsak Sriprapha
CO-ADVISOR	Prof.Dr. Katsunori Hanamura

ABSTRACT

From the previous research found that the soot contamination in used engine oils of diesel engine vehicles was about 1% by weight. This research aimed to investigate the effects of soot Nanoparticles on metallic wear characteristics using Four-Ball Wear Tester. Soot particle contamination in diesel engine oil was simulated using carbon black (CB). There were commercial carbon black which difference primary particle size. Micro - nanostructure of soot particles were studied by scanning electron microscopy (SEM), transmission electron microscopy (TEM) and laser diffraction spectroscopy (LDS). Wear and roughness measurement was investigated by high resolution optical microscopy (OM), 3D rendering optical technique and SEM image processing method. Base on four ball wear test, the 1% by weight of CB contamination shows 14% higher average WSD compare to the pure SAE0W30 engine oil, but the surface roughness was 22 % lower. Soot particle could be increase the rate of wear because it was large in comparison with the oil film and its hardness was higher than that of the steel ball. Moreover, in case of CB N660, soot particle was much larger than the oil film thickness. So, that it might be block the lubrication inlet to the contact, therefore resulting in unlubricated sliding wear which causes the largest wear scar diameter.

Keywords: Lubricant; Wear; Soot; Four-Ball wear tester; Electron microscopy; Laser diffraction spectroscopy

ACKNOWLEDGEMENT

I would first like to thank my thesis advisor Asst. Prof. Dr. Preechar Karin of the faculty of automotive engineering at king mongkut's institute of technology ladkrabang. His guidance helped me whenever I ran in to a trouble spot or had a question about my research or writing.

I would also like to thank my co-advisors Dr. Kobsak Sriprapha from National Electronics and Computer Technology Center (NECTEC), National Science and Technology Development Agency (NSTDA) and Prof. Dr. Katsunori Hanamur of the Departments of Mechanical Engineering, Tokyo institute of technology, Japan, for their support, technical recommendations, and collaboration all the time throughout the research project. I gratefully acknowledge the financial support from Bangchak Corporation Pub. Co., Ltd., FOCUSLAB Ltd., KMITL and NSTDA.

Finally, I must express my very profound gratitude to my parents and friends for providing me with unfailing support and continuous encouragement throughout my years of study and through the process of researching and writing this thesis. This accomplishment would not have been possible without them.

Warawut Amornprapa

TABLE OF CONTENTS

LIST OF TABLES

LIST OF FIGURES

CHAPTER 1
INTRODUCTION

1.1 Background

Recently, diesel engine is widely used as the powertrain in many fields of economy. It is an internal combustion engine which converts chemical energy within the fuel into mechanical energy. The contact movement of the moving parts inside the engine generate some frictional force. The force can increase the lubricant temperature which resulting in reducing oil film thickness. The direct metal to metal contact generate much amount of frictional force and heat that can make the material loss. Wear is a loss of material from a solid surface. It is often classified as abrasive, adhesive and fatigue wear. Common wear behavior is shown in Figure 1.1 [1]. Which starts with a running-in period that is a newly manufactured surfaces. It is followed by mild wear period. The life of the components ends when the wear rate was significantly increases and it causes an engine failure. Lubricant plays an importance role in reducing frictional force, prevent wear and removing frictional heat. It has an ability to minimize metal to metal contact by generating a lubricating oil film between the surfaces. The lubrication regimes can be divided into a boundary, mixed film, and full film lubrication.

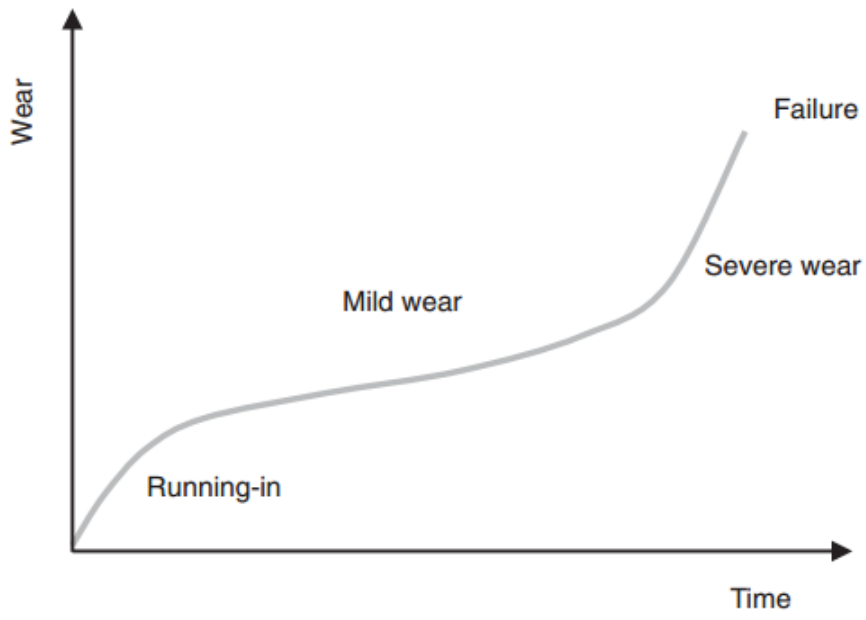

Figure 1. 1 The wear process depends on time.

However, the impurities are trapped in the engine oil which are in the form of solid, liquid, and gaseous contaminants. The high amount of contaminants from uncontrolled system can breakdown the lubricating oil which resulting in performance degradation and shorten oil service life and finally cause a component failure. The solid contaminants which including wear debris can damage the mechanical commonest. The liquid contaminates which including fuel and water can prevent the proper operation of lubricant and its additives. The Gaseous contaminates which including combustion products can wear a wear the components surfaces and break down the oil.

Soot is remain of incomplete combustion which consists mostly of carbon, hydrocarbon and metallic ash. The primary and agglomerated soot particles observed by Transmission Electron Microscopy (TEM) are in the range of 20 - 80 nm and 100 - 300 nm, respectively [2] . Soot hardness were measured by Li et al. [3]. Its hardness were determined by carbon plasmon energy methods which obtained from the electron energy loss spectra. They reported that the soot hardens was much higher than the hardness of steel. Soot can be entered into the engine oil through the piston ring clearance during the combustion process [2]. The predominant wear mechanisms due to soot contamination have been proposed as abrasive and oil starvation. The abrasive wear occurs where the soot particle abrades the steel surfaces. Because of its hardness was much higher than that of the steel ball. The oil starvation occurs where the dimensions of soot agglomerates was higher than the oil film thickness and blocks lubricant entry to the contact.

Biodiesel is an alternative fuel that plays an importance role in replacement using petroleum diesel. It is an oxygenated fuel that promotes more completely combustion. The soot diameter size and quantity from biodiesel engine emission is lower than that of diesel. However, soot induced wear mechanisms are still not fully understood. This research aimed to investigate the effects of soot Nanoparticles on metallic wear characteristics using Four-Ball Wear Tester, Laser Diffraction Spectroscopy, and Electron Microscopy.

1.2 Objective

To investigate the effect of soot nanoparticle sizes (28, 30, 40 and 50 nm) on metal wear mechanisms by using Four-ball wear tester.

1.3 Scope of work

1.3.1 The four types of carbon black (CB) with difference primary particle sizes are mixed in to the engine oil at 1% by weight per volume for simulating soot contamination. Only the mass of each types of CB are considered and controlled into 1 % by weight per volume but their number are not considered.

1.3.2 The investigation of both soot contamination on metallic wear were investigated using Four-ball wear tester.

1.4 Structure of the research

The research methodologies in this this are divided as follows.

Chapter 1 discuss the research background, objective, and scope.

Chapter 2 discuss the relevant theory and literature including fundamental of tribology, used oil analysis, fuel and soot contamination on metallic wear.

Chapter 3 discuss the research materials and methods.

Chapter 4 discuss the results of soot contamination on metallic wear by using Four-ball wear tester, optical microscopy, scanning electron microscopy and laser diffraction spectroscopy.

Chapter 5 is a conclusion and suggestions.

1.5 Expected benefits

This research can help to explain the possible effects of wear mechanisms on the biodiesel engine. The PM nanoparticle size and quantity of biodiesel engine is lower than that of the diesel.

CHAPTER 2
LITERATURE REVIEW

2.1 Tribological Contacts [1]

A tribological contact is defined as two solid bodies in contact under relative motion. It can be either unlubricated or lubricated. The tribological contact is characterized by its operating conditions (e.g. velocity, load and type of motions), material parameters (e.g. surface material, surface roughness and hardness), and environmental conditions (e.g. temperature and humidity) and, in the lubricated case, lubricant properties (e.g. viscosity) (see Figure 2.1). The tribological contact can be observed at different scales, that is at macroscopic scale (or macro scale) or at microscopic scale (or micro scale) (see Figure 2.2). The macro scale will give global information of the contact, while the micro scale will give local information within the contact. For example, a contact that appears smooth at macro scale may appear very rough and uneven at micro scale. The real contact area between the surfaces is the sum of a large number of small areas where surface peaks from the two surfaces get into contact. As a consequence, the apparent contact area at the macro scale is much larger than the real contact area between the two surfaces in contact.

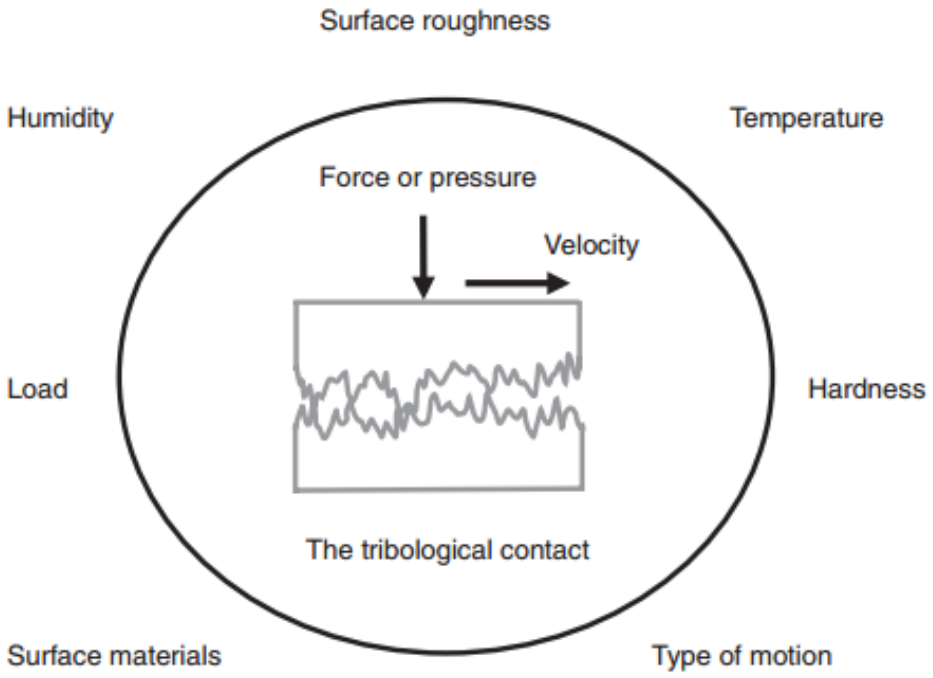

Figure 2. 1 Tribological contacts are affected by different conditions [1].

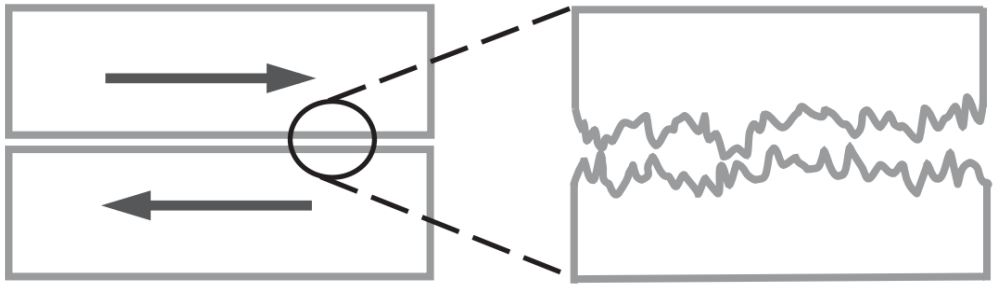

Figure 2. 2. The tribological in macro scale (left) and micro scale (right) [1].

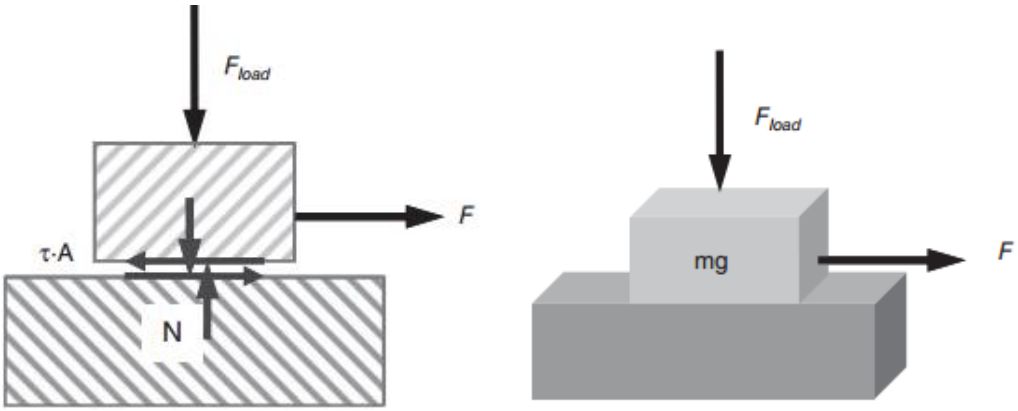

Figure 2. 3 Friction visualized as pulling a small box across a flat surface [1].

2.2 Friction [1]

Friction is the force resisting the relative motion between two surfaces in contact. It is commonly divided into dry friction and viscous friction. It may be static that is the solid bodies have no relative motion, or dynamic, when the solid bodies are moving relative to each other. Dry friction occurs between two dry solid bodies. Viscous friction occurs when the two solid bodies are more or less separated by a fluid, for example a lubricant.

The Coefficient of Friction

The coefficient of friction μ is defined as the ratio of the friction force F and the normal force N between the bodies, as shown in Figure 2.3 and expressed by

$$\mu = \frac{F}{N} \tag{2.1}$$

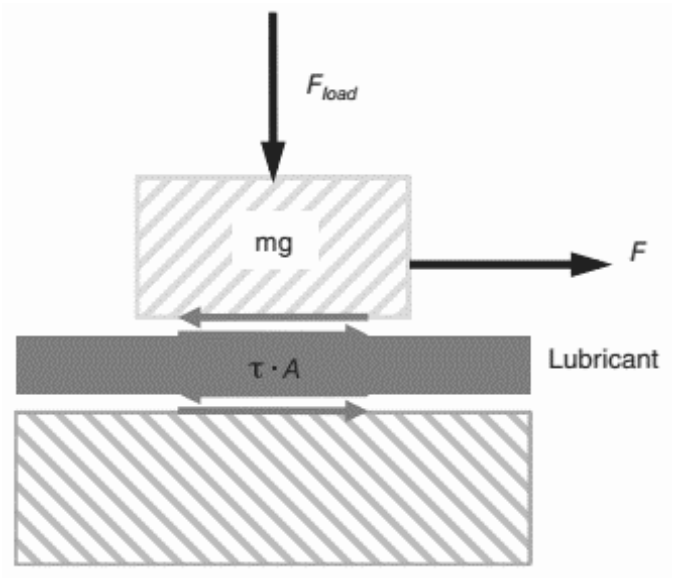

Figure 2. 4 Friction in tribological contact [1].

Where the normal force is actually the sum of the load of the mass mg and any externally applied load, F_{load}

$$N = mg + F_{load} \tag{2.2}$$

The normal force always acts perpendicular to the contact area. When sliding the mass the friction force is the force required to maintain the sliding and it always acts tangential (i.e. parallel) to the contact area.

For a contact where the surfaces are fully separated by a lubricant the friction force is commonly expressed by

$$F = \tau A \tag{2.3}$$

Where $\boldsymbol{\tau}$ is the shear stress in the lubricant and A is the contact area. The shear stress is determined by the lubricant properties, the velocity of the motion and the distance between the bodies. The forces in the lubricated contact act on both the solid bodies and the fluid, as shown in Figure 2.4.

2.3 Lubrication Regimes [1] [4]

A general description of the friction behavior in a lubricated contact can be seen in Figure 2.5, where the dependence of the coefficient of friction μ versus the film parameter ʌ is shown. The film parameter ʌ is calculated as

$$\Lambda = \frac{h}{\sqrt{R_{qA}{}^2 + R_{qb}{}^2}} \tag{2.4}$$

Where h is the lubricant film thickness and R_{qA} and R_{qb} represent the surface roughness of the two surfaces A and B in contact. The contact is classified as boundary, mixed or full flm lubricated depending on the degree of mechanical contact between the solid surfaces. The curve in Figure 2.5 originates from the Stribeck curve. Boundary lubrication implies heavy contacting between the asperities with a film parameter below 1. The load is carried by the solid surfaces in. The lubricant is mainly acting as a carrier of additives. The presence of additives is necessary to ensure the performance and build-up of a boundary film. This regime is characterized by high load and low speed. A slowly rotating shaft and a bushing mainly work in the boundary lubrication regime even if they are lubricated. In mixed film lubrication the surfaces are less separated than in the full film regime. The surfaces are close enough for asperity contact to occur occasionally. The mixed film lubrication regime is a combination of full film lubrication and boundary lubrication with film parameter between 1 and 3. Thus, the load is carried partly by a pressure in the fluid film and partly by the asperities in contact, as shown in Figure 2.6. The lubricant will support the contact with necessary additives to reduce wear. In full film lubrication the solid bodies are lubricated by a thick enough lubricant film to ensure full separation of the surfaces. In this regime the coefficient of friction is very low. A ʌ -value higher than 3 indicates full film lubrication. The lubricant film thickness h is determined by the lubricant the operating conditions, the contact geometry and the solid surface's material properties. In practice, typical lubricant film thicknesses are about 1–100 microns.

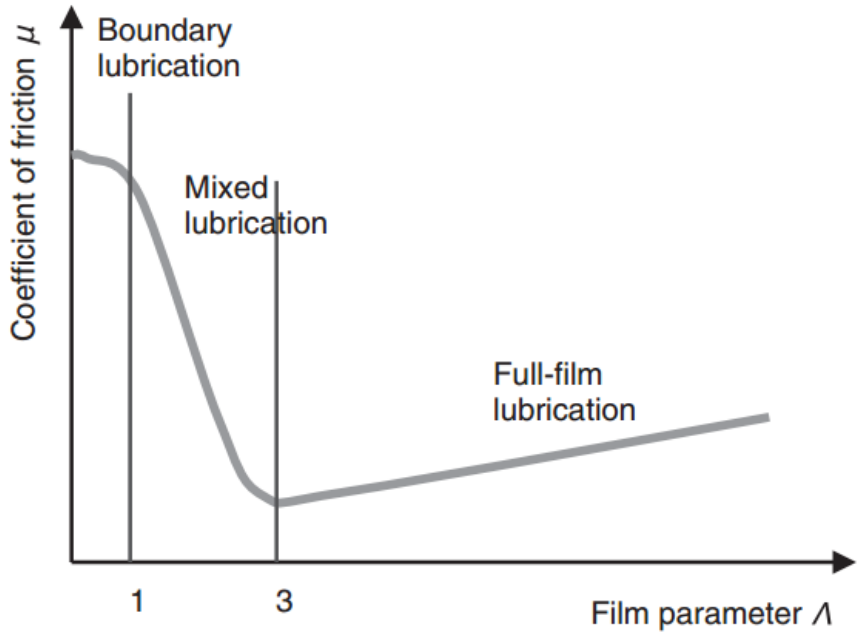

Figure 2. 5 Coefficient of friction versus film parameter [1].

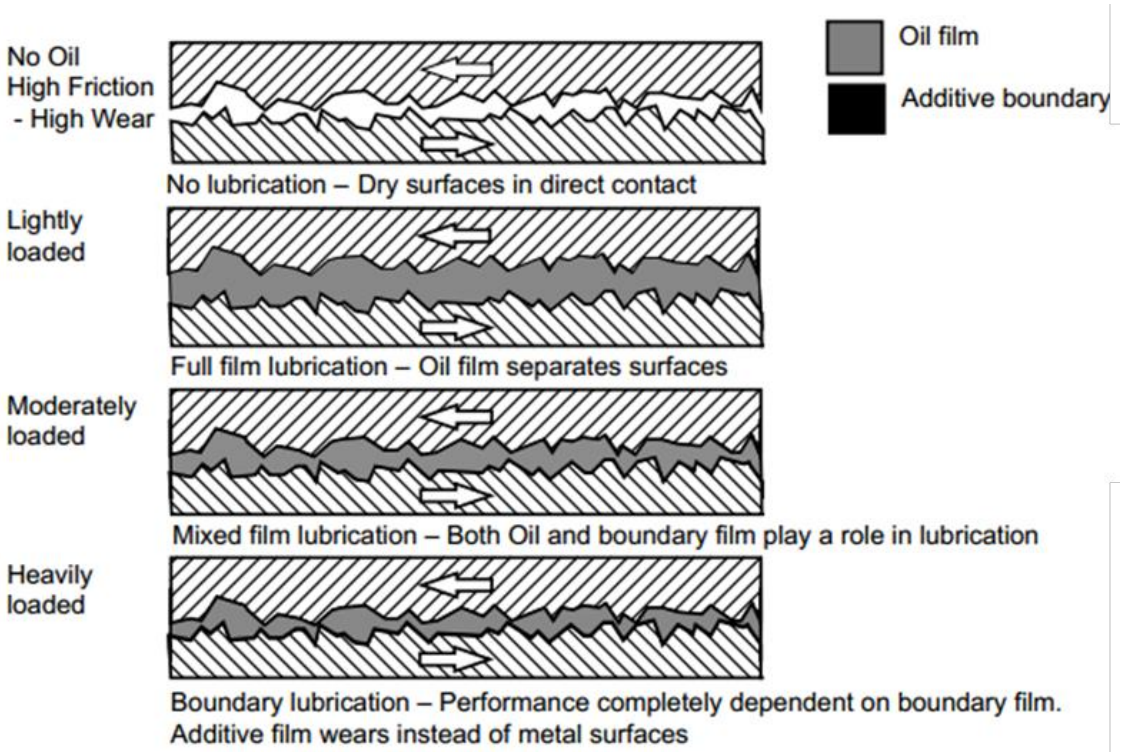

Figure 2. 6 Engine lubrication regimes [4].

2.3.1 Film Thickness Estimation between Two Sphere Contacts [5]

In this topic, the fundamental mechanisms of film generation in elastohydrodynamic contacts, together with the methods for calculating the minimum film thickness between spherical balls. The shape of the contact area depends on the shape (curvature) of the contacting bodies. For example, point contacts occur between two balls, line contacts occur between two parallel cylinders and elliptical contacts, which are most frequently found in many practical engineering applications, occur when two cylinders are crossed, or a moving ball is in contact with the inner ring of a bearing, or two gear teeth are in contact. The curvature of the bodies can be convex, flat or concave. It is defined by convention that convex surfaces possess a 'positive curvature' and concave surfaces have a 'negative curvature'. The following general rule can be applied to distinguish between these surfaces: if the center of curvature lies within the solid then the curvature is positive, if it lies outside the solid then the curvature is negative. This distinction is critical in defining the parameter characterizing the contact geometry which is known as the reduced radius of curvature. The configuration of two elastic bodies with convex surfaces in contact was originally considered by Hertz in 1881 and is shown in Figure 2.7

$$\frac{1}{R'} = \frac{1}{R_x} + \frac{1}{R_y} = \frac{1}{R_{ax}} + \frac{1}{R_{ay}} + \frac{1}{R_{bx}} + \frac{1}{R_{by}} \tag{2.5}$$

Where:

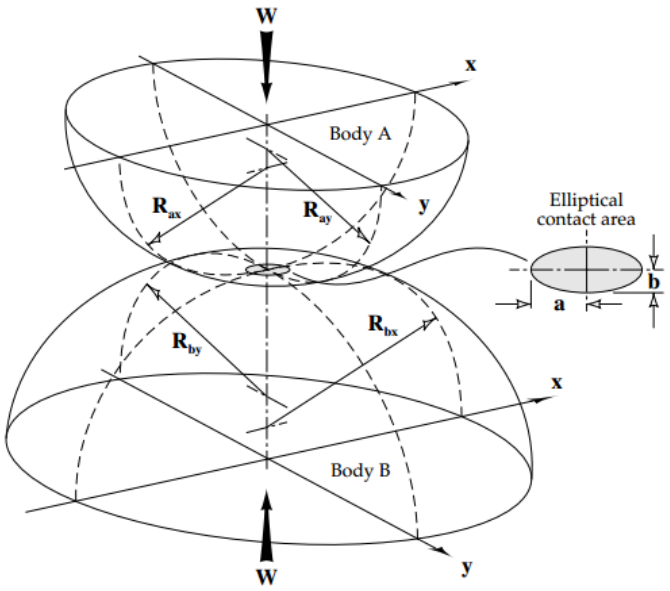

Figure 2. 7 Geometry of two elastic bodies with convex surfaces [5].

$$\frac{1}{R_x} = \frac{1}{R_{ax}} + \frac{1}{R_{ay}}$$

$$\frac{1}{R_y} = \frac{1}{R_{bx}} + \frac{1}{R_{by}}$$

R_x is the reduced radius of curvature in the x direction [m].

R_y is the reduced radius of curvature in the y direction [m].

R_{ax} is the reduced radius of curvature of body A in the x direction [m].

R_{ay} is the reduced radius of curvature of body A in the y direction [m].

R_{bx} is the reduced radius of curvature of body B in the x direction [m].

R_{by} is the reduced radius of curvature of body B in the y direction [m].

The reduced Young's modulus is defined as:

$$\frac{1}{E'} = \frac{1}{2}\left[\frac{1-\vartheta_A{}^2}{E_A} + \frac{1-\vartheta_B{}^2}{E_B}\right] \tag{2.6}$$

Where:

ϑ_A and ϑ_B are the Poisson's rations of the contacting bodies A and B.

E_A and E_B are the Young's moduli of the contacting bodies A and B.

It can be noted that for the spheres:

$R_{ax} = R_{ay} = R_A$ and $R_{bx} = R_{by} = R_B$

Where:

R_A and R_b are the radii of the spheres A and B, respectively.

Substituting into equation (2.6) gives:

$$\frac{1}{R'} = \frac{1}{R_x} + \frac{1}{R_y} = \frac{1}{R_A} + \frac{1}{R_B} + \frac{1}{R_A} + \frac{1}{R_B} = 2\left(\frac{1}{R_A} + \frac{1}{R_B}\right) \tag{2.7}$$

Where:

$$\frac{1}{R_x} = \frac{1}{R_y} = \frac{1}{R_A} + \frac{1}{R_B}$$

Elastohydrodynamic lubrication (EHL) is a mode of fluid-film lubrication in which hydrodynamic action is significantly enhanced by surface elastic deformation and lubricant viscosity increases due to high pressure. EHL conditions are typically obtained in nonconformal contacts such as ball on cylinder (elliptical contact), ball on ball (circular contact), and cylinder on cylinder (line contact).

Surfaces are deformed when two nonconformal bodies are brought in contact. A flat narrow contact zone is formed and contact width and pressure can be predicted by using the Hertz contact theory. At maximum Hertz pressure, the lubricant under goes a phase transition into a solid glassy state. From this point, the lubricant no longer behaves as a Newtonian fluid, and it can be considered as a pseudo-fluid. Figure 2.8 shows the lubricant which is entrained into the contact zone and formed the thickness profile. The flow profile has two components, Couette flow (surface driven flow) and Poiseuille flow (pressure driven flow). Due to continuity requirements, the total flow must be the same at all three positions. In the center of the contact, an oil is relatively incompressible and density of the lubricant does not vary more than a few percent and then the oil film thickness should be constant (hc). Further to the right, just before the outlet of the contact, there is a sudden decrease of the film thickness. This is the position where h min occurs. This flow constriction occurs in order to maintain continuity of

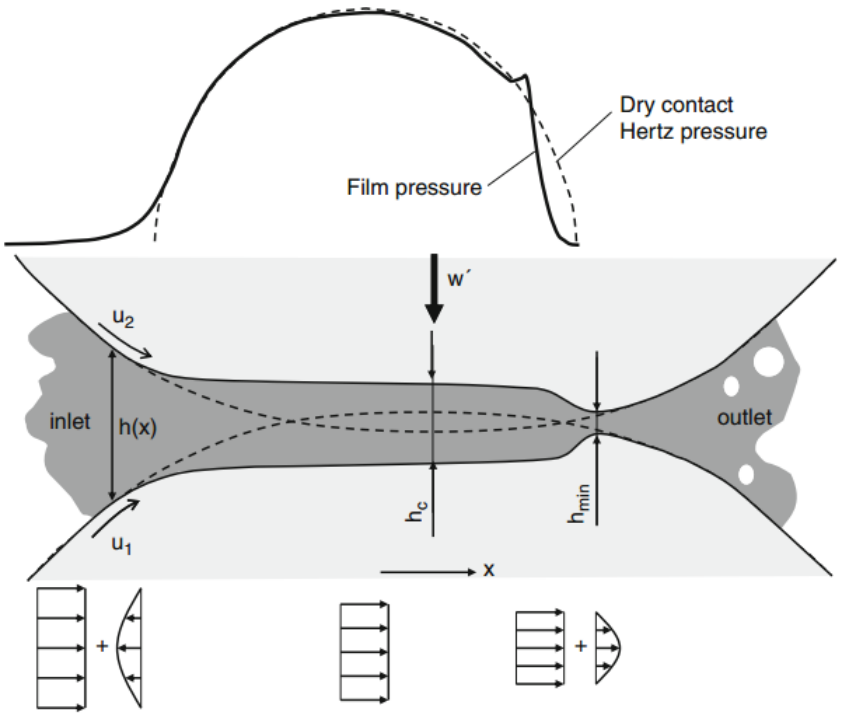

Figure 2. 8 Hydrodynamic pressure distribution in an elastohydrodynamic contact; hc is the central film thickness, h min is the minimum film thickness.

flow. The Poiseuille flow is significantly larger near the inlet and outlet due to the high pressure gradients. In the inlet it will counteract the Couette flow, while it will be in the same direction as the Couette flow in the outlet, and the gap must therefore be closed to balance flow into and out from the contact.

$$\frac{h_c}{R} = 2.69\left(\frac{U\eta_0}{ER}\right)^{0.67}(\alpha E)^{0.53}\left(\frac{W}{ER^2}\right)^{-0.067}\left(1 - 0.61e^{-0.73k}\right) \quad (2.8)$$

$$\frac{h_{min}}{R} = 3.63\left(\frac{U\eta_0}{ER}\right)^{0.68}(\alpha E)^{0.49}\left(\frac{W}{ER^2}\right)^{-0.073}\left(1 - e^{-0.68k}\right) \quad (2.9)$$

Where h_c is the central film thickness, h_{min} is the minimum film thickness, η_0 is viscosity at atmospheric pressure of the lubricant, R is Radius of curvature, U is Entering surface velocity, E is Young's modulus, α is Pressure-viscosity coefficient, W is contract load and K is Elasticity parameter.

2.4 Wear

Wear is loss of material from a solid surface. Wear can appear in many ways depending on the material of the interacting contact surfaces, the environment and the operating conditions. The wear mechanisms can be divided as abrasive wear, adhesive wear and surface fatigue.

2.4.1 Abrasive Wear [6]

An important aspect of abrasion is the issue of rolling on the surface or sliding. It is common to categorize abrasion produced as two-body or three-body abrasion. Two-body abrasion is produced by fixed abrasives. Three-body abrasion is produced by abrasive particles that are forced against a soft surface by something, a third body. The third body could be a solid or simply compacted particles, as in tilling soil.

Figure 2.9.a illustrates the concept of fixed abrasives. Approximately same size stones were "fixed" into a concrete cap on a stone wall to keep tourists from sitting and walking on the wall, but this is how fixed abrasive papers (sandpaper) and films are made. Approximately the same size abrasive particles are bonded to a flexible substrate with a thin film of adhesive. Grinding and cutoff wheels are made by adhesive bonding particles together (resin bonded wheels) or by using a glass as the glue between particles (vitrified wheels). Fixed abrasives tend to produce scratching abrasion (Figure 2.9), while loose abrasives can roll to indent a soft surface or become momentarily fixed to produce scratching abrasion.

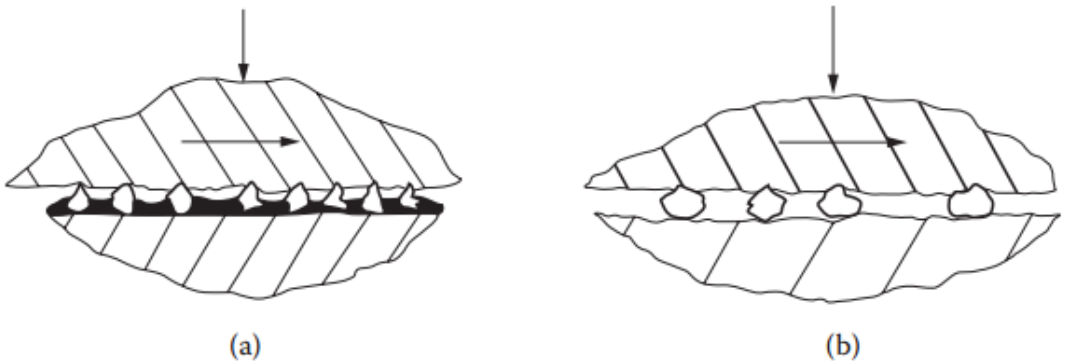

Figure 2. 9 (a) Two-body and (b) three body abrasion. [6]

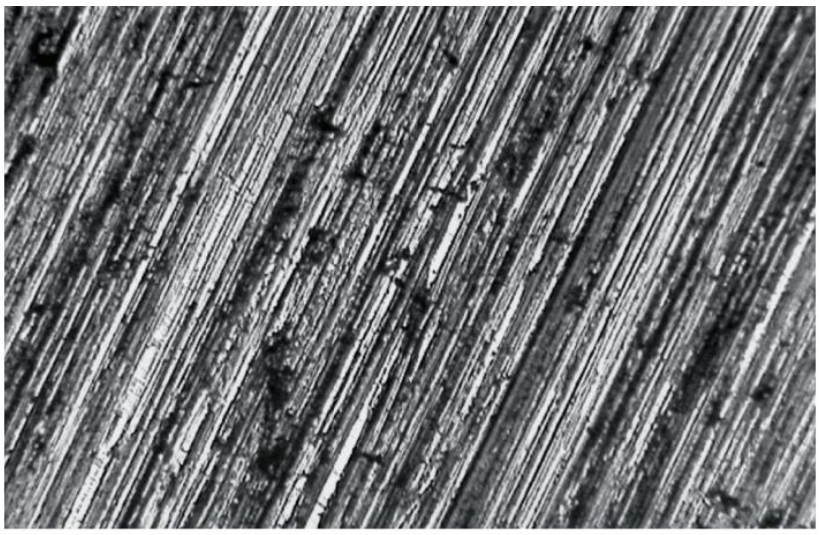

Figure 2. 10 Scratches produced by a 60-grit alumina [6].

2.4.2 Adhesive wear [6]

Adhesive wear is a very serious form of wear characterized by high wear rates and a large unstable friction coefficient. Sliding contacts can rapidly be destroyed by adhesive wear and, in extreme cases, sliding motion may be prevented by very large coefficients of friction or seizure. All surfaces are composed of atoms in either crystal form, as in most metals and ceramics; amorphous form, as in some coatings and treatments; or molecular form, as in plastics. When surfaces make contact with each other, the films that naturally occur on surfaces often separate the atoms or molecules so there is no tendency for adhesion. However, if the force pushing contacting surfaces becomes sufficient locally at spots in the real area of contact, films can break down and the atoms or molecules of the mating surfaces can make atomic contact (Figure 2.11) and atomic bonding can occur, depending on the nature of the atoms involved. Of course, like atoms (e.g., steel–iron on steel–iron) will want to bond to each other and adhesion is more likely. Atomic or molecular bonding is less likely with dissimilar atoms or molecules (e.g., steel sliding on a phenolic thermosetting (PF) plastic like countertop laminate). Thus, the mechanism of adhesion between rubbing surfaces is atoms of one surface in atomic contact with atoms of the contacting surface at the waveforms that make up the real area of contact.

Sometimes a material couple produces only microscopic excrescencies. The surface damage is the same as in galling, but more than the naked eye is necessary to see the damage. Usually a 7X loupe is sufficient. Hard metals often exhibit incipient galling. Gear teeth with moderate hardness are prone. There is a standard test for galling: ASTM G 98. This test uses a 360° rotation of a ½ in. diameter flat-ended pin (button) on a flat counter face (block). A test is conducted at a trial load to see if galling occurs. If it does, the load is lowered and the test is repeated until galling no longer occurs. The apparent stress that the couple can tolerate without galling is called the threshold galling stress. Incipient galling and adhesive transfer (Figure 2.12) are not called galling, but they still denote an unacceptable mating couple. Some researcher also reported that the plastically deformation of the worn surface which was larger than 20 microns was reflected to adhesive wear.

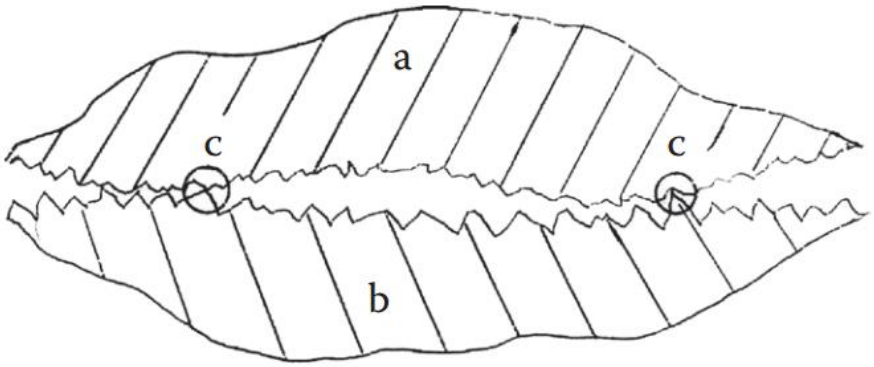

Figure 2. 11 Adhesion loci are produced by sites of real contact [6].

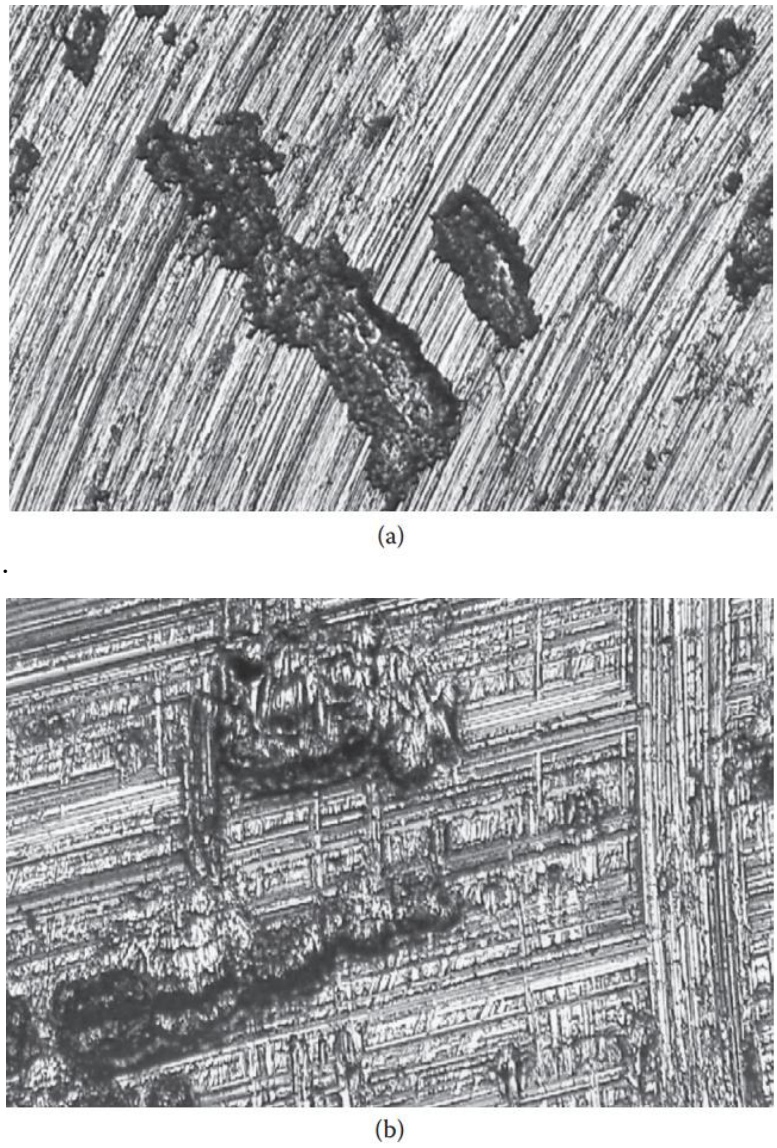

Figure 2. 12 Adhesive transfer of titanium (a) to steel (b) (100×) [6].

2.4.2.1 Adhesive scuffing wear [7]

To better understand scuffing, Figure 2.12.1 presents the interpretative models of the phenomena in different phases of this process, caused by the continuously increasing load. The models concern the contact between two balls of the four-ball tribosystem (the rotating upper ball with one of the three stationary lower balls) during the testing of the automotive gear oils of API GL-4 and GL-5 performance levels. The lower graph presents the friction torque curve (Mt) obtained at continuously increasing load (P).

The phase ‘‘mixed friction’’ concerns the first stage of the run from the moment of the start of the relative movement between the test balls to the scuffing initiation reflected by a sharp rise in the friction torque. In this phase, the load is mainly carried by the micro EHL films and the mating surfaces are protected from a direct contact by the boundary layer. But at some micro-zones, due to the failure of the micro-EHL film surface, asperities locally collide. Collisions of the surface asperities without the protective chemically modified layers make the temperature increase. The oil viscosity decreases, and, due to the continuously increasing load, the oil film thickness drops, which leads to an increase in the number of collisions of asperities and further temperature rise. In a relatively short time and at a relatively low load for GL-1 oils, the collapse of the oil film occurs and scuffing initiates, indicated by a sharp friction torque increase.

Yet another ‘chain of events’’ (not invoked in the model) leading to the lubricating film collapse is possible, not directly related to the surface asperities collisions. At the low oil film thickness, surface roughness causes high local pressure values, with the potential to raise lubricant viscosity and thus increase fluid traction. The latter can give rise to heating of the inlet to the contact, reducing the oil film thickness further and making local contact pressures more severe. High local pressures allow plastic deformation of the surface, which leads to changes of topography (i.e., roughening) and, if this creates significant surface valleys, then the local oil pressure can drop down through the side leakage, allowing the oil film to collapse. The fact that so many phenomena happen simultaneously in a tribological contact necessitates some circumspection when their interpretation, and the respective models related only to the collisions of the surface asperities, presented in Figure 2.12.1, should be considered to be very simplified.

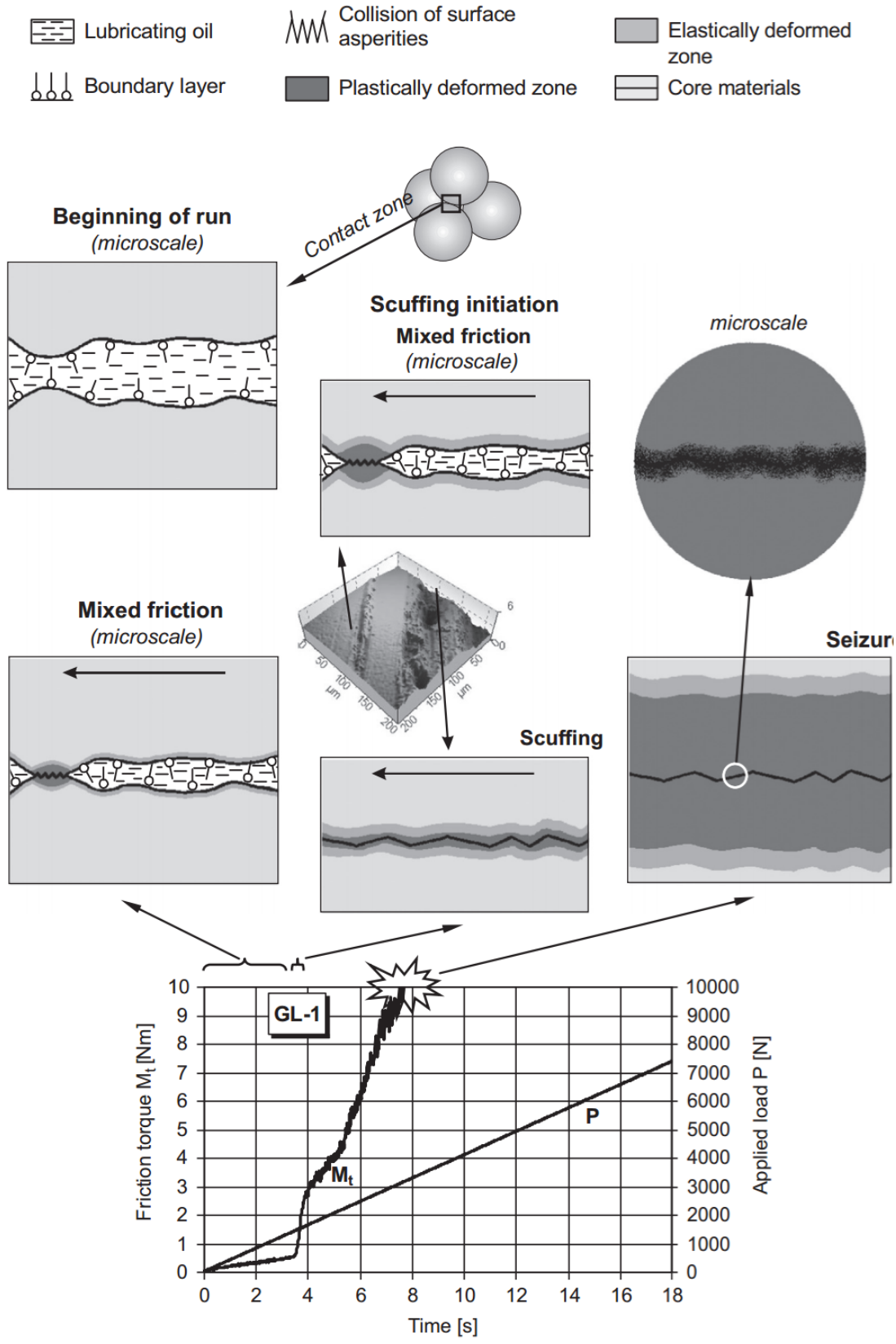

Figure 2.12.1 Models of scuffing in different phases for the gear oils [7].

2.4.3 Rolling Contact Fatigue [6]

Rolling contact fatigue is material removal/damage caused by repeated rolling of a solid shape on a contacting solid surface. One more definition is in order. The ASTM G 2 Committee on Wear and Erosion defines *rolling* as "motion of a sphere, cylinder, or revolute shape in a direction on another surface characterized by no relative slip between contacting surfaces" (Figure 2.13). It is this subsurface stress that produces the tendency for rolling contacts to produce subsurface cracks that propagate to produce material removal (Figure 2.14). Spalling is defned as material removal from a solid surface in the form of a platelet or similar shape caused by propagation of subsurface fractures to a free surface.

In summary, the mechanism of rolling contact fatigue is fracture of material from a solid surface that is subject to repeated compressive stressing from contact with a rolling body. The material removal starts with the development of a subsurface crack that, with repeated stressing, propagates upward in multiple directions so that a piece of material is free to be ejected from the surface.

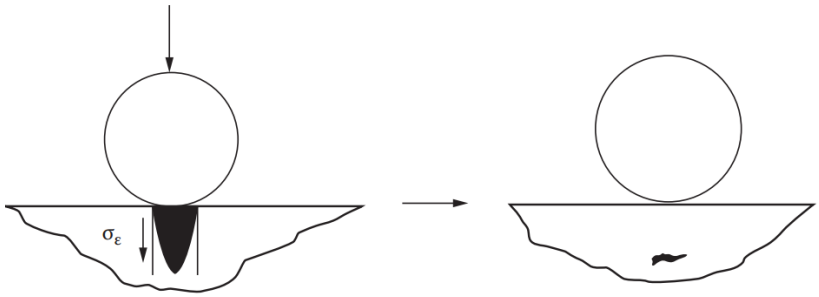

Figure 2. 13 Peak stress in the compressive profile on a flat surface. [6].

Figure 2. 14 Spalling of hard chromium on the hard steel after reciprocating [6].

2.5 Combustion Engines [1]

The engine operation will be described from the four-stroke engine perspective (see Figure 2.15). During intake, air is sucked into the combustion chamber. Fuel is injected during the compression stroke. Different fuels are used for different engines. Fuels generally consist of carbon and hydrogen, CxHy. They may include gasoline, diesel or biodiesel (having 10–15 carbons), ethanol or gaseous fuels (e.g. natural gas, biogas.). Fuel and air react during the compression stroke (having 5–12 carbons), diesel or biodiesel (having 10–15 carbons), ethanol or gaseous uels (e.g. natural gas, biogas.). Fuel and air react during the compression stroke. The combustion energy released pushes the piston downwards, yielding power, heat and friction during the expansion stroke. The final stroke releases the exhaust components. The current emission legislation has limits on the allowable exhaust components. Emissions may be reduced by after-treatment of the exhaust gas or optimizing the combustion. The whole engine uses one single lubricant, which should lubricate, for instance, the piston ring-cylinder, the bearings and the valve train, as well as cool the pistons. The piston ring cylinder operates in the boundary regime at the turning points and reaches full-film lubrication in between the turning points.

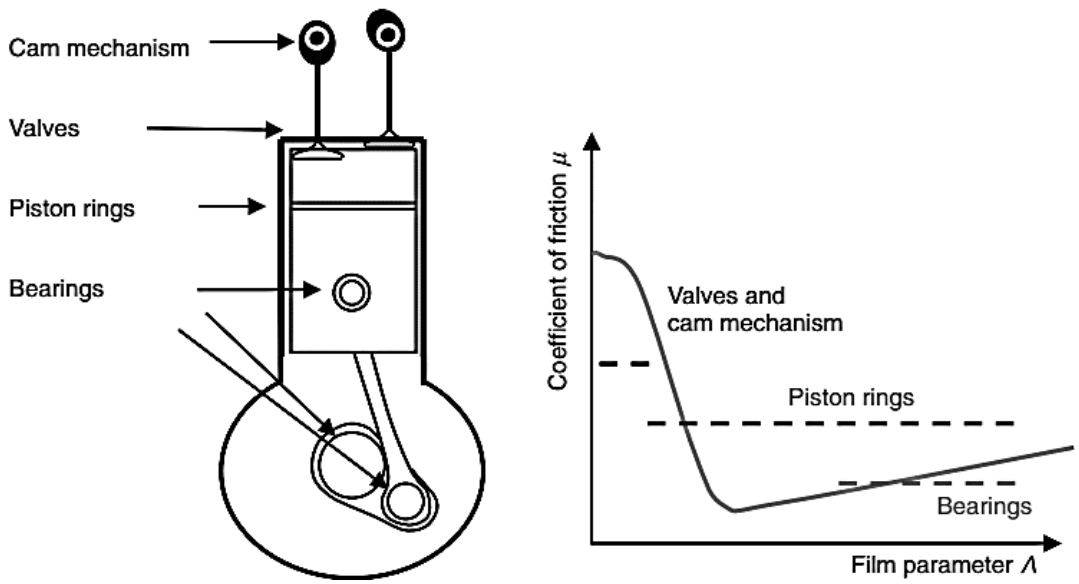

Figure 2. 15 The engine lubricated parts (left) and the conditions (right) [1].

2.6 Oil and wear analysis [8].

Oil analysis is an extensive subject whose focus can be subdivided into (a) fluid Composition and thermo physical properties (e.g., room temperature viscosity, volatility, thermal conductivity, temperature-viscosity coefficient), (b) external contamination level, and (c) tribosystem-generated wear debris. It can help to indicate how much wear is occurring, from where the debris is originating, and even what form of wear is taking place.

Trending is an important element of oil analysis. By studying periodic oil samples, it is possible to track the progression of wear (including running-in) within a tribosystem in which the individual components may be difficult or impossible to inspect without disassembly. For example, oil analysis from an internal combustion engine may reveal whether wear is occurring in the main bearings, on the piston skirts, or piston rings. It may indicate whether the wear is abrasive in nature (cutting chip like debris) or more adhesive (metallic flakes). Therefore, OA can indicate both the locations and types of wear in a tribosystem.

2.6.1 Viscosity [8]

The viscosity values most frequently reported for a lubricant are at 40 °C and 100 °C at atmospheric pressure and low-shear rates. Viscosity is a measure of a fluid's resistance to flow. The basic unit for absolute or dynamic viscosity is the Pascal-second (10 Poise). The common unit of absolute viscosity is centipoise, cP (1 mPa·s). The most common method of viscosity measurement is described in the ASTM D445 standard. Viscometers are devices that are used to measure viscosity. Most depend on the force of gravity to drive the fluid through a capillary. The viscosity value thus obtained is referred to as kinematic viscosity. The unit of kinematic viscosity is Stoke (St) or cent-Stokes (CST=0.01 St). One centistoke equals $1mm^2/s$. Absolute viscosity in centipoise (cP) is equal to kinematic viscosity in centistokes multiplied by the density of the fluid in kg/m^3 Viscosity index (VI), which is a measure of a lubricant's viscosity-temperature relationship, is based on 40 °C and 100 °C viscosity values (ASTM D2270).

2.6.2 Density and Specific Gravity [8]

Density of a substance is defined by mass per unit volume and in liquids, such as lubricants, is expressed as gram/ milliliter (g/mL). Relative density, also known as

specific gravity, is a measure of the density of a material relative to another material. Specific gravity of the liquids is equal to the density of the liquid divided by the density of water, and in gases, it is the density of the gas divided by the density of air. Specific gravity has no units. For liquids, density, hence specific gravity, is typically measured at 60°F or 15.6°C. Density of a material depends upon both pressure and temperature. Density change with temperature is called coefficient of thermal expansion and for liquids the more appropriate term is volumetric thermal expansion coefficient. This coefficient in liquids affects volume and is more sensitive to the boiling point of the hydrocarbon material or the component than to its density. Specific gravity is often used to identify specific lubricants, for example to distinguish between primarily paraffinic, naphthenic, and aromatic-based stocks.

2.6.3 Wear debris analysis [9] [10]

Ferrography is a very useful and comprehensive analysis for trending and reporting. At a minimum, the use can obtain an analytical means of monitoring the wear condition; and, at the same time, accrue the necessary sample points required to establish a wear particle concentration baseline and retain the presence of non-magnetic particles for visual inspection and evaluation as shown in Figure 2.16.

Industrial application of Ferrography entails the non-interruptive machine condition monitoring of heavily used lubricated mechanical systems. Hence, an operational baseline can easily be established by sampling every 50-500 hours of operation (approximately every one to three months, depending on system criticality), and used for quantitative trending analysis. Any anomalies in the wear particle

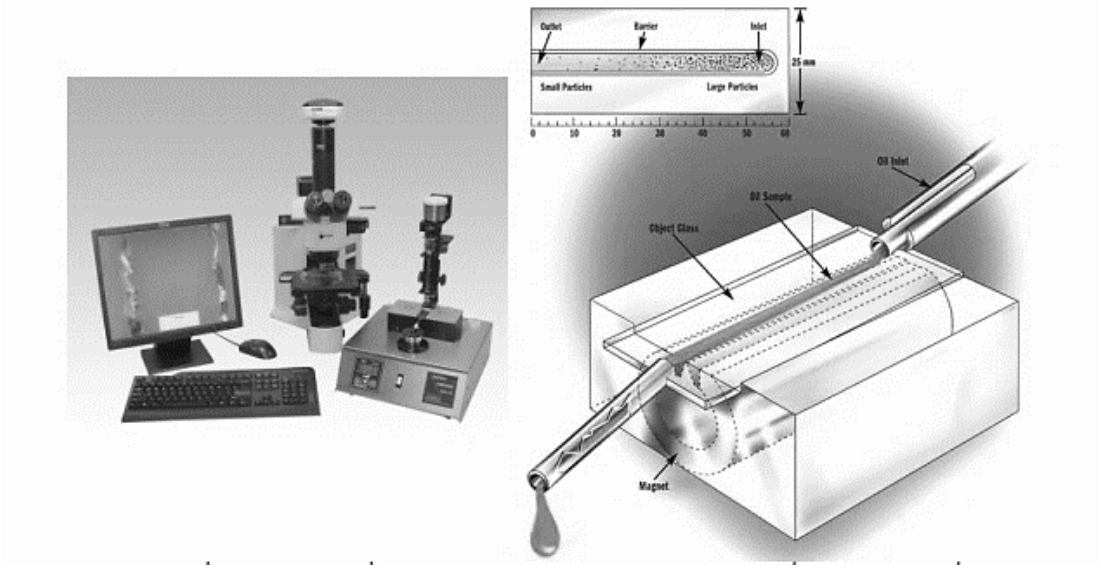

Figure 2. 16 Bichromatic microscope and Ferrogram analysis method [9] [10].

concentration, especially in the generation rate of large particles (>20 microns), is symptomatic of the onset of failure. For consistent results and accurate trending, lubricant samples are taken from the same places in the system each time. The method of sample extraction assures that the lubricant samples contain a Representative selection of wear particles. The samples are then ferrographically Analyzed both quantitatively and qualitatively.

	**Normal rubbing wear** Individual particles are generally 5 Microns and below. The quantity of these particles determines the wear Rate. There should be little or no visible texture to the surface, and the thickness should be 1 µm or less**.**
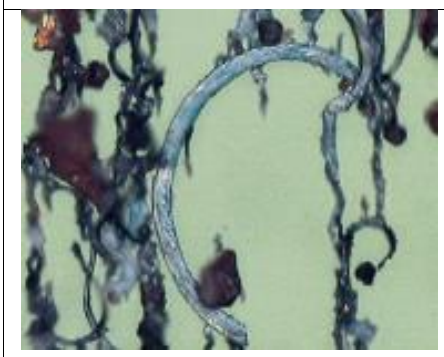	**Curled cutting wear particles** Such as this are usually generated as a Result of misalignment or abrasive particle embedded in a Babbitt bearing cutting wear particles may resemble wire, drill turnings, whittling chips, or gouged-out curls.
	**Red oxide** These particles resemble severe sliding wear particles, except that they are usually gray. They are formed in conditions of inadequate lubrication.

Figure 2. 17 Wear particle and wear mechanisms [10].

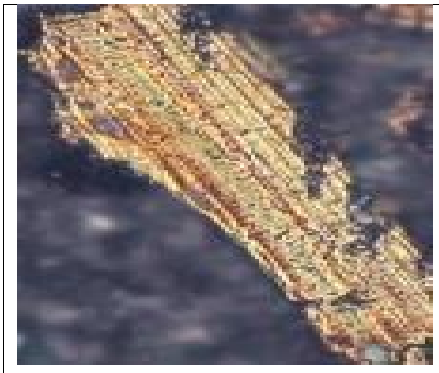	**Severe sliding wear** These particles are identified by parallel striations on the surface. Sliding wear particles sometimes show evidence of temper colors, which may change the appearance of the particle after heat treatment.
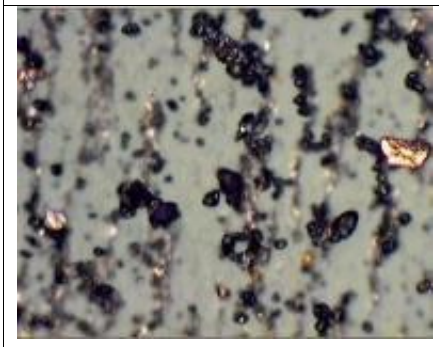	**Black oxides** Black oxides are dark gray to black, and they resemble pebbles. More iron is being consumed in the oxidation process, as a result of inadequate lubrication.
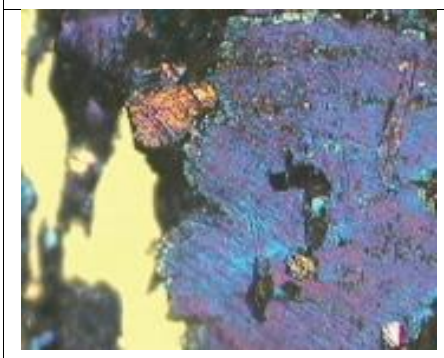	**Chunks** Chunks are generally greater than 5 μm in major dimension, with the length-to-thickness ratio being less than 5:1. There is generally some surface texture, and the particles do not appear flat. Instead, they are rough and shaped like chunks, but they are thinner.
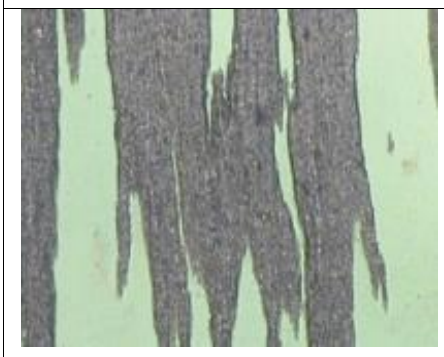	**Corrosive wear** When acids and other corrosive agents attack the surfaces of the machine and its wear particles, submicron-sized free metal particles, oxides, and other metal compounds are yielded. The size of this deposit can warn of chemical attack on the equipment
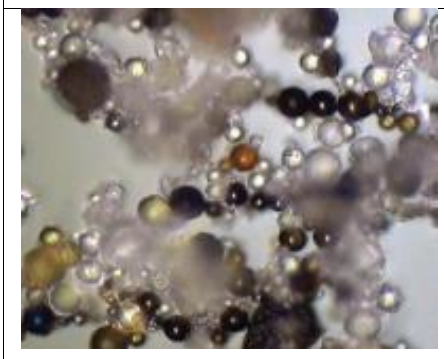	**Dirt and dust** Dirt and Dust are contaminants particles which are transported into the engine oil during combustion process.

Figure 2.17 Wear particle and wear mechanisms (continues) [10].

2.6.3.1 Scanning electron microscope [11]

The scanning electron microscope (SEM) uses a focused beam of high-energy electrons to generate a variety of signals at the surface of solid specimens. The signals that derive from electron-sample interactions reveal information about the sample including external morphology (texture), chemical composition, and crystalline structure and orientation of materials making up the sample. In most applications, data are collected over a selected area of the surface of the sample, and a 2-dimensional image is generated that displays spatial variations in these properties as shown in Figure 2.18. Areas ranging from approximately 1 cm to 5 microns in width can be imaged in a scanning mode using conventional SEM techniques (magnification ranging from 20X to approximately 30,000X, spatial resolution of 50 to 100 nm). Electrons are produced at the top of the column, accelerated down and passed through a combination of lenses and apertures to produce a focused beam of electrons which hits the surface of the sample. The sample is mounted on a stage in the chamber area and, unless the microscope is designed to operate at low vacuums, both the column and the chamber are evacuated by a combination of pumps. The level of the vacuum will depend on the design of the microscope. The position of the electron beam on the sample is controlled by scan coils situated above the objective lens. These coils allow the beam to be scanned over the surface of the sample.

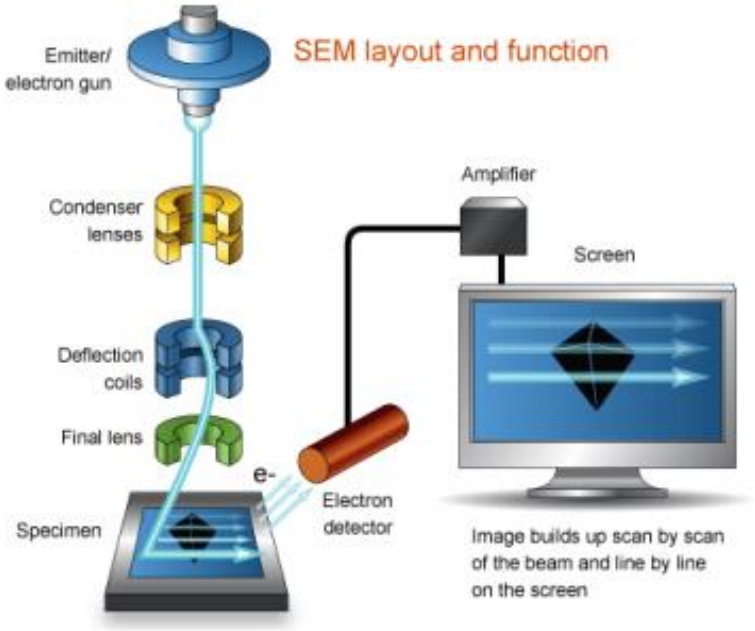

Figure 2. 18 Schematics of scanning electron microscopy operation [11].

2.6.3.2 Transmission electron microscope [11]

The transmission electron microscope (TEM) is a very powerful tool for material science. A figure 2.19 shown schematic of transmission electron microscopy operation by a high energy beam of electrons is shone through a very thin sample, and the interactions between the electrons and the atoms can be used to observe features such as the crystal structure and features in the structure like dislocations and grain boundaries. Chemical analysis can also be performed. TEM can be used to study the growth of layers, their composition and defects in semiconductors. High resolution can be used to analyze the quality, shape, size and density of quantum wells, wires and dots. The TEM operates on the same basic principles as the light microscope but uses electrons instead of light. Because the wavelength of electrons is much smaller than that of light, the optimal resolution attainable for TEM images is many orders of magnitude better than that from a light microscope. Thus, TEMs can reveal the finest details of internal structure - in some cases as small as individual atoms.

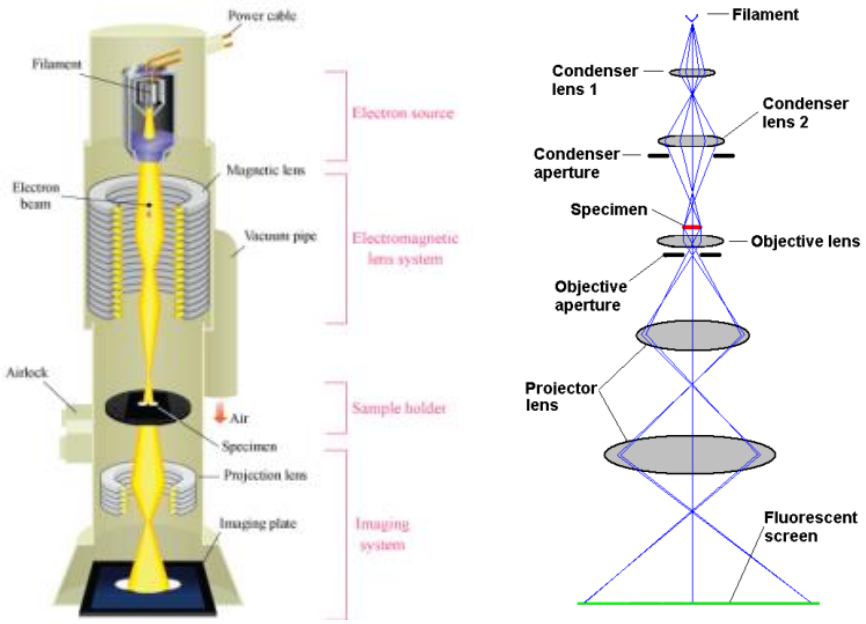

Figure 2. 19 Schematics of transmission electron microscopy operation [25].

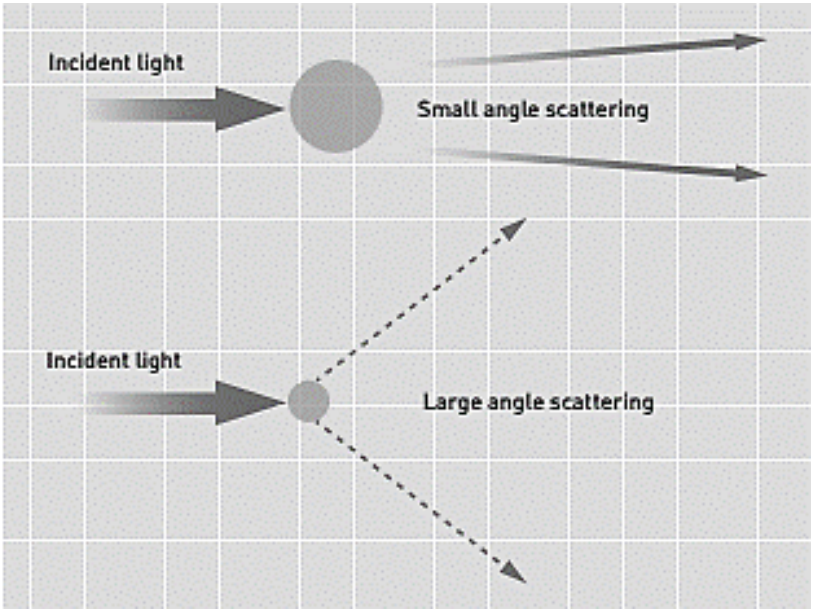

Figure 2. 20 light scatted pattern of the small and large particle [12][11]

2.6.3.3 Laser Diffraction spectroscopy [12]

Laser Diffraction spectroscopy is widely used for ranging a particle size distribution from hundreds of nanonetrs yp tomilimaters in size. It hits a laser beam passes through a particle and measure the intensity of the scattered light. Diffracted and refracted light is useful for this purpose; absorbed and reflected light works against this purpose and must be taken into account during measurement and size calculation. Large particles scatter light at small angles relative to the laser beam and small particles scatter light at large angles as shown in Figure 2.20. The angular scattering intensity data is then analyzed to calculate the size of the particles that created the scattering pattern using the Mie theory of light scattering. The particle size is reported as a volume equivalent sphere diameter. In this study used MALVERN Mastersizer 3000. The machine is capable for measuring particles between 0.01 and 20000 microns.

2.6.4 Oxidation Stability

Most lubricant applications are in the presence of air or oxygen; hence a lubricant to have good oxidation stability is highly desirable. All hydrocarbon materials undergo oxidative degradation. Unlike thermal stability which is inherent to the base stock, oxidation stability can be greatly improved by the use of the oxidation inhibitors. The consequences of oxidation are a lubricant's viscosity increase and the formation of

acids and deposits, such as varnish and sludge. A wide variety of tests are available to assess a lubricant's oxidation stability. These include tests that are described in the ASTM Standards D2272 and D1313. These tests are suitable for measuring a lubricant's stable life and the effectiveness of the oxidation inhibitors. To monitor the oxidation process, a micro-oxidation test, such as the Penn State micro-oxidation test, has been developed along with the analytical procedures based on gel permeation Chromatography (GPC) and atomic absorption spectroscopy (AAS).

2.6.5 Nitration

Nitration: The combustion chambers of engines provide one of the few environments where there is sufficient heat and pressure to break the atmospheric nitrogen molecule down to two atoms that can react with oxygen to form nitrous oxides (NOx). This becomes a major problem for some engines, especially EGR engines. When nitrogen oxide products enter the lube oil through EGR and normal blow-by, they react with moisture present in the lube and become very acidic and rapidly accelerate the oxidation rate of the oil. The GCF Filter controls the effects of nitration in the same ways it controls oxidation. By delivering cleaner oil to offer as a seal between the ring and liner, blow-by of NOx is kept to a minimum. Also, the GCF Filter keeps the oil chemically dry and prevents the mixing of NOx and moisture, which controls NOx acid formation and accelerated oxidation of the oi*l.*

2.6.6 Total base number

The total base number, or TBN, of the detergent reflects its ability to neutralize acids. In the case of the basic suffocate and phosphate detergents, only the over based portion of the detergent, i.e., the carbonate and the hydroxide, possess this capability. The neutral metal sulfates and phosphates, or the soaps, lack this ability. However, in the case of the basic carboxylates, salicylates, and phonates, the soaps also possess the acid neutralizing ability. This is because unlike the sulfates and phosphates that are strong acid—strong base salts, metal carboxylates, metal salicylates, and metal phonates are strong base-weak acid salts. This makes them Lewis bases, hence the acid neutralizing ability. The total acid number (TAN) of oil is synonymous with neutralization number. The TAN of oil is the weight in milligrams of potassium hydroxide required to neutralize one gram of oil and is a measure of all the materials in oil that will react with potassium hydroxide under specified test conditions.

2.6.7 Elemental and Structural Analysis

Petroleum, or crude oil, contains a wide variety of elements, some of which are present at percent levels and others at parts per million levels. However, refining processes used to manufacture fuels and mineral base oils remove most elements other than carbon, hydrogen, oxygen, nitrogen, and perhaps sulfur. Additives used to formulate lubricants contain elements that are used either to facilitate their solubility in base fluids or impart special properties. Common elements include nitrogen, sulfur, phosphorus, alkaline earth metals, zinc, copper, and molybdenum. A list of elements That are generally used in lubricants is provided in Table 2.1, along with their role X-Ray Fluorescence Spectrometer (WDXRF) is a powerful analytical instrumental method used in a wide variety of industries to determine the elemental composition of various materials.

Table 2. 1 Chemical elements present in lubricants and their role [1]

Element	Compounds	Performance
Boron (B)	Borax and esters	Anti-wear agents, oxidation inhibitors, deodorant cutting oils
Barium (Ba)	Sulfonates, phenates, phenates, dialkyl phosphates, phosphonates and thiophosphonates	Detergents inhibitors, corrosion inhibitors, detergent and rust inhibitors
Calcium (Ca)	Sulfonates, phenates, carboxylates, and salicylates	Detergents, detergent inhibitors, dispersants
Magnesium (Mg)	Sulfonates and phenates	Detergents inhibitors
Molybdenum (Mo)	Molybdenum disulfide and alkyl phosphate	Extreme-pressure additives
Phosphorus (P)	Metal dialkyl dithophosphates	Oxidation inhibitors, anti-wear agents, rust inhibitors
Zinc (Zn)	Dialkyl dithiophosphates, dithiocarbamates and pheolates	Oxidation inhibitors, corrosion inhibitors, detergents, extreme – pressure additive and anti-wear agents, rust inhibitors

2.7 Literature reviews

2.7.1 Particulate matters morphology and nanostructures

Soot is a microscopic carbonaceous particle that is a product of incomplete combustion of hydrocarbons. An artist's conception of diluted and cooled diesel PM is illustrated in Figure 2.21 [13]. It consists of carbon, ash, and unsaturated (unburned) hydrocarbons. The unsaturated hydrocarbons are essentially acetylene and polycyclic aromatic hydrocarbons. These components have particularly high levels of acidity and volatility. Measurements have shown that it typically contains 90 per cent carbon, 4 per cent oxygen, and 3 per cent hydrogen with the remainder consisting of nitrogen, sulphur, and traces of metal. Individual or primary soot particles from diesel combustion have been measured to be approximately 40 nm. Because of soot's colloidal properties, the particles agglomerate up to a maximum of approximately 500 nm, with a mean soot agglomerate size of 200 nm. The TEM micrograph of diesel engine soot is shown in Figure 2.22.

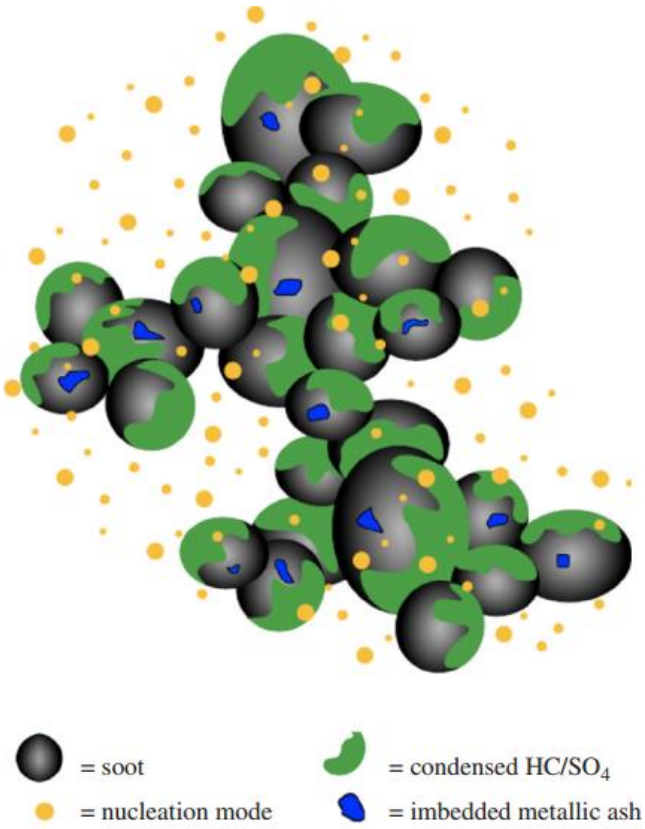

Figure 2. 21 Artist's conception of diesel particulate matter [13].

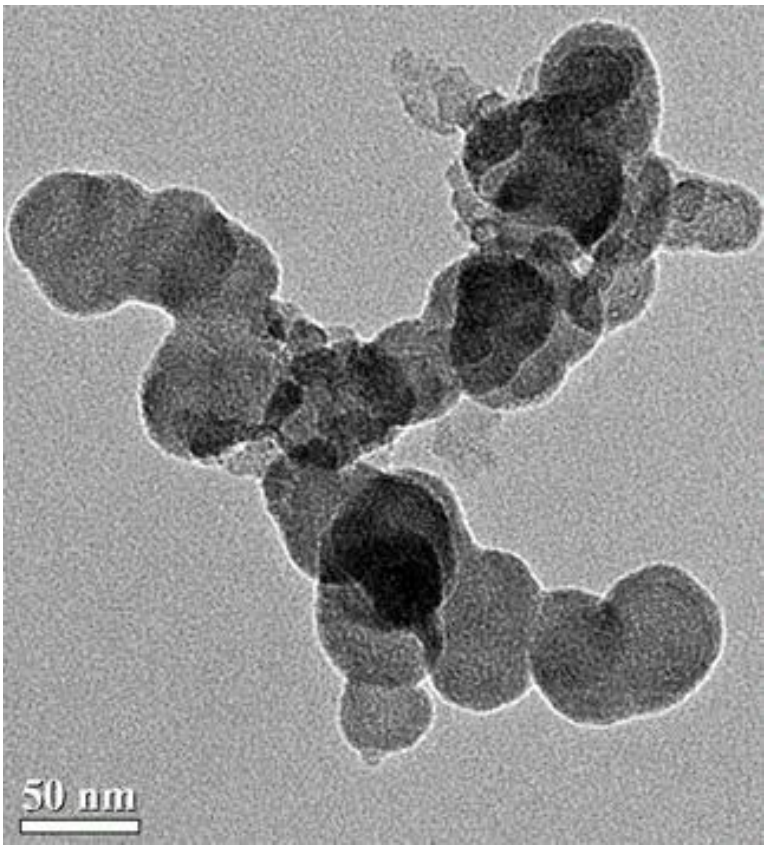

Figure 2. 22 TEM micrograph of diesel engine soot

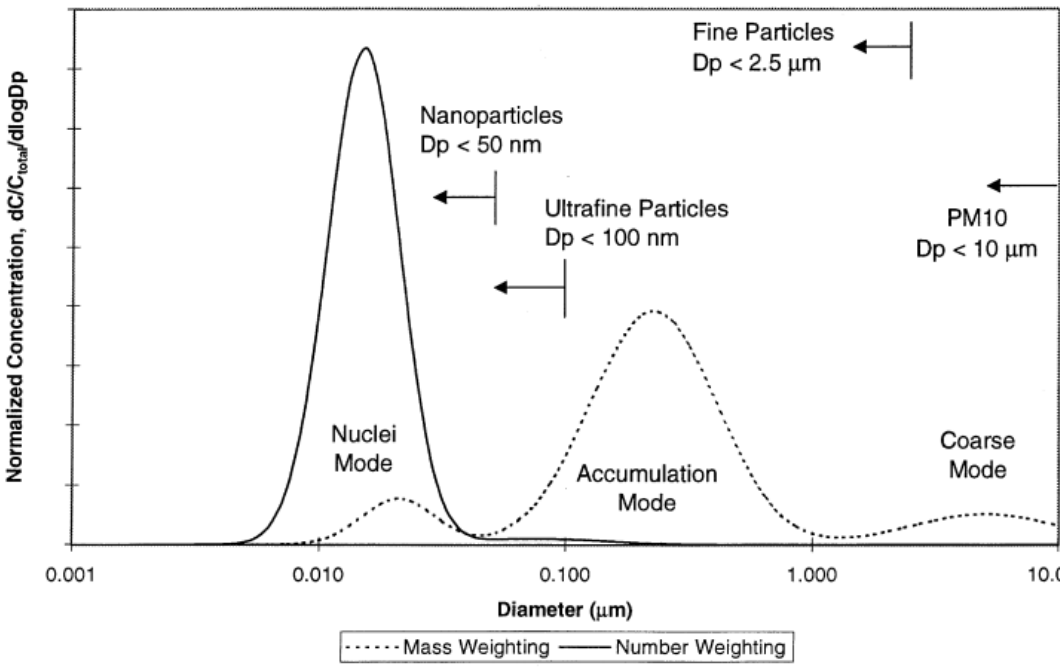

Figure 2. 23 Idealized diesel exhaust particle number and mass weighted size distributions [26].

The idealized diesel exhaust particle number and mass weighted size distributions is shown in Figure 2.23. It was proposed by D. B. Kittelson [13]. The particle size distribution are trimodal distribution which consisting of nucleation, accumulation and coarse mode. The nucleation mode consists of the particle from a few nanometer to 50 nm and the larger particle which in the range of 0.01 – 0.3 microns are in agglomeration mode. The particles in the coarse mode which consists of the nucleation and accumulation mode are larger than 1 microns.

The impact of small compression ignition (CI) engine operation conditions on diesel and biodiesel particulate matters (PMs) was investigated by Siricholathum et al [14] They found that the smoke intensity of biodiesel engine's PMs are around the half of the diesel engine's PMs. The physical characterization of those PMs were also investigated by using TEM. Figure 2.24 shows TEM micrographs of diesel and biodiesel engine's PMs under 40% engine load and 1,600 rpm of engine speed. The primary particle size were in the range of 10-60 nm. It was clearly observed much amount of particle diameters were in the range of 30-40. Moreover, the primary particle size distribution are also shown in Figure 2.25. The result of measuring particle sizes is in the range of 10-60 nm. It was clearly observed much amount of particle diameters are in the range of 30-40 nm. Figure 2.26 shows Average size distribution of Primary particle particulate matter from diesel and biodiesel under 20, 40, 60 and 80% of engine load and 1600 rpm of engine speed particle diameter size decreased when increasing engine speed for both of diesel and biodiesel particulate matter. When focus on the effect of biodiesel fuel, the particulate matter from biodiesel combustion is emitted smaller size than that of diesel combustion.

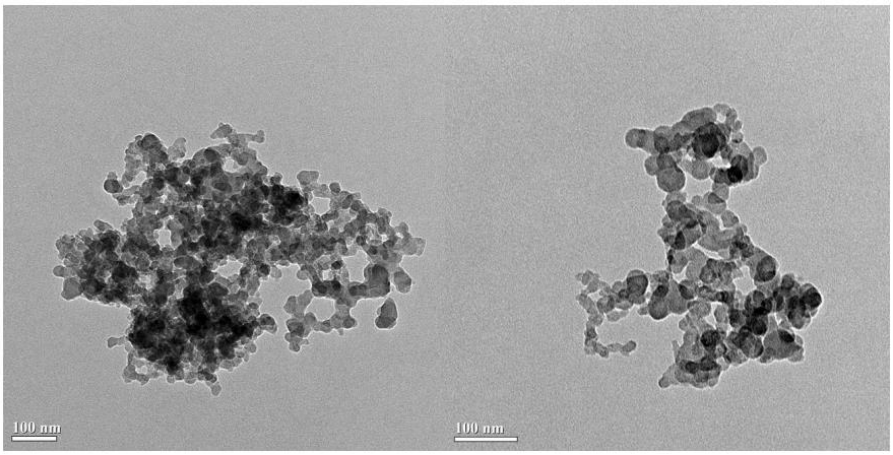

Figure 2. 24 TEM micrograph of diesel and biodiesel engine PMs under 40% engine load and 1,600 rpm of engine speed [14].

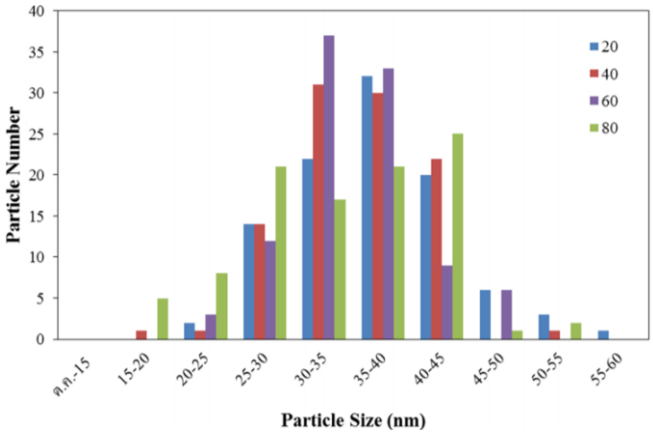

(a) Diesel engine 1600 rpm

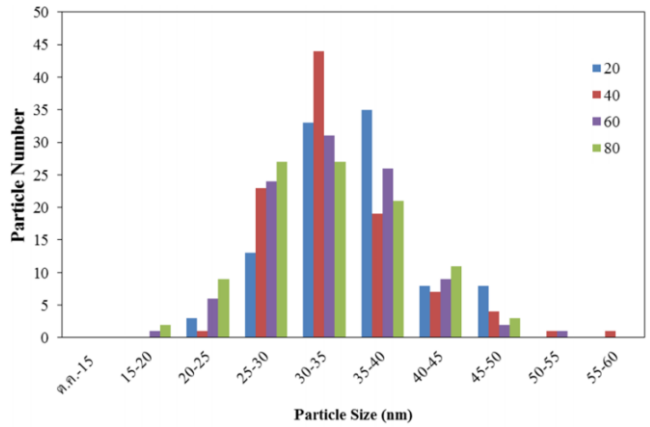

(b) Biodiesel engine 1600 rpm

Figure 2. 25 Size distribution of primary particulate matter from (a) diesel and (b) biodiesel at 1600 rpm of engine speed [14].

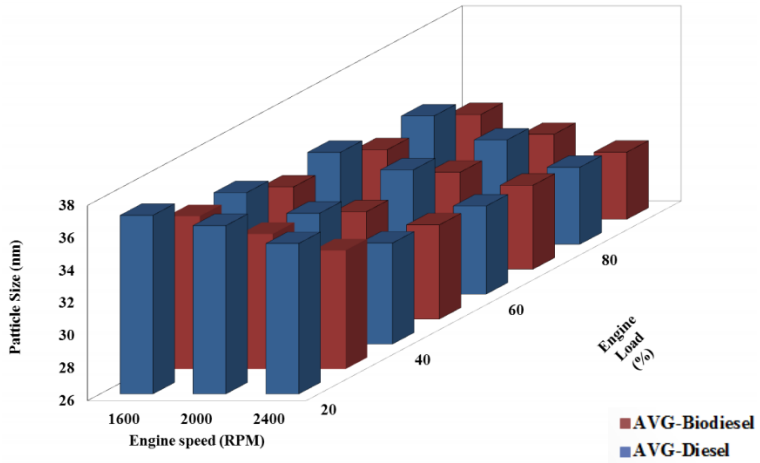

Figure 2. 26 Comparison primary particle size distribution between diesel and biodiesel engine soot under difference engine speed and engine load [14].

2.7.1.1 Carbon atom density calculation

The nanostructures of particulate matters emitted from combustion was investigated by [15]. They used TEM to characterize the nanostructures of diesel soot particle as shown in Figure 2.27. Single particles are nearly sphere shape even though surface are not so smooth. Carbon platelets in the surface of particle are not so close distance and look like not so strong contact with other platelets. TEM image shows the different structure of inner core zone and outer shell zone of PMs. The inner core diameters are approximately 5 to10 nm. Moreover, the structure of carbon platelet inside inner core zone shows short length and non-homogeneous platelets, whereas long length and homogeneous platelets could be clearly observed in outer shell zone. Single particle could be observed two to four inner core portions. In the first process of PM formation, agglomerated inner core portion might be accumulated to be a single primary particle. After that, surface of single primary particle growth up by carbon atom with time until approximately 100 nm of diameter depended on engine operation condition which might be strongly effect on density of carbon atom per volume.

PM is investigated for number of carbon atom include in the particle. TEM image is used for numerate platelet number that aggregate layered in the particle. Each of platelet is consisted properly by carbon atom from incomplete combustion product. Figures 2.28.(a-c) are the images of original 10 nm2 focused area, after post processing of two colors and after post processing of skeleton carbon platelet length estimation, respectively. The focused areas of all images are homogeneous platelet area in each outer shell zone. Original gray color could be successfully changed to two colors images in the first step. The lengths of each platelet in each sample are quite different, whereas the distances of each platelet are also not too different. From the skeleton images, the carbon platelets inside the PM were measured by image processing program. The skeleton carbon platelets, which have 1 unit pixel width for each platelet, were measured for the white area in the image to be a carbon platelet length. The estimated of platelet sizes distribution in each condition are shown in Fig.2.28. The average of diesel and biodiesel PM carbon platelets is in the range of 0.1-7.0 nm. Another result of carbon atom number per volume is also estimated.

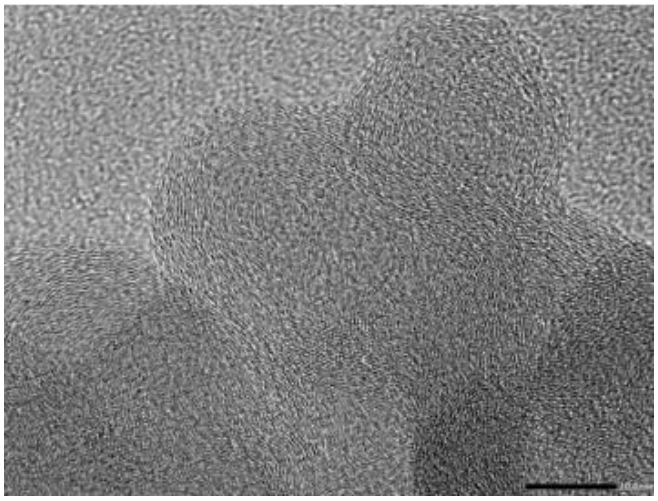

Figure 2. 27 TEM micrograph of diesel single PMs [15].

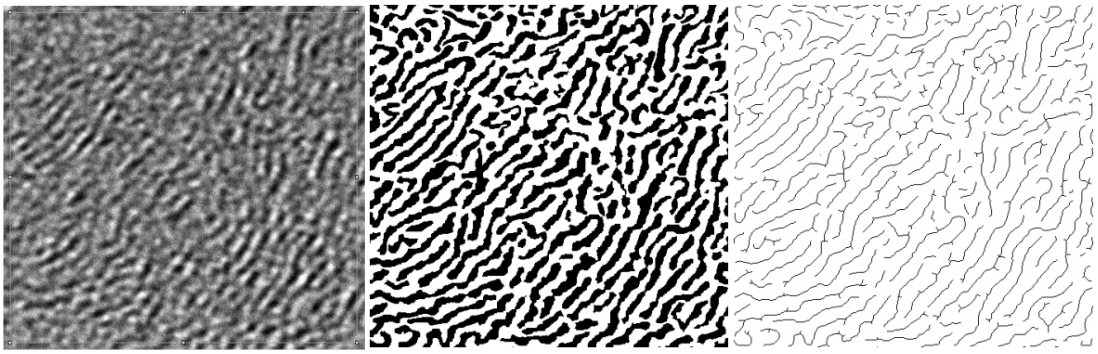

(a) TEM focused area (b) two-colors (c) Skeletonized

Figure 2. 28 TEM micrographs of (a) diesel single PMs focused area, (b) two color post processing and (c) skeletonized images of crystallites [15].

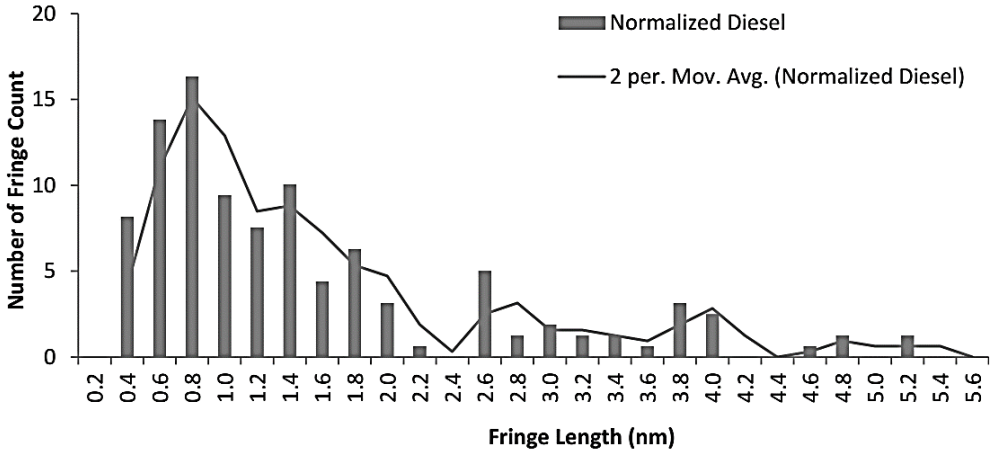

Figure 2. 29 Diesel's crystallite size distribution [15].

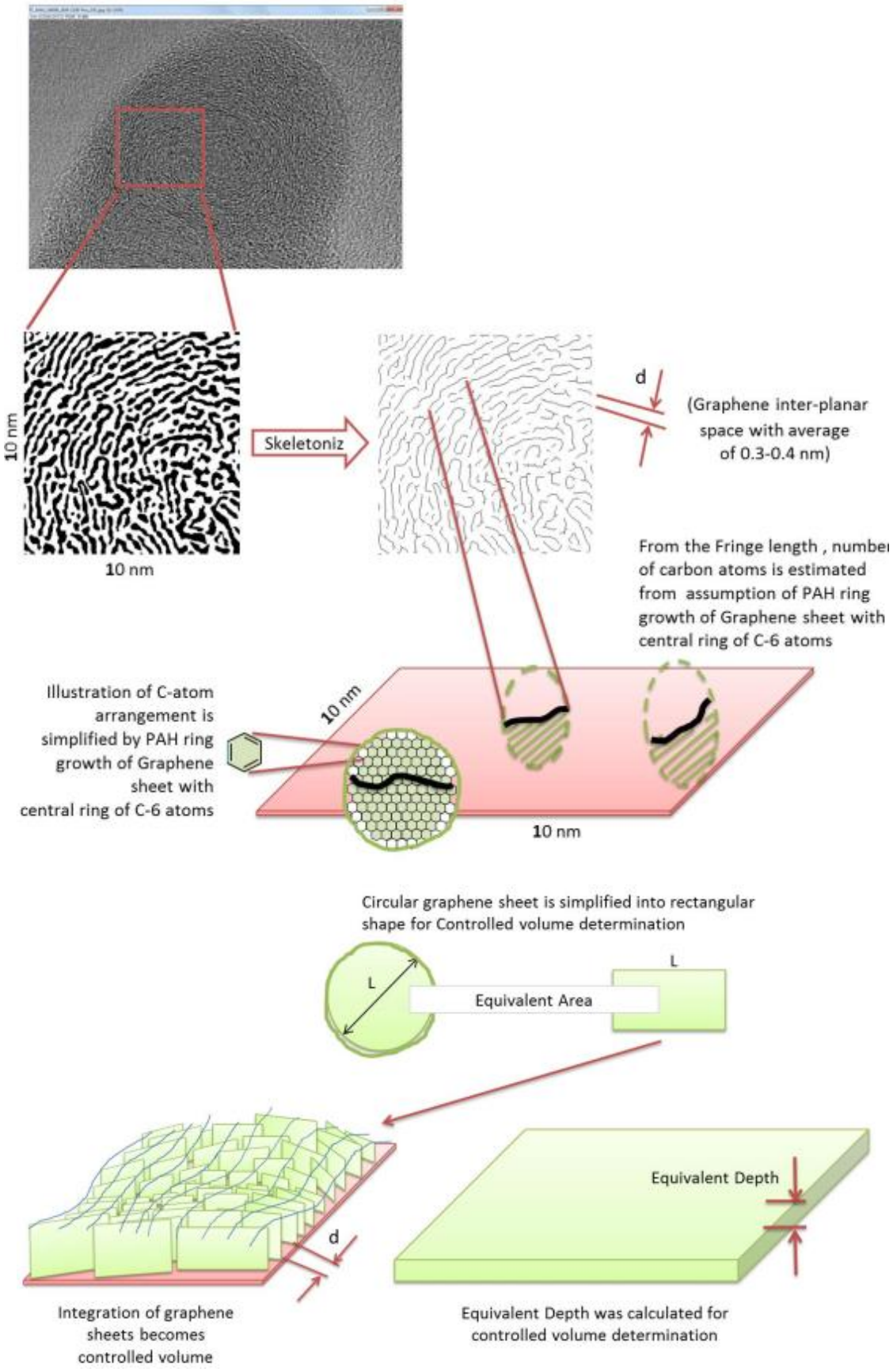

Figure 2. 30 Conceptual model for calculating carbon atom density. [15].

Figure 2. 31 Comparison of carbon atom and soot density of BE20, B100, and Diesel [15].

Items	BE20	B100	Diesel	Graphite	Carbonblack
Total crystallite length (nm/image)	189.13	208.38	227.45		
Total C atoms	9786.92	14700.46	17695.83		
Control volume (nm^3)	110.86	162.27	171.61		
Carbon atom density (atom/nm^3)	88.28	90.59	103.12		
Soot density (g/cm^3)	1.76	1.81	2.06	1.7-1.8 [a]	1.8 – 2.1 [b]

a : http://www.chemicalbook.com/ProductMSDSDetailCB3109508_EN.htm ;
http://www.inchem.org/documents/icsc/icsc/eics0471.htm

b : Poco Graphite - An Entegris Company

Watanawongskorn et al. proposed a model to determine a controlled volume from the 2-dimension captured image as shown in Figure 2.30. The crystallite platelet was assumed to form a circular sheet because of chemical bonding stability. In order to estimate an accurate volume, the graphene sheets were simplified into rectangular shape. Integration of all sheets becomes a closed volume which is ready for carbon atom density calculation. The concepts of estimation are "the molecule of carbon-6 (C6) is the possible smallest size" and "there are 3 layers arranged to be a platelet". Such molecules are agglomerated to be the large ring of carbon then becomes a platelet. Figure 2.31 shows calculation results of carbon atom density compared among B100, BE20, and diesel‟s soot particle. Carbon density of diesel‟s soot is apparently higher than B100‟s and BE20‟s which agrees with the Black and White image from the image processing. Also, all calculation results of soot density are close to practical values of industrial graphite and carbon black properties.

2.7.1.2 Soot hardness calculation [3]

Soot particles are generally assumed to be extremely hard individually and much softer when agglomerated. The harnesses of a variety of soots produced during a standard Cummins M-11 engine test were measured by Li et al. [3]. They were determined by carbon Plasmon energy methods, obtained from the electron energy loss spectra, which were measured using a high-resolution transmission electron microscope as shown in Figure 2.32. In order to calculate soot hardness, they created the relationship between carbon atom density and hardness. Figure 2.33 (a) shows the

correlation between carbon density and mechanical hardness of the diamond, graphite and diamond-like carbons according to the literature. The hardness of glassy carbon is about 250 kilogram per square millimeter but the hardness of diamond is about 10,000 kilogram per square millimeter. The solid line is the best linear least-squares fit of all four data points. The results in Figure 2.33 (b) were obtained according to the best-fit scale. It shows the calculated hardness of CB, diesel, biodiesel engine soot and the hardness from the reference. It is clearly indicates that the hardness of soot is higher than that of the metal. That means soot is hard enough to abrade the metal engine parts.

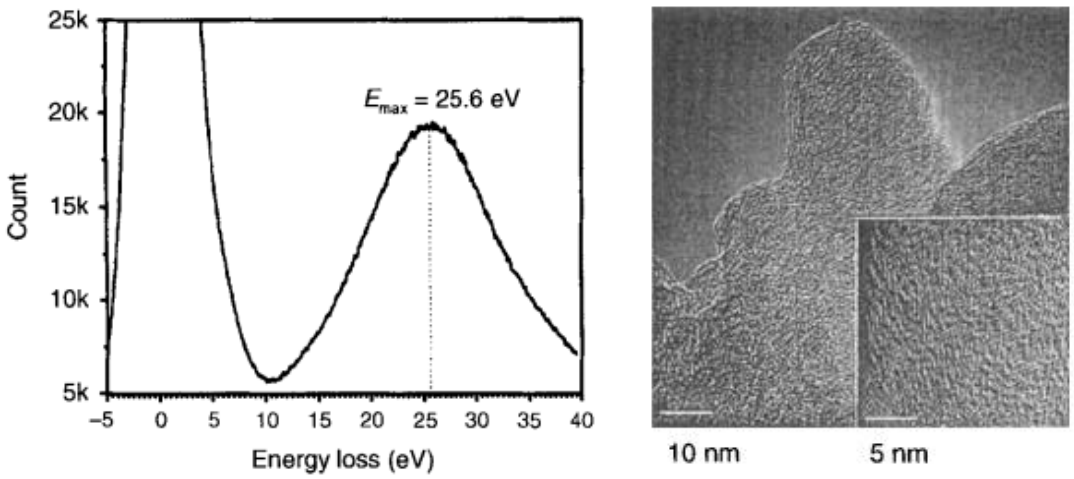

(a) Low-loss energy-loss spectrum (b) TEM image of soot particle

Figure 2. 32 Low-loss spectrum and TEM image of an individual soot particle [3].

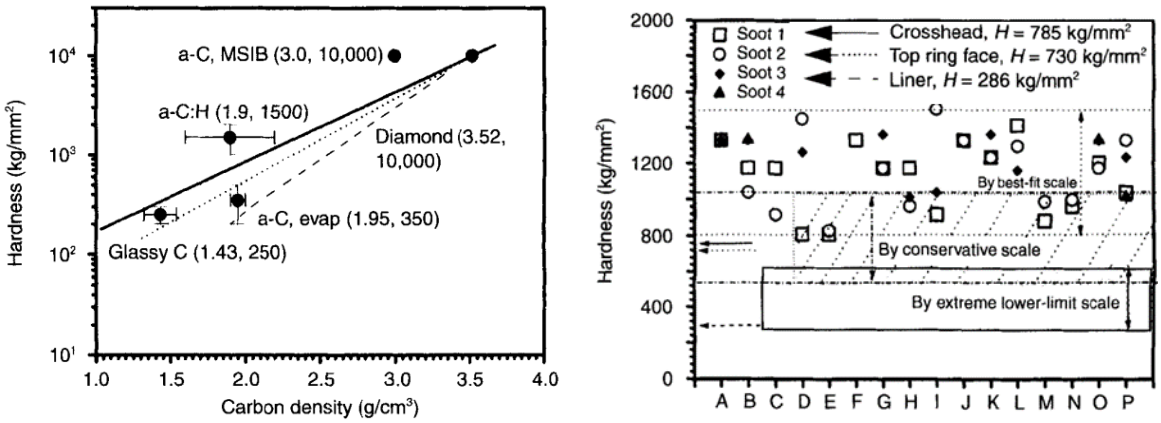

(a) Carbon density and soot hardness. (b) Hardness of soot and engine parts

Figure 2. 33 Carbon density and its hardness and Hardness of soot and engine parts [3].

2.7.1.3 Soot Simulants [16]

Carbon black particles do have the capability of mimicking the behavior of soot from engine oils, investigated by Supanamok et al [16] . Findings showed that, whenlooking at primary soot particles (30–50 nm) using electron microscopy techniques, there is very little difference between engine soot and carbon black. There was a great deal of similarity in particle size and structure, confirming that the two are essentially the same on a nanometer scale. When investigating agglomerated soot and carbon black particles (up to 500 nm), carbon black was again found to be similar to engine soot, although a slight difference was discovered. The carbon black particles disperse in a similar fashion, but create a larger agglomerate diameter than extracted engine soot, greater by approximately 50 nm. Chemical analysis of soot and carbon black particles showed that contents. Oxygen and hydrogen were shown to concentrate on the surface of the carbon black, creating a relatively polar surface, meaning it will tend to have a greater tendency to interact with other polar species, for example, other carbon black particles. Prior to extraction from its lubricant, the engine soot displays a higher polar surface than carbon black, but, once the soot has been extracted from the lubricant, it becomes less polar than carbon black. This explains why carbon black particles created a larger-diameter agglomerate than extracted engine soot. Carbon black particles display higher carbon contents and lower ash and volatile.

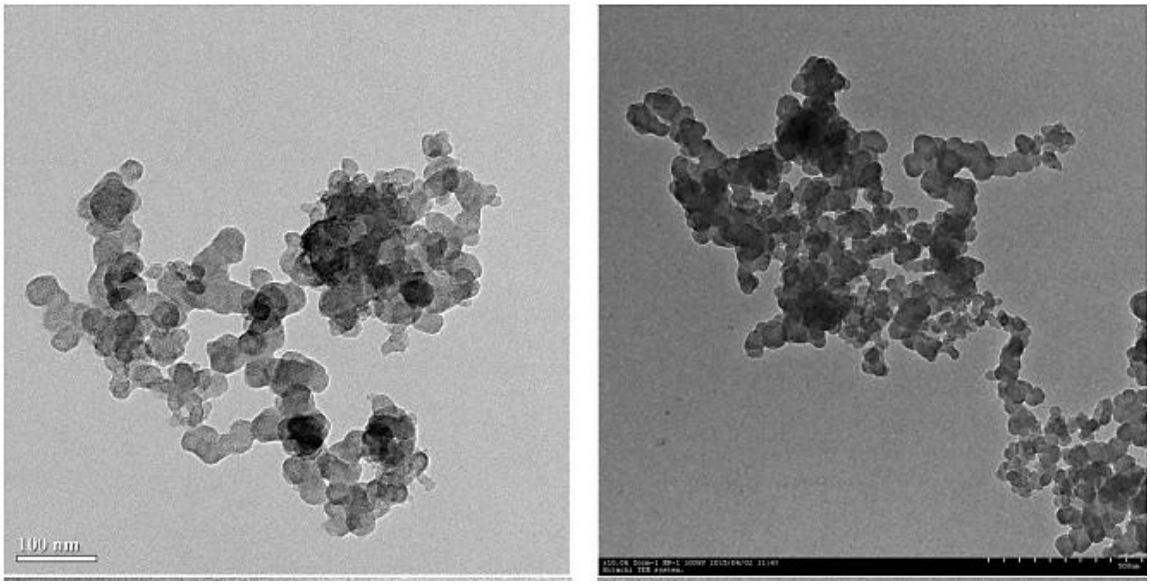

Figure 2. 34 Morphological of diesel soot (left) and carbon black (right) [16]].

2.7.2 Soot transport and entrainment in component contacts

It has been shown that, of the soot produced within the engine, only 29 per cent reaches the atmosphere through the exhaust pipe, with the remainder being deposited on the cylinder walls and piston crown. Of the soot that is retained in the engine (mainly in the lubricant), 3 per cent is attributable to blow-by gases; the remainder results from piston rings scraping away soot deposits in the cylinder, which then end up in the sump. It is then transported around the engine where it can be entrained into component contacts. Within the valve train, there are many component interfaces, all of differing geometries and motions, as shown in Figure 2.35. Sliding, rolling–sliding, and reciprocating contacts exist, some of which are conformal and some non-conformal. Because of the varying motion and loads at each interface, different regimes of lubrication will be apparent. This is further complicated by the mechanisms for lubrication application, which range from contacts where positive lubrication is used, to those where lubricant reaches the contact indirectly by splash lubrication. In some cases, contacts receive little lubrication because of their location, and starvation problems can exist; the presence of soot will further exacerbate this.

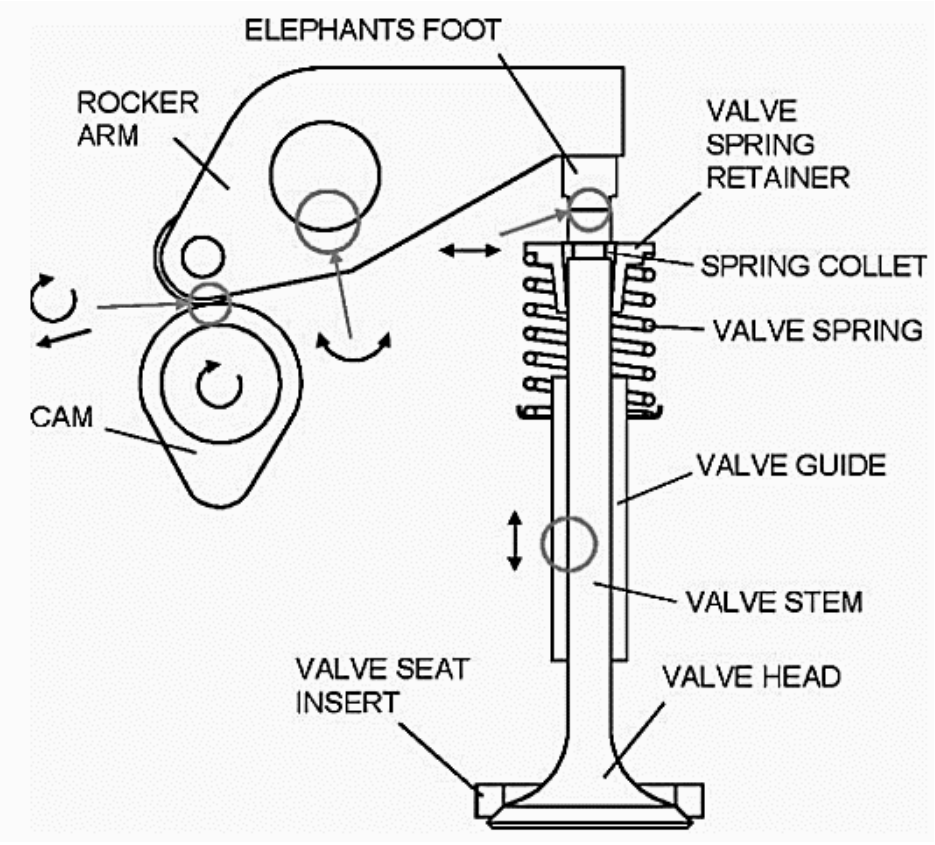

Figure 2. 35 Sample valve train component contacts [2].

2.7.2.1 Soot and metallic wear contamination in used engine oil [17]

The used engine oils were collected from the small diesel engine vehicles with different oil changed interval by [17]]. The engine oil‘s mileage and oil aged were in the range 3,000-20,000 and 0-10,000 km, respectively. After that, the engine oil conditions and contaminants were measured. They are including kinematic viscosity, fuel, soot and metallic wear contamination. The used oil’s kinematic viscosity at 40 and 100 °C were measured as shown in Figure 2.36.a and b. The viscosity at 40 °C fall in the range of 45 – 37 Cst and the average value was 36.63 Cst. The viscosity at 100 °C also fall in the range of 10 – 8 cSt and the average value was 8 cSt. The results shows that the viscosity decrease with the increasing of the engine mileage and oil aged. Two major factors are mainly responsible for lubricant oil viscosity changes, (i) formation of resinous products because of oil oxidation, evaporation of lighter fractions, depletion of anti-wear additives and contamination by insoluble compounds tend to increase viscosity and (ii) moisture addition, fuel dilution and shearing of viscosity index improvers tend to reduce the oil viscosity.

Fuel and soot contamination in used oils were measured as shown in Figure 2.36.c. and d**,** respectively**.** The fuel contamination were in the range of 1.57 – 2.5 percent by weight. And the soot contamination were in the range of 0.6 – 1 percent by weight. The oil analysis showed that the fuel and soot contamination increased as the mileage and oil age increase**.** Fuel and soot are remain of the incomplete combustion process that can be transported to the engine oil during combustion process. The average fuel contamination in the small diesel engine vehicles was about 2 % by weight and the average soot was about 0.69 % by weight.

Total wear metal contamination in used oils were also measured as shown in Figure 2.36.e. The wear contamination were in the range of 9 – 280 ppm. The oil analysis showed that the wear contamination increased as the mileage and oil age increase.

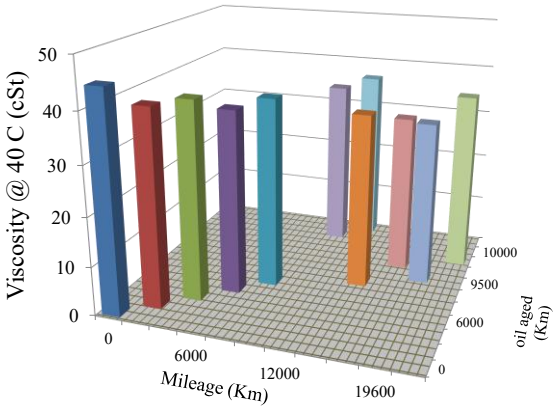

(a) Kinematic viscosity @ 40 °C (cSt.)

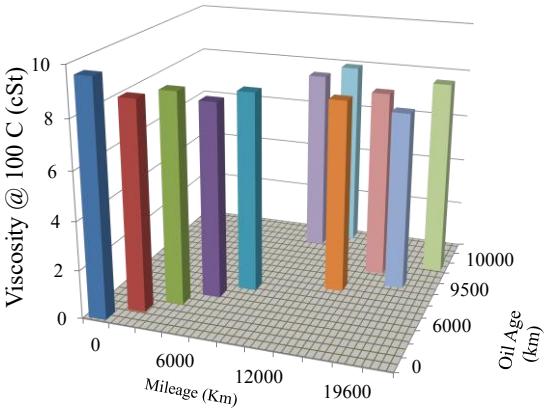

(b) Kinematic viscosity @ 100 °C (cSt.)

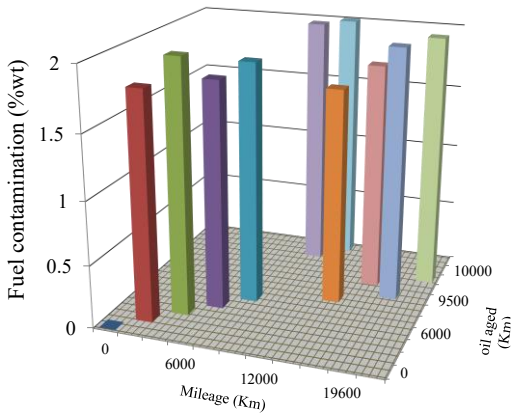

(c) Fuel contamination (%wt.)

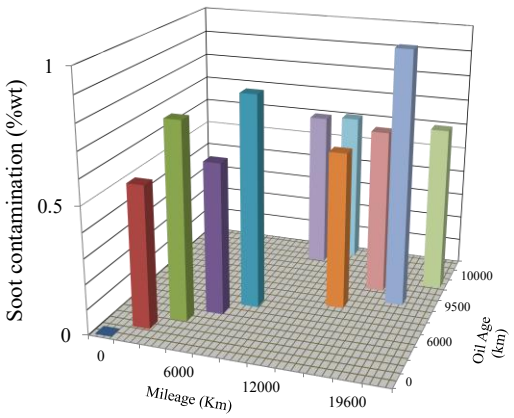

(d) Soot contamination (%wt)

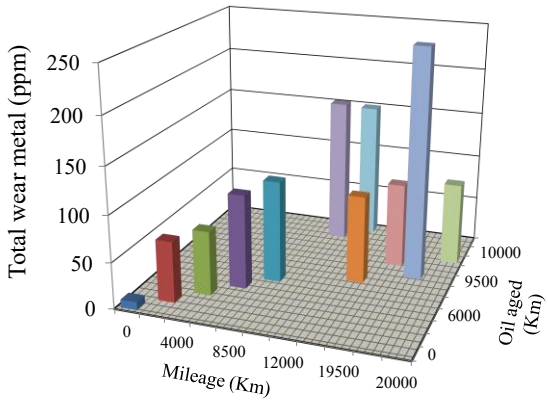

(e) Total wear metal contamination (%wt.)

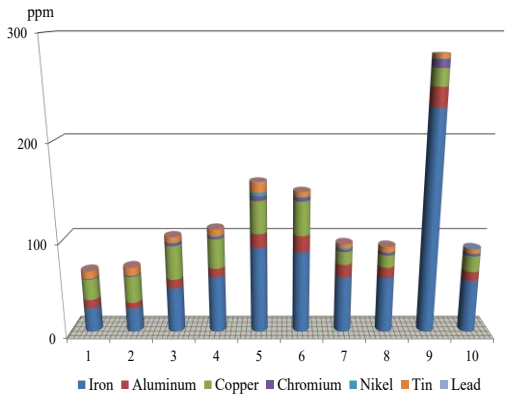

(f) Total wear metal elements (ppm)

Figure 2. 36 kinematic viscosity, fuel, soot, and wear metal contamination in the used oil of the small diesel engine and wear metal elements [17].

2.7.3 Tribology Tests [1]

Torbacke. [1] wrote an introduction to tribological test methods that there are many reasons for carrying out tribology test or tribotest. One reason is to study wear and friction mechanism appearing in specific tribological application. Other reasons are ranking of materials and lubricants for existing equipment or selection of materials and lubricants for new application. Tribotesting may also be performed for general characterization of wear and friction. Tribotests can be classified into tests that simulate the function of real components or tribological systems and tests that simulate the critical tribological load. The former class includes field tests, bench tests and component tests. The latter class comprises different model tests. All testing aims at increasing the tribological understanding at the fundamental or system level in order to enable development of design, construction and function of tribological systems. The complexity of testing may differ as well as the time and cost for testing.

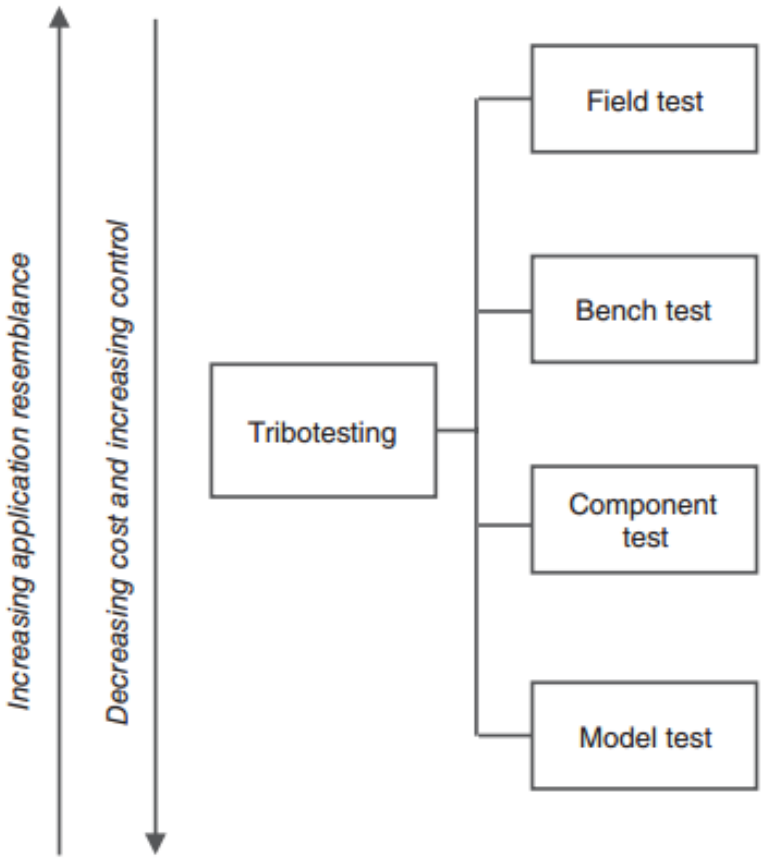

Figure 2. 37 Different types of tribological tests [1].

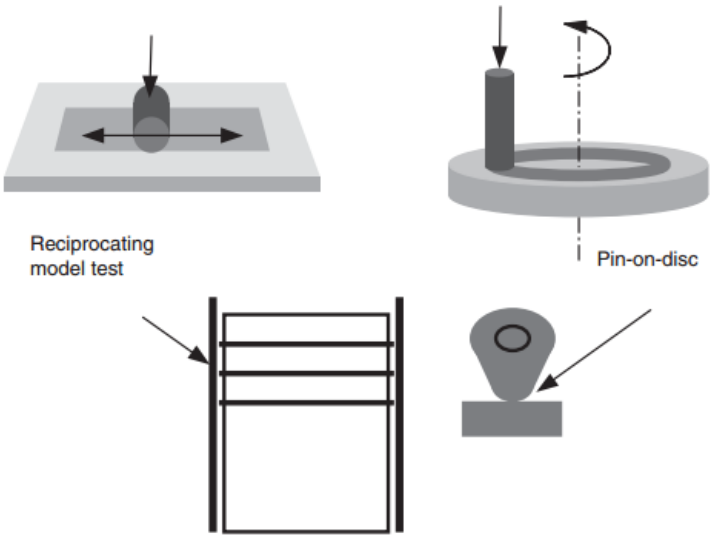

Figure 2. 38 Tribology selection for typical combustion engine [1].

With testing involving contaminants, it is essential that a good representation of the contact motion, loading, and geometry is achieved if bench testing is to be used. Entrainment of the contaminants will be directly affected by these and is key to determining which wear process may occur. This means that the best approach would probably be to use actual components. Engine tests are always problematical. It is difficult to control many of the test parameters and to provide good wear measurements. However, standard engine test cycles designed to promote soot production have been defined, as will be outlined in a later section, that allow soot wear studies to be carried out. The model test selected should provide the closest possible resemblance to the application in mind. The first step is to evaluate the contact geometry that is the form or shape of the contacting bodies and whether the contact is formed. The contact geometry directly affects the local conditions in the contact and is considered to be the primary variable for selecting model test and for scaling up and scaling down of tests. Finally, the test duration must be set long enough for the test to be correctly evaluated.

The combustion engine is lubricated with one lubricant operating in the boundary to the full-film regime. Two parts of a combustion engine have been selected to show the use of model testing, seeing on Figure 2.38. The piston–cylinder liner and the cam–follower represent two different types of lubricated contacts in an engine. Due to the combustion in the engine, the piston–cylinder is exposed to very high temperatures.

2.8 The effect of biodiesel contamination on metallic wear [17]

The pure engine oil and engine oil with difference types of biodiesel contamination were brought to test four-ball wear tester under controlled condition, 60 minutes duration, apply load 392 N, speed 1200 rpm, and temperature at 75ºC. The wear scar diameters (WSD) and surface roughness of the lower balls were measured by using an optical microscope and 3D rendering analysis, they were the average value of the three lower balls. In addition, the micro surface analyses were investigated by using Scanning Electron Microscopy (SEM). Figure 2.39 shows wear surfaces under 3D optical microscope and scanning electron microscope of each sample the engine oil without fuel and engine oil containing 2% wt. of Biodiesel (b) B7, (c) B20, (d) B50 and (e) B100. The average wear scar diameter and surface roughness were shown in Table 2.2. The results showed that WSD increased when the concentration of biodiesel was increased but the surface roughness were not significantly changed. It might be expected that Fuel contamination may decreases the viscosity of the engine oil that resulting in reducing oil film thickness, Moreover, it might decreases the strength of anti-wear additives that make higher wear on metal surface.

After Four-ball tests, the Four-ball tested oils were measured the particle size distribution by using laser particle size analyzer. The particles sizes were in the range of 0- 125 μm. The size distributions occur as bimodal distribution. The first and the second fraction were in the range of 0-15 μm and 15-125 μm, respectively. The results showed that the EB7 and EB20 consist mostly of the small particles. However, the NE, EB50 and EB100 consist mostly of the large particles.

Table 2. 2 WSD and Roughness of each sample.

Samples	**Wear Scar Diameter (Micron)**	**Roughness (Micron)**
Lubricating oil without biodiesel	533	1.32
Lubricating oil with B7	588	1.18
Lubricating oil with B20	569	1.17
Lubricating oil with B50	604	1.21
Lubricating oil with B100	615	1.68

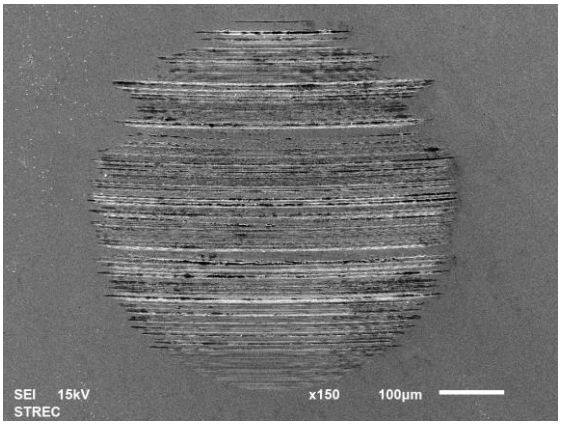

(a) The engine oil without fuel

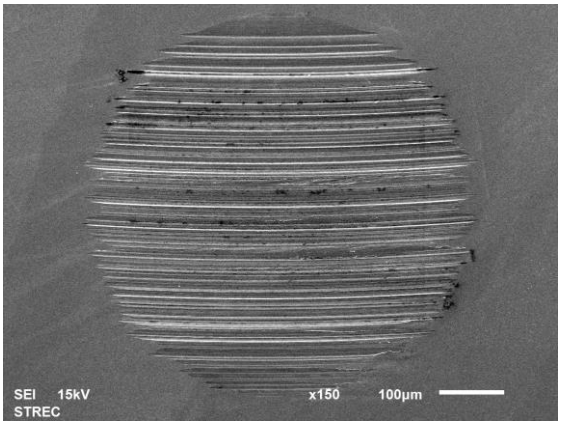

(b) The engine oil containing B5-7.

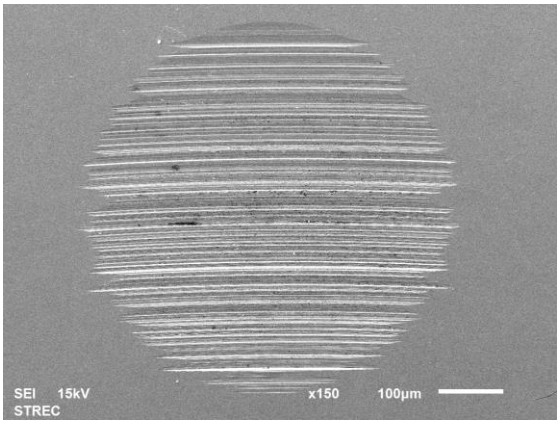

(c) The engine oil containing B20.

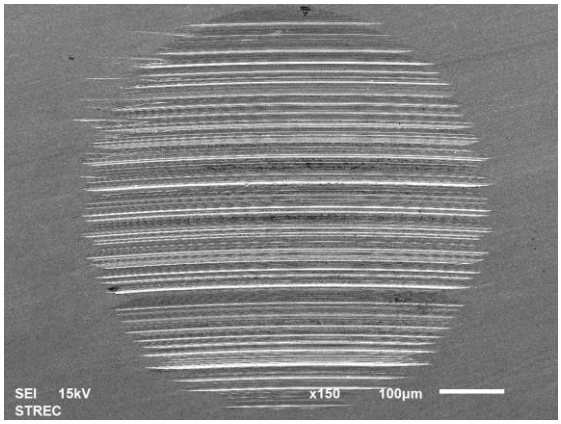

(d) The engine oil containing B50.

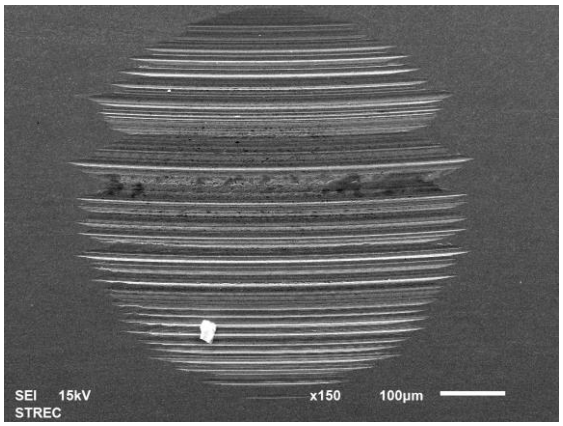

(e) The engine oil containing B100.

Figure 2. 39 SEM micrographs of the ball from (a) engine oil without fuel and engine oil with 2% by weight of (b) commercial diesel, (c) B20, (d) B50, and (e) B100 [17].

2.8.1 The effect of biodiesel contamination on metallic wear

Rounds et al [18] performed tests on a four-ball wear testing machine with soot contaminated oils. The test conditions were 15 kg of loads, 93 degree Celsius of oil temperature, 1,500 rpm of testing speed and 30 minutes of test. The balls were 12.7 mm CVD 5210 steel. The effect of diesel soot contamination on wear was evaluated by using the used engine oil from the diesel engine (1-2 %) and the engine oil with added soot (3-5 %). It was shown in Figure 2.40 (a). As can be seen, wear increased with increasing soot concentration until the wear car reached the range of base oil alone, and at the higher soot loading no further increase in wear occurred. These results indicated that at soot concentration above 3.5 percent the antiwar performance of the ZDP in engine oil was completely destroyed by the presented of soot.

The carbon black N 990 was mixed with oil to see if CB was the important constituent in diesel soot causing high wear. Figure 2.40 (b) shows the antiwar performance of ZDP when added to the vase oil alone, the base oil plus ashless succinimide dispersant or the base oil plus dispersant and carbon black. Adding the ZDP to the base oil alone gave the expected decrees in wear with increasing ZDP concentration. The ashless dispersant gave some antiwear benefit by itself, but the dispersant interacted strongly with the ZDP. When 5 percent carbon black was present in the dispersant blend, adding ZDP had no effect until the ZDP concentration exceeded 0.45 percent Zn, well above a typical ZDP concentration. These results demonstrated that carbon black can have a large adverse effect on ZDP antiwear performance and suggested that the effect of diesel soot on wear is primarily a result of its carbon content.

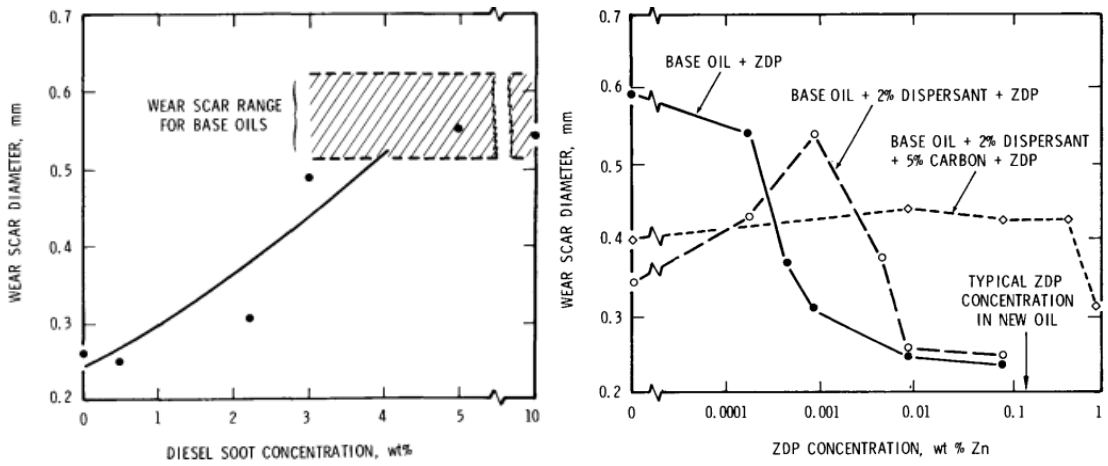

(a) diesel soot contamination (b) CB N990 contamination

Figure 2. 40 Effect of (a) diesel soot and (b) Carbon contamination on wear using Four-ball wear tester [18].

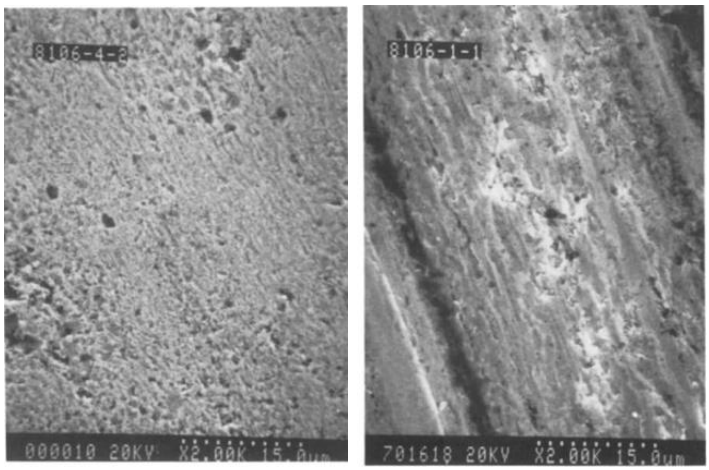

(a) oil alone (b) oil with Cab-O-Si

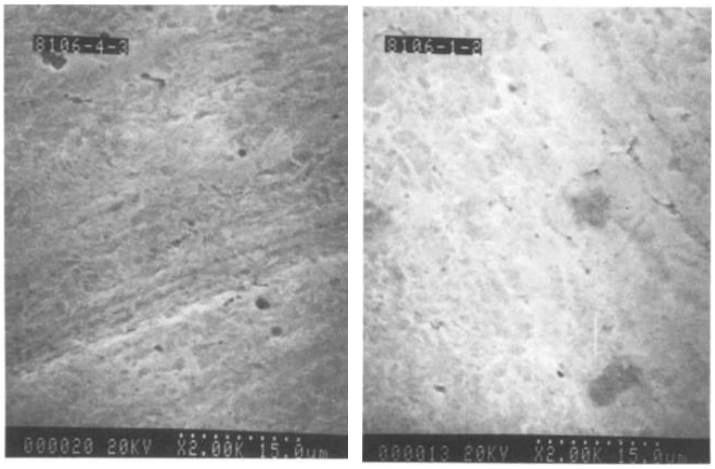

(b) oil with Alon C (d) oil with Carbon black

Figure 2. 41 SEM micrographs of the ball surface in the oil (a) alone and oil containing (b) Cab-O-Si, (c) Alon C and (d) Carbon black [19]

Ryason et al [19] performed wear tests on a ball-on flat- disk tribometer using carbon black and steel balls made of AISI 52100 steel. Wear tests were performed on carbon black, alumina and silica. Investigations were carried out on the wear scars from the tests using scanning electron microscope (SEM) and electron probe microanalysis as shown in Figure 2.41. The SEM pictures showed that the scars on the surfaces of the balls worn in the presence of oils containing carbon black, alumina and silica were similar, and differ from that of the ball worn in the presence of oil alone. Ryason concluded that the wear that occurred was polishing in nature. He also suggested that although the wear was abrasive in nature, the cutting of the material did not take place. The soot particles ploughed through the surface, forming a groove with a smooth curved cross-section, depressed at the center and raised at the edges.

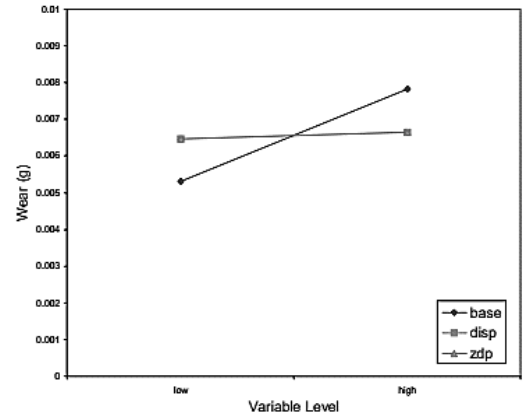

(a) Oil without soot

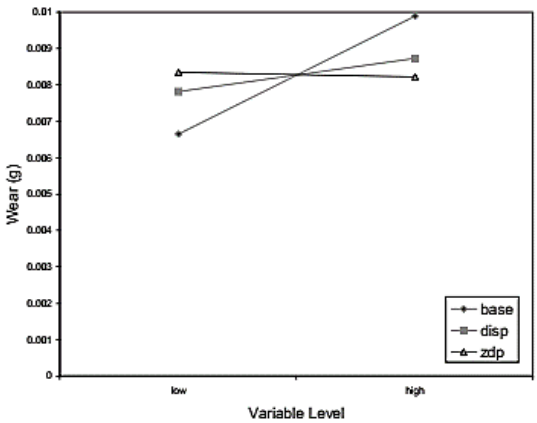

(b) Oil with soot

Figure 2. 42 Oil Wear Performance of the (a) engine oil alone and (b) oil with soot [20].

Gautam et al [20] investigated the effects of soot contaminated engine oil on three-body wear. Phosphorous level, dispersant level and sulfonate substrate level were the three oil additives they tested and concluded that there is an interaction between oil additives and soot in reducing the oil's anti-wear properties. They also concluded that wear increases with higher soot concentration and decreases with higher phosphorous concentration. They also performed tests on the ball-on-flat-disk setup with soot and alumina and compared their wear ratios. It was concluded that abrasion could be the major mechanism involved in the diesel engine wear. They also investigated the effects of base stock, dispersant level, and ZDP level on three-body wear. The study considered soot at two levels and hence could not determine the non-linear effect of soot on three-body wear. Results indicated that the oil's anti-wear properties were reduced as a result of soot. The statistical analysis led to the conclusion that base stock and dispersant levels were significant on oil's wear.

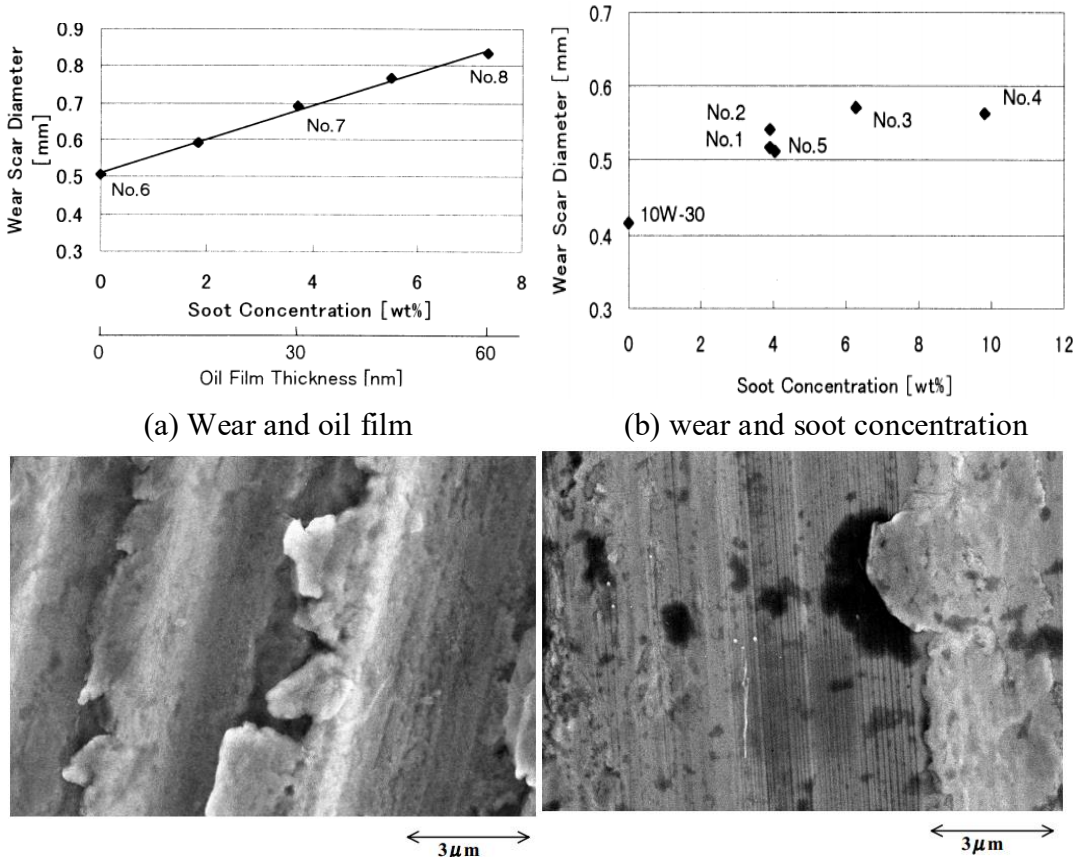

(a) Wear and oil film (b) wear and soot concentration

(c) Oil without soot (d) Used oil with soot 7.7%wt.

Figure 2. 43 Relation between (a) soot concentration and oil film thickness and (b) wear, SEM micrograph of the (c) engine oil alone and (d) used oil with soot [21].

Sato et al [21]. investigated the effects of soot concentration, and soot diameter and oil film thickness on metallic wear by using four-ball wear tester. Soot particle in the engine oil was observed by TEM, and the wear scar by SEM. It was found that particle diameter of primary soot was about 30nm, but these diameter wasn't very changed by the influence of burning method. Wear increases proportionally to the soot concentration when the characters of soot and fresh oil are same as shown in Figure 2.43 (a). Wear rate was rather small when oil film thickness was larger than particle diameter of primary soot, and accelerated when soot particle diameter was equivalent to oil film thickness as Figure 2.43 (b). In the latter case, the fine streaks are formed in the wear scar. It could be considered that those fine streaks are scraped by primary soot particles directly, and the abrasive wear is one of main factors on wear as shown in Figure 2.43(c-d).

.

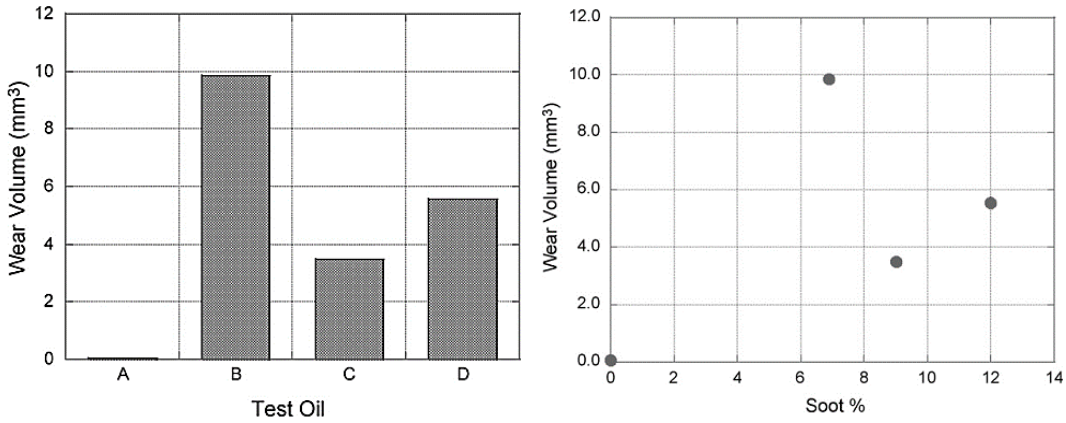

(a) Wear and oil film (b) wear and soot concentration

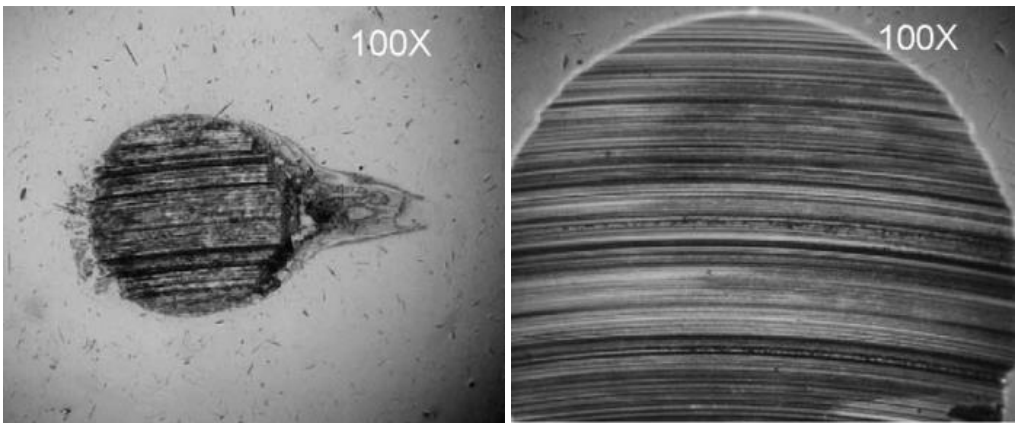

(c) Oil without soot (d) Used oil with soot 7.7%wt.

Figure 2. 44 Relation between soot concentration on wear and SEM micrograph [22].

Adajah et al [22] investigated the effects of soot concentration on metallic wear by using four-ball wear tester. Soot particle in the engine oil and the wear scar were examined by SEM. The variation of ball wear volume with the percent soot content in shown in Figure 2.45 (a-b) which include the result for fresh oil at 0% soot content. Although the number of data points is very limited, there appears to be no clear relationship between the soot content and ball wear in the present study. The wear scars on both the stationary ball and the rotating balls from the test with new oil A are shown in Figure 2.45(c). The scratches running the direction of sliding indicate that abrasive wear is the predominant wear mode. Figure 2.45(d) shows the wear track from tests with used oils B. Clearly, the wear scars are much larger, and the abrasive scratches are grooves and much larger. The predominant operating wear mode was abrasion, perhaps aided by corrosion. In the test using oil with the highest soot content (12%), wear also occurred by a scuffing mechanism in addition to the abrasive mechanism.

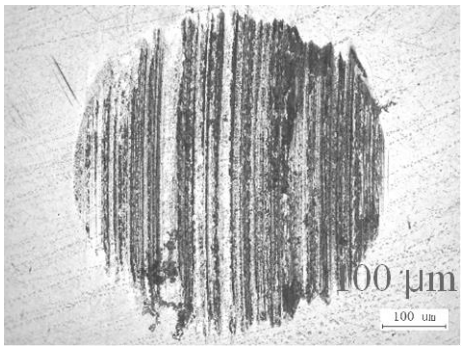

(a) Lube A without CB

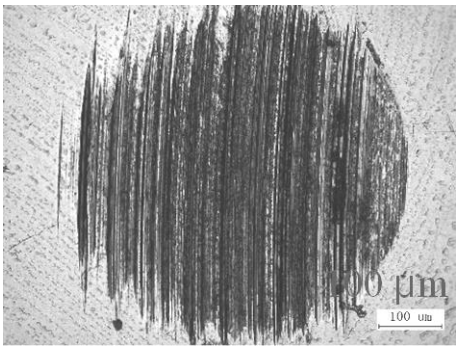

(b) Lube A with CB

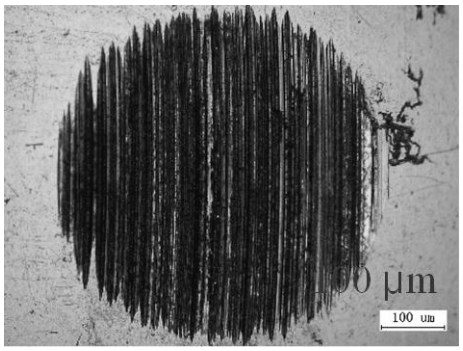

(c) Lube A without CB

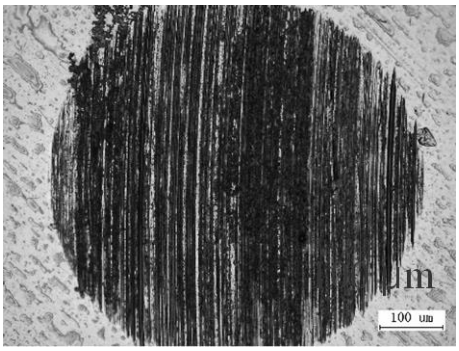

(d) Lube A with CB

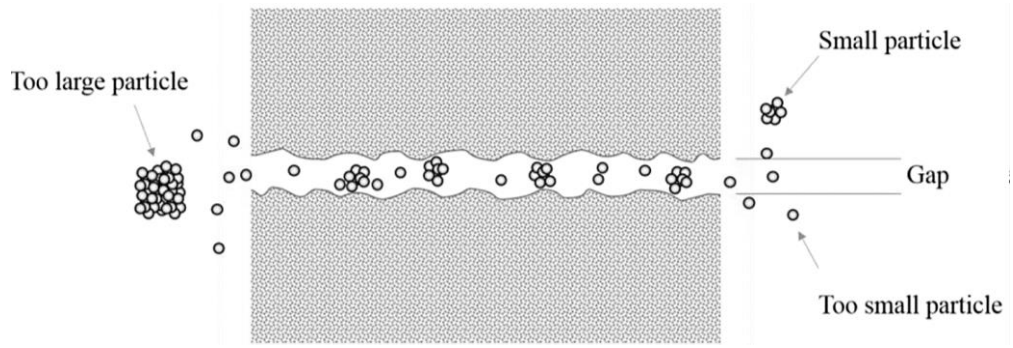

(e) Soot introduced wear model

Figure 2. 45 TEM micrographs of (a) diesel engine soot and (b) carbon black and comparison size distribution [16].

Supanamok et al [16] investigated the characteristics of soot in the internal combustion engine affecting on the abilities of lubricating oil and leading to result in engine components wear. The behavior was studied by means of a Four Ball tribology test with friction and wear measured and also investigate wear roughness in micro-scale by high resolution optical microscope and 3D rendering optical technique. Soot particle contamination was simulated using carbon black. Effects of oils with different additive on size distribution was studied by laser diffraction technique. Morphology and nanostructure of particles were studied by transmission electron microscope as shown in Figure 2.45. Moreover, physical and chemical properties of used oil were investigated and determined soot contamination.

The results showed that soot contaminated in engine used oil is about 1% by weight and it affected on changing oil's properties. Modern oil additives can control the agglomeration of soot very well by keep soot size in small diameter. Based on tribology test, soot contamination in oil made more wear on tested steel ball and reduced friction during test comparing to the test with fresh oil. In conclusion, the appropriate particle size, which is near to oil film thickness between metal surface contacts, is the dominant cause of making wear. By the way, the too large particle size compared to oil film thickness will escape out and too small particle size will not effect on wear. Furthermore, high level of proper particle size contaminated in oil will increase probability of rubbing process then make contact surface smoother or make lower in roughness.

After analyze all of the data, they may be explained that soot or carbon black which are mixed into tested lubricants, the too small particles may not affect to the metal surfaces. The too large particles may also escape out from scrubbing areas because they cannot enter to that clearance. They are limited by the gap length between two metal surfaces which defined by oil film thickness. There are just only the proper particle which near to film thickness can be introduced to the gap and scratch the metal surfaces and make them wear. This is demonstrated by a drawing in Figure 2.45.

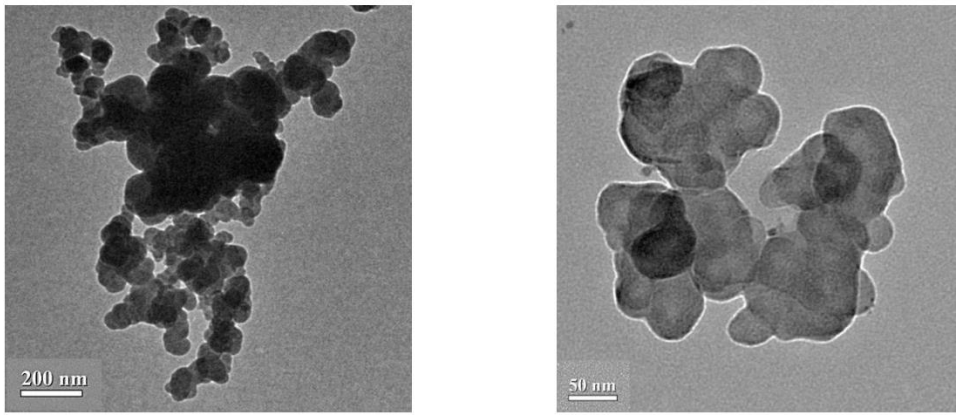

(a) Carbon Black Ultrafine Particle

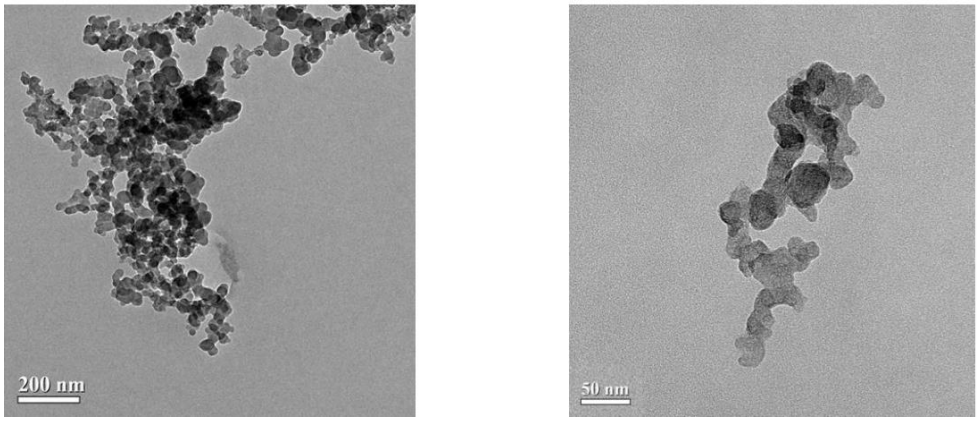

(b) Diesel Engine's Ultrafine Particle

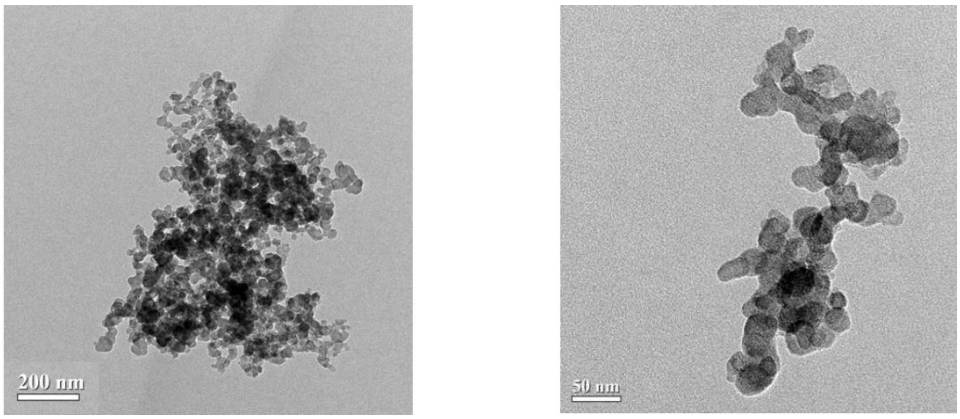

(c) Biodiesel Engine's Ultrafine Particle

Figure 2. 46 TEM images of (a) carbon black, (b) diesel engine's ultrafine particles and (c) biodiesel engine's ultrafine particles in the operation condition 80% of engine load and 2400 rpm of engine speed [27]

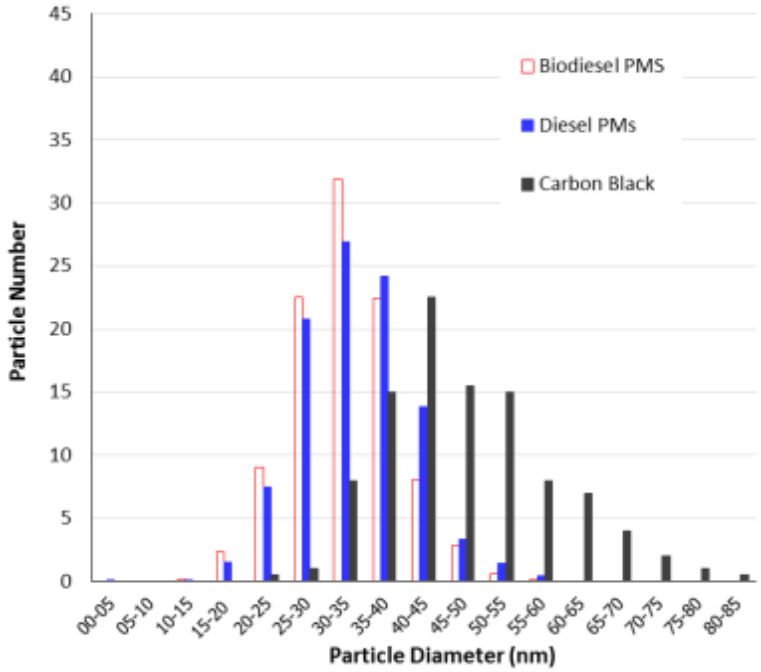

Figure 2. 47 Size distribution of carbon black versus average particle size distribution of diesel engine's nanoparticles and biodiesel engine's nanoparticles under 20, 40, 60 and 80% of engine load and 1600, 2000 and 2400 rpm of engine speed using TEM image processing method. [27]

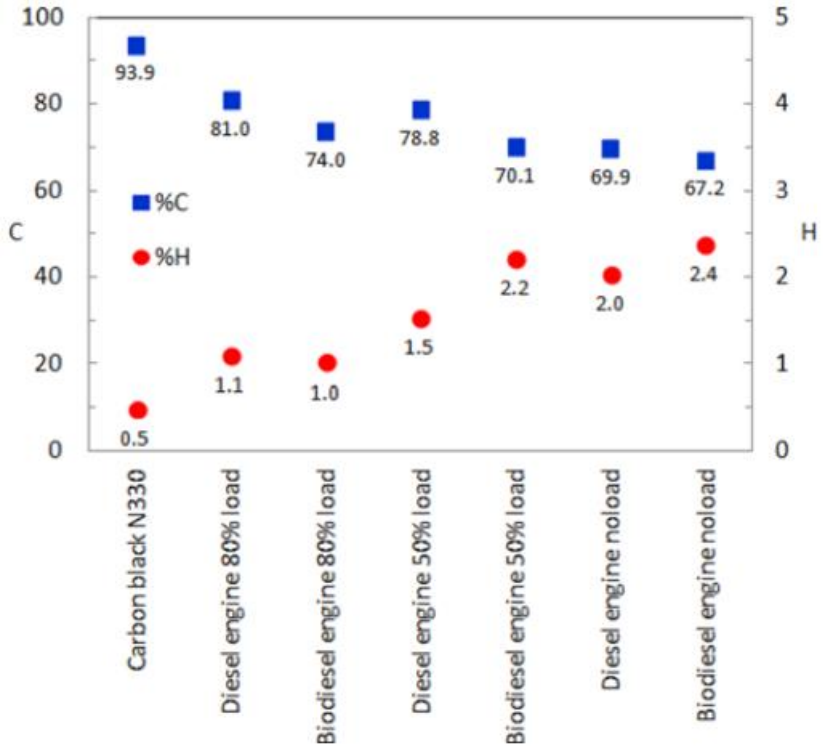

Figure 2. 48 Chemical consistent of diesel and biodiesel PMs using CHN analyzer. [28]

Karin et al [27-28] investigated the impact of biodiesel fuel on morphology and oxidation kinetics of engine's PMs on conventional DPF powders by using TEM and TGA, respectively. PM size distribution and oxidation apparent activation energies would be calculated by using TEM image processing method and Arrhenius plots of PM oxidation kinetics for better understanding and future design of DPF configuration for biodiesel blends diesel engine application.

Figure 2.46 show TEM images of biodiesel and diesel engine's ultrafine PMs under the condition 80% of engine load, 2400 rpm of engine speed and carbon black ultrafine particles. The average agglomerated ultrafine particle's diameter of carbon black is significant larger than that of diesel and biodiesel engine PMs. Primary nanoparticles of both diesel and biodiesel engine's PMs were measured using image processing method The primary nanoparticle diameters are in the range of 10-60 nm. It was clearly observed much amount of particle diameters are in the range of 30-40 nm. The average diameter of primary nanoparticles emitted from engine all operation conditions and carbon black are in the range of 10-60 nm and 20-90 nm, respectively, as shown in Figure 2.47. The average single particle sizes of carbon black, diesel and biodiesel engine's PMs are approximately 48, 34 and 32 nm, respectively.

The estimated carbon and hydrocarbon content inside PMs are agree with the results of CHN analysis, as shown in Figure 2.48. Carbon fraction inside carbon black is higher than that of diesel and biodiesel engine PMs, respectively due to unburned oxygenated hydrocarbon of biodiesel PMs. It was clearly observed that carbon fraction inside low load engine PMs are lower that of high load engine operation condition due to unburned fuels.

CHAPTER 3
RESEARCH METHODOLOGY

3.1 Experimental equipment

3.1.1 Formulated SAE 0W30 engine oil

A formulated engine oil which had the same grade as SAE0W30 was used in this research. The engine oil condition including viscosity, oxidation, nitration and total base number were measured according to ASTM standard test methods. Oil additives were measured by x-ray fluorescence. The standard for testing the new engine oil are following:

- Kinematic viscosity @ 40ºC (ASTM D-445)
- Kinematic viscosity @ 100ºC (ASTM D-445)
- Oxidation (ASTM E-2412M)
- Nitration (ASTM E-2412M)
- Total base number (ASTM D-4739)

3.1.2 Carbon black [23]

Carbon black is a synthesis soot which has similar particle size and physical properties to engine soot. In this study, a commercial carbon black was used as soot representative. In order to investigate the effect of soot Nano particle size on metallic wear, the commercial carbon black which have different primary particle sizes were used. They were Commercial carbon black N220, N330 N550 and N660.

Figure 3. 1 carbon black N330 [23]

3.1.3 Transmission Electron Microscope

Transmission Electron Microscope (TEM) was employed to investigate morphology and nanostructure parameters of carbon black primary particles. The main target is to define the average carbon black primary particles size and primary particle size distribution. The TEM machine (JEOL JEM-2010) which used in this study is shown in Figure 3.2.

Figure 3. 2 Transmission electron microscope (JEOL JEM-2010)

3.1.4 Laser Diffraction Spectroscopy

Laser diffraction Spectroscopy was used to measure particle size distribution in liquid which could range a particle size from hundreds of nanometers up to several millimeters. In this study, the different types of carbon black size distribution before wear test and wear particle size distribution after ball wear were both measured by this technique. The TEM machine (JEOL JEM-2010) which used in this study is shown in Figure 3.3.

Figure 3. 3 MALVERN Laser Diffraction Spectroscopy.

3.1.5 Four ball wear tester [24]

The four-ball wear tester is well-known a tribology test bench. This test method can be used to determine the relative wear preventive properties of lubricating fluid in sliding contact under the prescribed test conditions. The test methods and conditions followed the standard test ASTM D4172 as shown in Figre3.4. The machine consists of four chrome alloy steel, made from AISI standard steel No. E-52100, with diameter of 12.7 mm (0.5 in.) Grade 25 EP (Extra Polish) 12.7 mm. The three lower balls were held in a steel cup with fixed position and the top ball was pressed with 300 N of force. The operating temperature was regulated at 75 °C and the top ball was rotating at 1,200 rpm for 60 min. Circular wear scars will appear on the three lower balls, while a circular wear track will appear on the upper ball. The more details of test conditions are also shown in Table 3.1.

Figure 3. 4 Schematic of Four-ball wear tester followed ASTM - D4172.

Table 3. 1 ASTM D-4172 conditions tests [24]

Test conditions		**Ball material**	
Parameter	**Specification**	**Parameter**	**Specification**
Rotational speed	1200 rpm	Ball material grade	25 EP
Load	392 N	Surface roughness	0.005 microns
Duration per load	60 min	Ball hardness	64 – 66 (HRC)
Temperature	75°C	(Rock well)	

3.1.6 Optical Microscope

Optical Microscope (OM) was used to measure the wear scar diameter of the three lower balls after four ball wear test. The average wear scar diameter was the average value which was used to compare the scar diameter of each oil samples. Moreover, the surface roughness of three lower balls were also measured using 3D rendering system and it were reported as average roughness. This test will help us to know more details in wear mechanism.

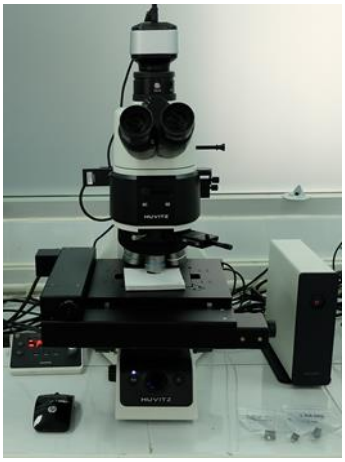

Figure 3. 5 Optical microscopy.

3.1.7 Scanning Electron Microscope

Scanning Electron Microscope and Energy Dispersive X-Ray Spectrometer (SEM-EDS) is a powerful tool for studying worn surface and wear elements analysis. The SEM permits the observation of materials in macro ranges. When used with EDS, the analyst can perform an elemental analysis on microscopic sections of the material or contaminants that may be present. The SEM-EDS machine (JSM-6610LV and X-MaxN 50) which used in this study is shown in Figure 3.6.

Figure 3. 6 Schematics of SEM-EDS (JSM-6610LV and X-MaxN 50).

3.2 Experimental procedure.

3.2.1 The study of commercial carbon blacks morphology

Transmission Electron Microscope (TEM) was used to investigate the physical properties and nanostructure parameters of different types of commercial carbon black. The main target is to define the average carbon black's primary particles size and primary particle's size distribution. The commercial carbon black which including N220, N330, N550 and N660 were used. The CB sample was prepared by following method. The CB powder was isolated by using ultracentrifugation with heptane as the diluent and it was adhered to TEM grid. Then, the CB which was adhered on the grid was observed in Nano - scale by using TEM. After that, the TEM micrographs of CB was used to determine the primary particle size distribution by using measurement program (Image J). The area of primary particle were measured by using an elliptical shape selection and convert that area to diameter as shown in **Figure 3.7.** The results showed a comparison of primary particle size distribution of each tpyes of comercial carbonblack.

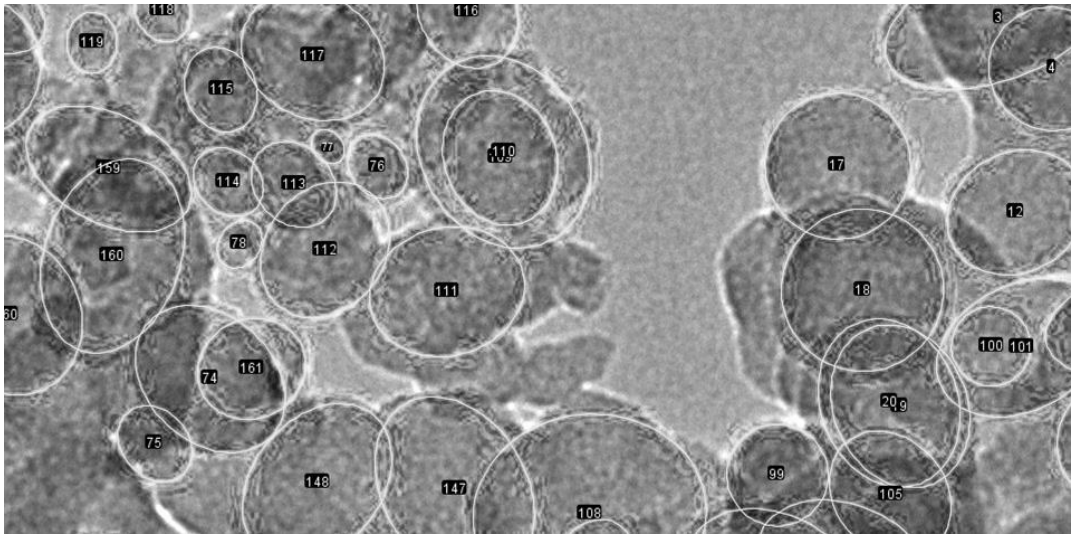

Figure 3. 7 The measurement of carbon black primary particle.

3.2.2 The Impact of Biodiesel and Soot Contamination on Metallic Wear

The wear preventative properties of the engine oil and engine oil with contamination was investigated using four ball wear tester. The test methods and conditions followed the standard ASTM D4172 as shown in Table 3.1. The major conditions for this wear test was to investigate The impact soot Nano particle sizes on metallic wear. The different types of carbon blacks (CB) were mixed with the engine oil at 1% by weight per volume. The types of commercial Carbon black N220, N330, N550 and N.660 The details of oil samples and CB average particle size were shown in Table 3.2. After the four ball wear tests, the balls and the tested oil were collected for the additional tests as follows:

1) The ball worn surface analysis.

1.1) Wear scar diameter measurement by Optical microscopy.

1.1.1) The ball wear scar diameter of the three lower ball and one upper ball were measured using OM as shown in Figure 3.7. After that, the average wear scar diameter of the three lower balls is used to compare the effect of contaminant on metallic wear.

1.1.2) The ball surface roughness of the three lower ball and one upper ball were also measured using 3D rendering system of the OM as shown in Figure 3.5 above. After that, the average surface roughness of the three lower balls is used to compare the effect of contaminant on metallic wear.1.2) Microscopic surface analysis by using Scanning electron microscopy. The microscopic worn surface of the four balls of each oil samples were investigated using SEM. SEM is a powerful tool for studying worn surface and wear elements analysis.

Particle size distribution laser diffraction spectroscopy.

The particle size distribution before and after four ball wear test were measured by using laser diffraction spectroscopy. The different type of commercial carbon black (CB) particle size distribution in the formulated SAE0W30 engine oil were also measured. The oil samples before wear test are follows:

- New SAE0W30 engine oil.
- New SAE0W30 engine oil + 1 %wt. CB N220.
- New SAE0W30 engine oil + 1 %wt. CB N330.
- New SAE0W30 engine oil + 1 %wt. CB550.

- New SAE0W30 engine oil + 1 %wt. CB N6600.

Moreover, the tested oil of SAE0W30 containing with different types of CB after wear tests were also measured as follows:

- New SAE0W30 engine oil + wear metal.
- New SAE0W30 engine oil + 1 %wt. CB N220 + wear metal.
- New SAE0W30 engine oil + 1 %wt. CB N330 + wear metal.
- New SAE0W30 engine oil + 1 %wt. CB550 + wear metal.
- New SAE0W30 engine oil + 1 %wt. CB N6600 + wear metal.

Table 3. 2 Engine oils mixed with carbon black.

Samples	Carbon Black	Average Primary Particle size according to standard (nm)	% CB (wt. / vol.)
NE	-	-	-
EC2	N220	21	1 %
EC3	N330	31	1 %
EC5	N550	53	1 %
EC6	N660	63	1 %

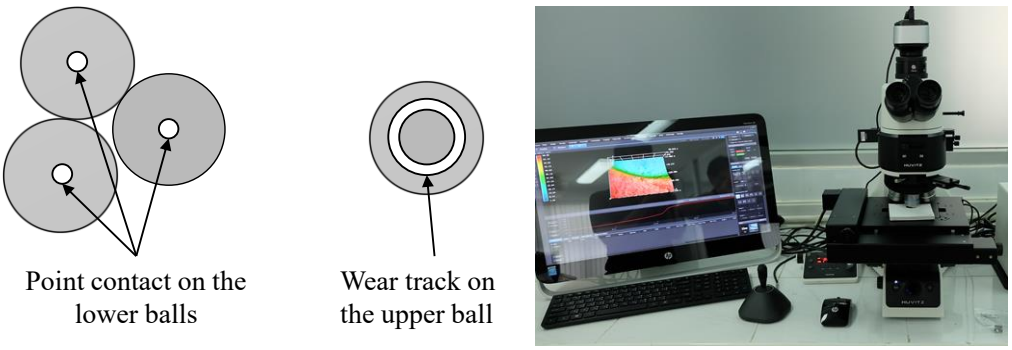

(a) Point contacts and circular wear (b) WSD and roughness measurement

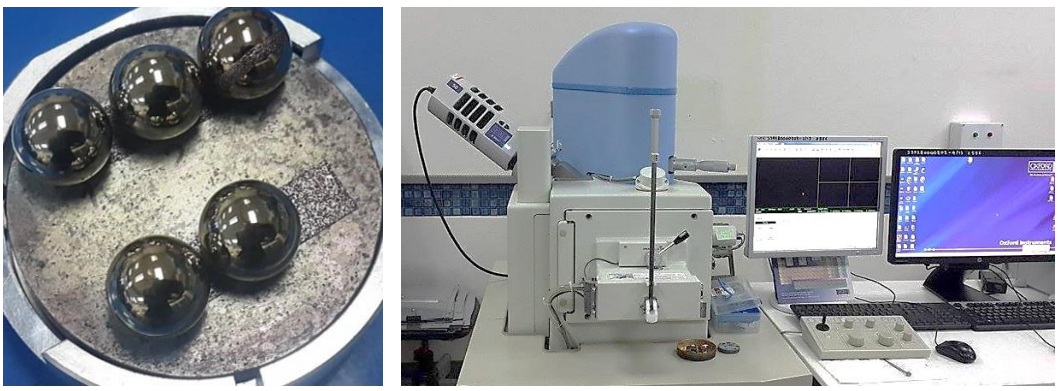

(c) Tested ball coated with gold (d) microscopic analysis by SEM

Figure 3. 8 WSD measurement and microscopic analysis of the tested balls

CHAPTER 4
RESULTS AND DISCUSSION

A formulated engine oil which had the same grade as SAE0W30 was used in this research. The engine oil condition including viscosity, oxidation, nitration and total base number (TBN) were measured according to ASTM standard test methods. Oil additives were measured by x-ray fluorescence. Additives used to formulate lubricants contain elements that are used to impart special properties. The oil conditions and additives are shown in Table 4.1. The sources of each element can be classified as following:

Sulphur (S) is a natural constituent of base oil, so it appears in almost all oil samples. It is also found in many additives, including anti-wear, antioxidant, extreme pressure, corrosion inhibitor and metal deactivator additives.

Calcium (Ca) is often found in conjunction with magnesium and forms the detergent and corrosion inhibitor part of the additive package.

Zinc (Zn) is found in chemicals used to make anti-wear, anti-oxidant, detergent and corrosion inhibitor additives.

Phosphorus (P) is a non-metal and is found in many additives. These include: anti-wear, anti-oxidant, extreme pressure, corrosion inhibitor, friction modifiers, metal deactivator, and biocide chemicals.

Magnesium (Mg) is used in the formulation of detergents and corrosion inhibitors.

Molybdenum (Mo) is seen as an additive in engine oils as part of the antioxidant package.

Table 4. 1 Properties of SAE0W30 engine oil

Oil conditions			**Oil additives**		
Kinematic Viscosity @ 40 °C	cSt	44.5	S	%	214.0
Kinematic Viscosity @ 100 °C	cSt	9.6	Ca	%	166.0
Oxidation	Abs	18.1	Zn	ppm	847.0
Nitration	Abs	6.1	P	ppm	779.0
TBN	mg KOH/g	5.6	Mo	ppm	454.0

4.1 Commercial carbon blacks primary particle size distribution

Figures 4.1 shows TEM micrographs of Commercial Carbon Black (a) N220, (b) N330, (c) N550 and (d) N660. The samples were prepared by using the ethanol solvent extraction technique and were put on the copper grid plates. These images of primary particle are quite difficult to measure the primary size of single particle because they are stacking together, so we cannot determine diameter of all particulates. The idea is just only measuring some of them that clearly appear. After that, the TEM micrographs of CB was used to determine the primary particle size distribution by using measurement program. The area of primary particle were measured by using an elliptical shape selection and convert that area to diameter. It might be the fallibility from the uncertainly of measurement technique such as the unclear image from TEM and the accuracy of measurement technique. These reasons cause to not too much different on size distribution of the diesel and biodiesel primary particulate matter.

Finally, more than 600 particles of each CB samples were investigated. Figure 4.2 shows Carbon Black's primary nanoparticle size distribution. The primary nanoparticle diameters were in the range of 5-90 nm. It was clearly observed much amount of particle diameters were in the range of 20-65 nm. The average primary nanoparticles of CB N660 was significant larger than that of N220.

The statistical data has been concluded in Table 4.2. It shows that the average primary particle size of CB N660 was largest and the average primary particle of CB N220 was smallest. The average primary particle size of CB N220, N330, N550 and N660 were 28.1, 30.5, 40.3 and 49.8 nm, respectively.

Table 4. 2 Statistical data of Commercial Carbon Black

Statistical Data	Carbon Black			
	N220	N330	N550	N660
Particle Count	1204	1070	784	625
Maximum (nm)	76.5	70.7	107.6	102.9
Minimum (nm)	6.4	7.9	11.7	15.9
Average (nm)	28.1	30.5	40.3	49.8
SD	10.0	9.2	12.6	15.7

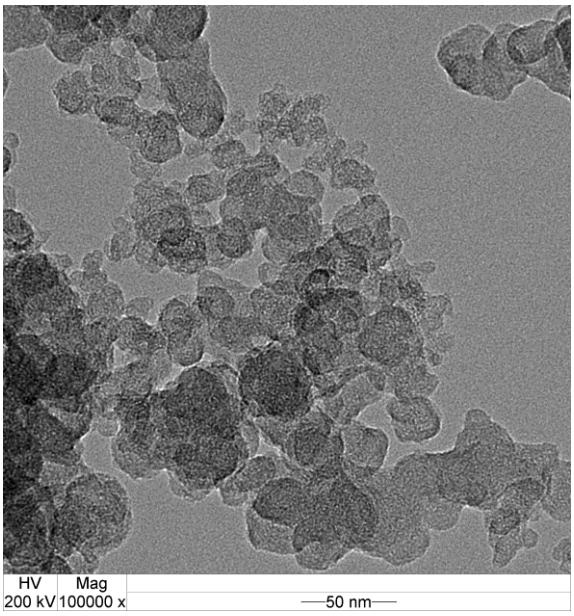

(a) Carbon black N220.

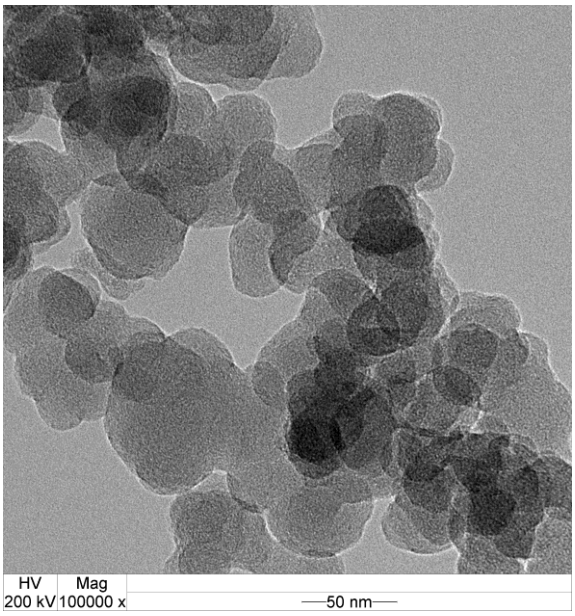

(b) Carbon black N330.

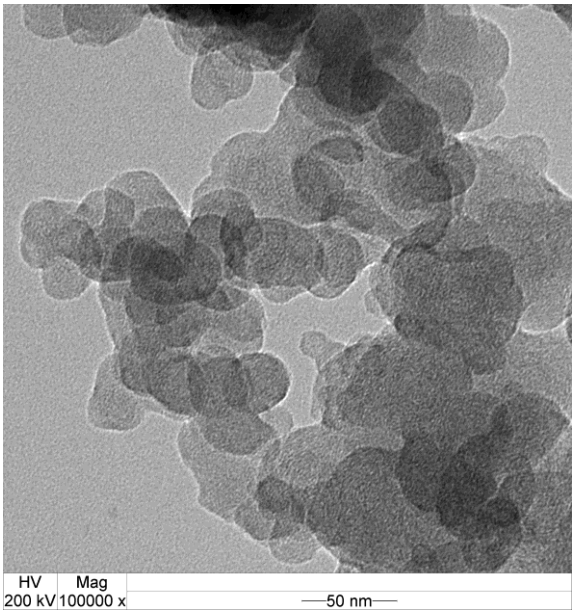

(c) Carbon black N550.

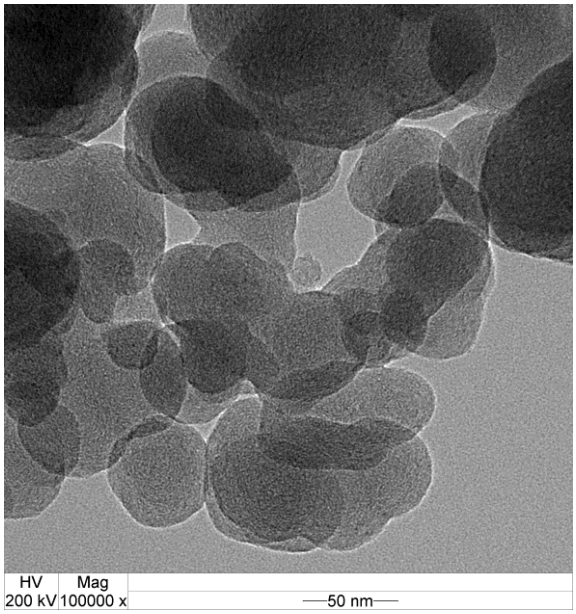

(d) Carbon black N660.

Figure 4. 1 TEM micrographs of commercial carbon black.

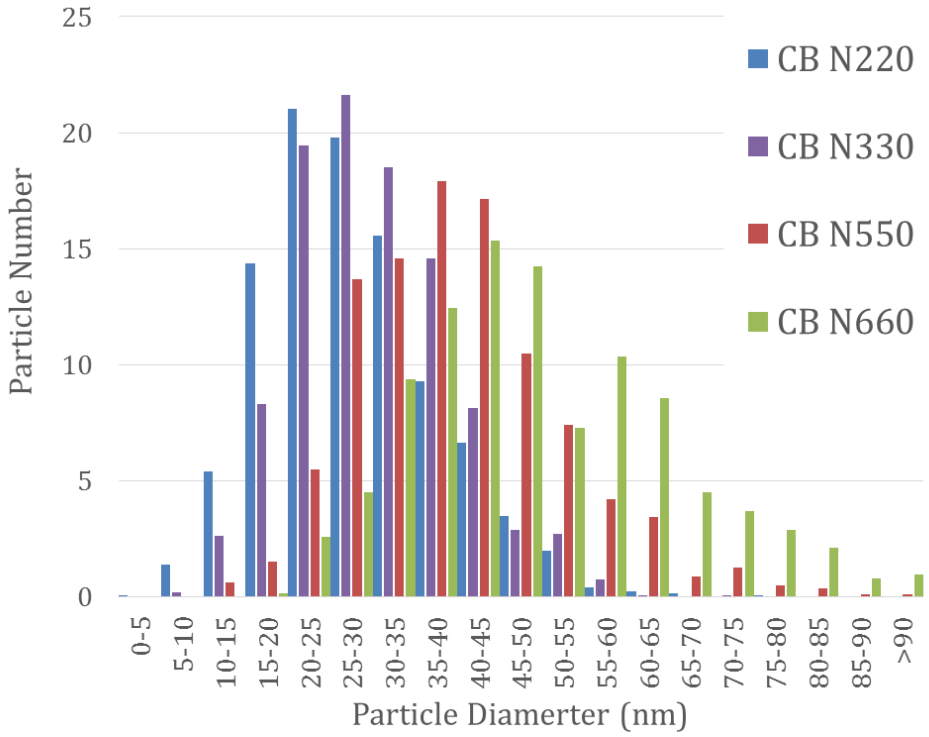

Figure 4. 2 Size distribution of commercial carbon black Nano particles

4.2 Carbon black particle distributing in engine oil

Figure 4.3.a shows size distribution of different types of carbon black mixing in the engine oil which measured before Four-ball wear test. There were CB N220, N330, N550 and N660, respectively. The results showed that the different types of soot dispersing in the engine oil were not significantly different. There were in the range of 0.01 – 300 microns, which were small particle that have size of 10 - 100 nm. The first and second groups of agglomerate were in the range of 0.1 - 2 micron and 2 – 300 micron, respectively. D. B. Kittelson [13] proposed that the soot particle from a few nanometer to 50 nm were in the nucleation mode and the larger particle which in the range of 0.01 – 0.3 microns were in agglomeration mode. The particles in the coarse mode which consists of the nucleation and accumulation mode were larger than 1 microns.

Figure 4.3.b shows cumulative size distribution of different types of carbon black mixing in the engine oil which measured before Four-ball wear test. There were CB N220, N330, N550 and N660, respectively. The particle in the range of 0.01 – 0.1 microns of the engine oil containing CB N220, N330, N550 and N660 were at 8.17 %, 17.85 %, 22.69% and 20.67 % cumulative, respectively.

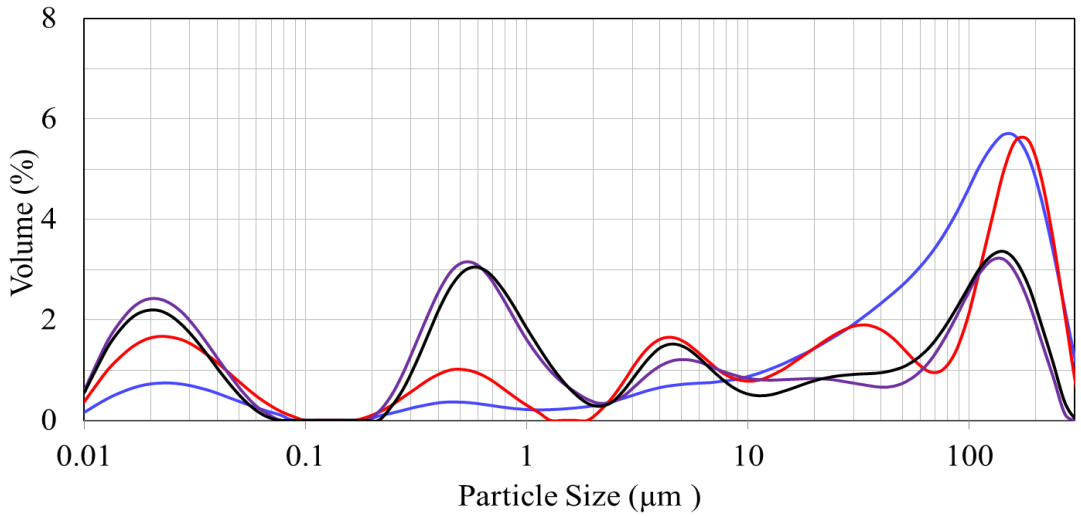

(a) Particle size distribution

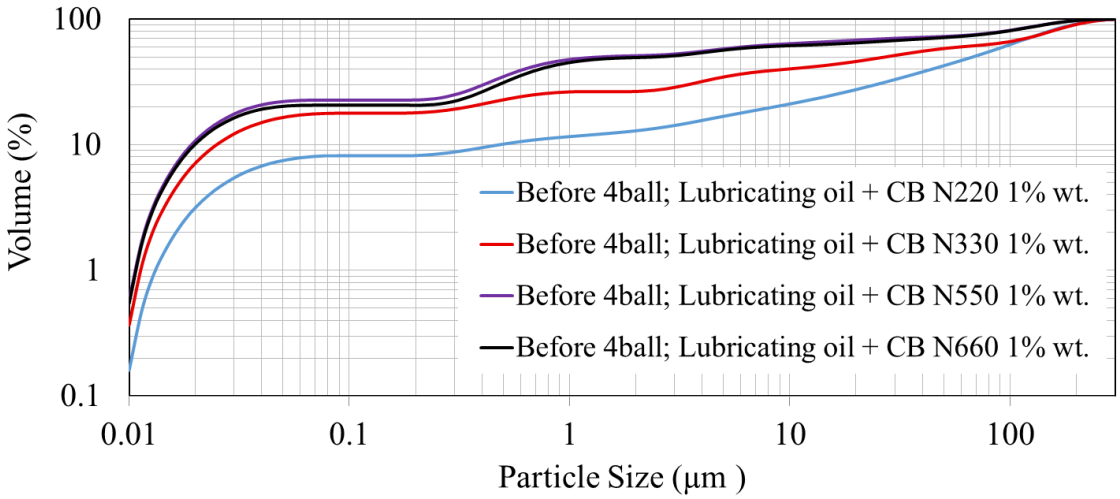

(b) Particle cumulative volume

Figure 4. 3 Carbon black (a) size distribution and (b) cumulative volume in lubricating oil before Four-ball wear test using Laser Particle Diffraction Spectroscopy.

The particle in the range of 0.01 – 1 microns of the engine oil containing CB N220, N330, N550 and N660 were at 11.61 %, 26.37 %, 47.72% and 45.12 % cumulative, respectively. Moreover, the particle in the range of 0.01 – 10 microns of the engine oil containing CB N220, N330, N550 and N660 were at 21.05 %, 40.13 %, 63.80% and 61.52 % cumulative, respectively.

It shows that engine oil with CB N550 contain the higher amount of a small particle which was lower than 0.1 microns at about 22.69 % cumulative. On the other hand, the oil with CB N220 contain the lowest amount of a small particle which was about 8.17 % cumulative.

4.3 Film thickness calculation using EHL

In this topic, the fundamental mechanisms of film generation in elastohydrodynamic contacts, together with the methods for calculating the minimum film thickness between spherical balls.

$$\frac{1}{R'} = \frac{1}{R_x} + \frac{1}{R_y} = \frac{1}{R_{ax}} + \frac{1}{R_{ay}} + \frac{1}{R_{bx}} + \frac{1}{R_{by}} \tag{2.5}$$

Where:

$$\frac{1}{R_x} = \frac{1}{R_{ax}} + \frac{1}{R_{ay}}$$

$$\frac{1}{R_y} = \frac{1}{R_{bx}} + \frac{1}{R_{by}}$$

R_x is the reduced radius of curvature in the x direction [m].
R_y is the reduced radius of curvature in the y direction [m].
R_{ax} is the reduced radius of curvature of body A in the x direction [m].
R_{ay} is the reduced radius of curvature of body A in the y direction [m].
R_{bx} is the reduced radius of curvature of body B in the x direction [m].
R_{by} is the reduced radius of curvature of body B in the y direction [m].

The reduced Young's modulus is defined as:

$$\frac{1}{E'} = \frac{1}{2}\left[\frac{1-\vartheta_A{}^2}{E_A} + \frac{1-\vartheta_B{}^2}{E_B}\right] \tag{2.6}$$

Where ϑ_A and ϑ_B are the Poisson's rations of the contacting bodies A and B.
E_A and E_B are the Young's moduli of the contacting bodies A and B.
It can be noted that for the spheres: $R_{ax} = R_{ay} = R_A$ and $R_{bx} = R_{by} = R_B$

Where R_A and R_b are the radii of the spheres A and B, respectively. Substituting into equation (2.6) gives:

$$\frac{1}{R'} = \frac{1}{R_x} + \frac{1}{R_y} = \frac{1}{R_A} + \frac{1}{R_B} + \frac{1}{R_A} + \frac{1}{R_B} = 2\left(\frac{1}{R_A} + \frac{1}{R_B}\right) \tag{2.7}$$

Where $\frac{1}{R_x} = \frac{1}{R_y} = \frac{1}{R_A} + \frac{1}{R_B}$

According to the Four-ball wear test. The radii of the balls are $R_A = R_B = 6.35 \times 10^{-3}$ [m]. The Young's modulus for both balls is E = 2.1×10^{11} [Pa] and the Poisson's ratio of steel is ϑ = 0.3.

Reduced Radius of Curvature

Since $R_{AX} = R_{AY} = R_{BX} = R_{BY} = = 6.35 \times 10^{-3}$ [$\boldsymbol{m}$]. The reduced radii of curvature in the 'x' and 'y' directions are:

$$\frac{1}{R'} = 2\left(\frac{1}{R_A} + \frac{1}{R_B}\right) = 2 \text{ x } (0.157 + 0.157)$$

$$R' = 1.59 \text{ x } 10^{-3} \text{ [m]}$$

Reduced Young's Modulus

$$\frac{1}{E'} = \frac{1}{2}\left[\frac{1-{\vartheta_A}^2}{E_A} + \frac{1-{\vartheta_B}^2}{E_B}\right] = \frac{1}{2}\left[\frac{1-0.3^2}{2.1\ x\ 10^{11}} + \frac{1-0.3^2}{2.1\ x\ 10^{11}}\right]$$

$$E' = 2.3\ x10^{11} \text{ [Pa]}$$

The objective of using lubricating oil is to get advantage from ability of film layer forming by lubricant, whereas film thickness is depended on viscosity at operating temperature. Then the viscosity of SAE 0W 30 was used to estimate oil film thickness. Central and minimum film thickness were calculated according to the following equation (2.1, 2.2):

Elastohydrodynamic lubrication (EHL) is a mode of fluid-film lubrication in which hydrodynamic action is significantly enhanced by surface elastic deformation and lubricant viscosity increases due to high pressure. EHL conditions are typically obtained in nonconformal contacts such as ball on cylinder (elliptical contact), ball on ball (circular contact), and cylinder on cylinder (line contact).

Surfaces are deformed when two nonconformal bodies are brought in contact. A flat narrow contact zone is formed and contact width and pressure can be predicted by using the Hertz contact theory. At maximum Hertz pressure, the lubricant under goes a

phase transition into a solid glassy state. From this point, the lubricant no longer behaves as a Newtonian fluid, and it can be considered as a pseudo-fluid. Figure 4.4 shows the lubricant which is entrained into the contact zone and formed the thickness profile. The flow profile has two components, Couette flow (surface driven flow) and Poiseuille flow (pressure driven flow). Due to continuity requirements, the total flow must be the same at all three positions as shown in Figure 4.4. In the center of the contact, an oil is relatively incompressible and density of the lubricant does not vary more than a few percent and then the oil film thickness should be constant (hc). Further to the right, just before the outlet of the contact, there is a sudden decrease of the film thickness. This is the position where h min occurs. This flow constriction occurs in order to maintain continuity of flow. The Poiseuille flow is significantly larger near the inlet and outlet due to the high pressure gradients. In the inlet it will counteract the Couette flow, while it will be in the same direction as the Couette flow in the outlet, and the gap must therefore be closed to balance flow into and out from the contact.

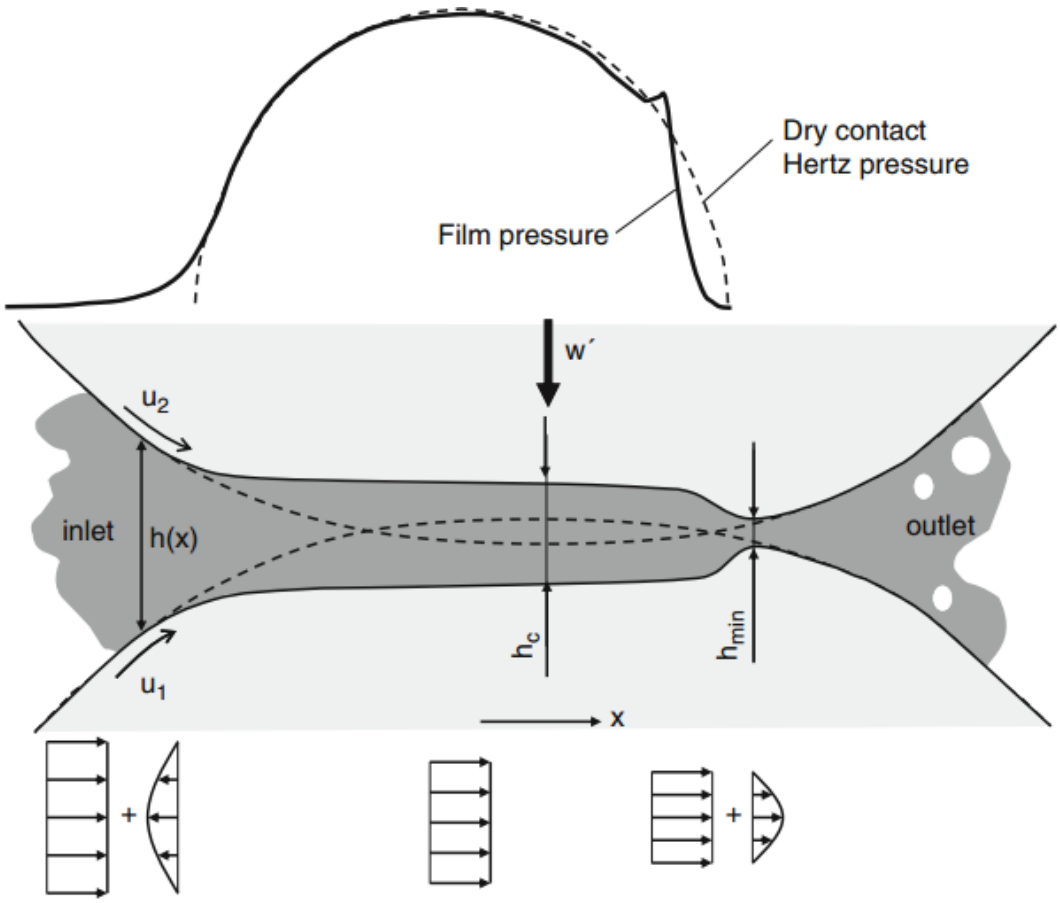

Figure 4. 4 Hydrodynamic pressure distribution in an elastohydrodynamic contact; hc is the central film thickness, h min is the minimum film thickness.

The exact analysis of elastohydrodynamic lubrication by Hamrock and Dowson [5] provided the most important information about EHL. The results of this analysis are the formulae for the calculation of the minimum film thickness in elastohydrodynamic contacts. The formulae derived by Hamrock and Dowson apply to any contact, such as point, linear or elliptical, and are now routinely used in EHL film thickness calculations. They can be used with confidence for many material combinations including steel on steel even up to maximum pressures of 3-4 [GPa]. The numerically derived formulae for the central and minimum film thicknesses are in the following form

$$\frac{h_c}{R} = 2.69\left(\frac{U\eta_0}{ER}\right)^{0.67}(\alpha E)^{0.53}\left(\frac{W}{ER^2}\right)^{-0.067}\left(1-0.61e^{-0.73k}\right) \quad (2.8)$$

$$\frac{h_{min}}{R} = 3.63\left(\frac{U\eta_0}{ER}\right)^{0.68}(\alpha E)^{0.49}\left(\frac{W}{ER^2}\right)^{-0.073}\left(1-e^{-0.68k}\right) \quad (2.9)$$

Where h_c is the central film thickness, h_{min} is the minimum film thickness, η_0 is viscosity at atmospheric pressure of the lubricant, R is Radius of curvature, U is Entering surface velocity, E is Young's modulus, α is Pressure-viscosity coefficient, W is contract load and K is Elasticity parameter.

Table 4. 3 Estimation of oil film thickness of the SAE0W30

Items	SAE 0W30		
	40 ℃	75 ℃	100 ℃
kinematic Viscosity (cSt)	44.5	24.4	9.6
Mean oil film thickness (nm)	51.25	31.97	18.34
Minimum oil film thickness (nm)	30.47	19.90	10.74

4.4 Soot hardness calculation

In order to investigate the number of carbon density, the TEM micrograph was used to calculate the carbon platelet number. Each of platelet is consist of carbon atom from incomplete combustion product as shown in Figure 4.5. The TEM micrographs of 10 nm2 focused area. was changed to be two color images. Then, it was convert to be a skeleton image by image processing software. From the skeletonize image, the line represents carbon crystallite each of which consist of carbon platelet. Each of platelet is a pair of graphene sheet

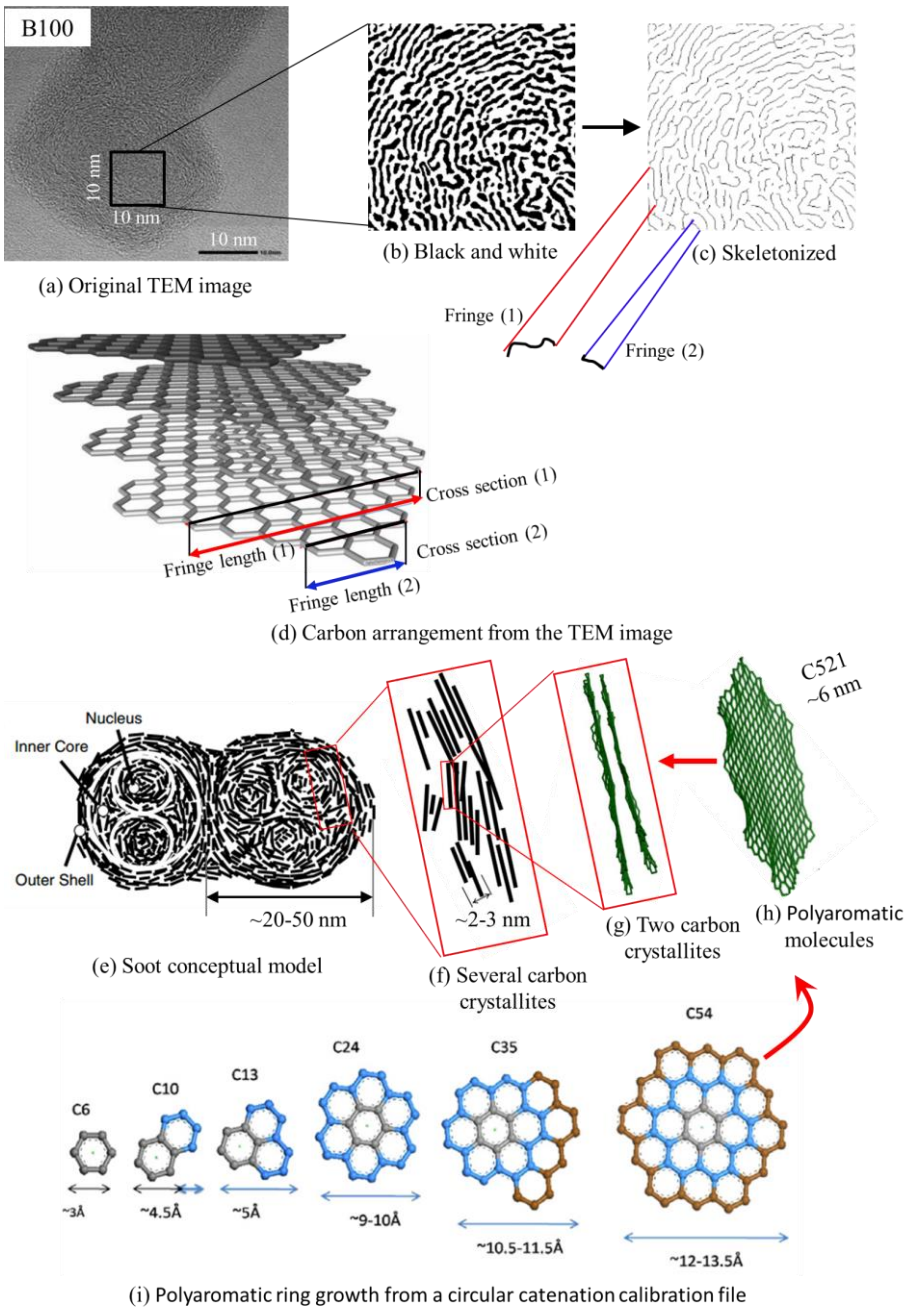

Figure 4. 5 Soot primary particle conceptal model for calculating carbonatomdensity

(modifided from (Watanawongskorn, Karin, Hanamura, & Chollacoop, 2017; Eastwood, 2008; Fernandez-Alos , Watson, Wal, & Mathews, 2011)).

Figure 4.6 shows the TEM micrographs of soot primary particle, 10 nm^2 focused area, black and white image as well as skeletonize of carbon black N330 (CB). It were four images of CB N330 that used to calculate carbon atom density. From the TEM images, it can be seen significantly difference.

(a) Carbon black N330-A

(b) Carbon black N330-B

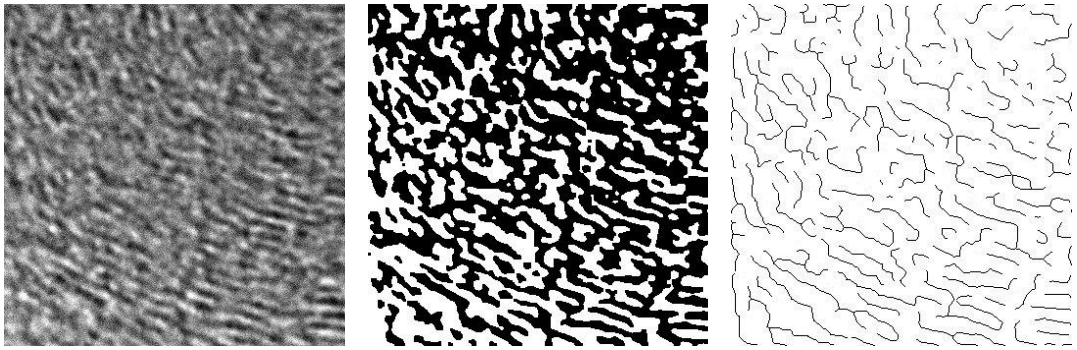

(c) Carbon black N330-C

(D) Carbon black N330-D

Figure 4. 6 TEM micrographs , black and white and skelotonize image of CB N 330.

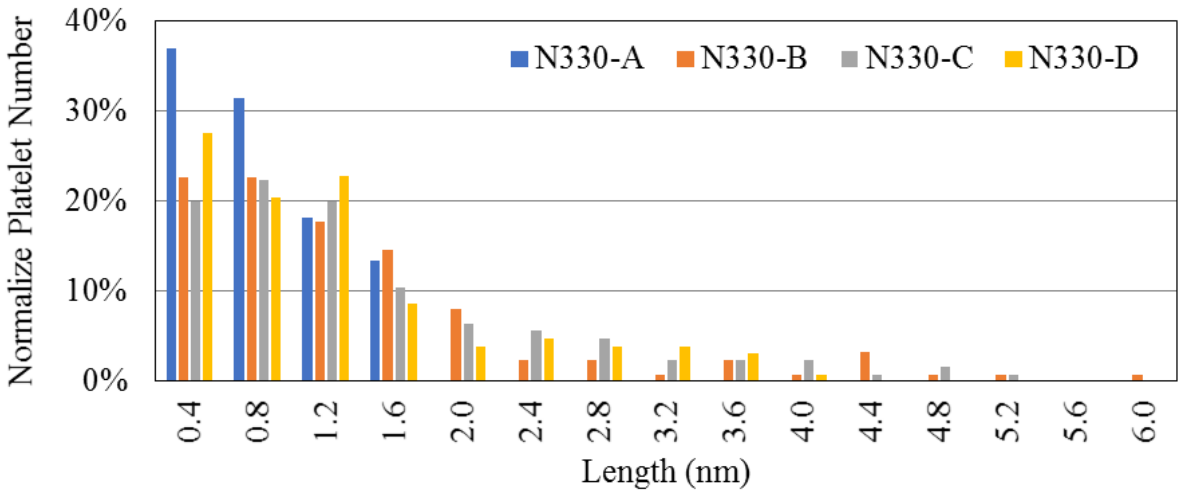

(a) Carbon platelet size distribution

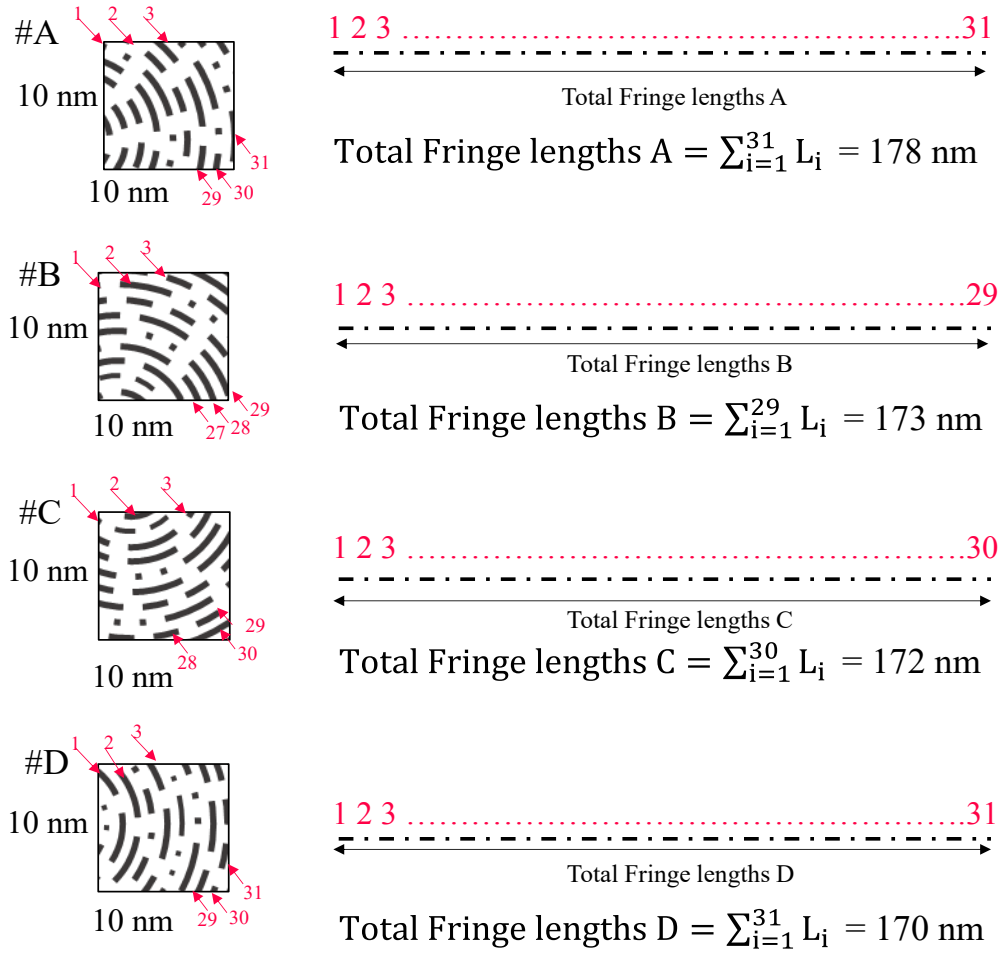

(b) Total fringe lengths

Figure 4. 7 Carbon platelet size distribution and total fringe lengths of carbon black N 330 from difference images.

The carbon platelet size distributions of each images are shown in Figure 4.7. It is clearly shown that the platelet size distributions are not significantly difference. Figure 4.7b shows the skeletonize TEM micrographs of 10 *10 nm^2 focused area of carbon black N330 (CB). It were four images of CB N330. The total fringe lengths of each sample are 178, 173, 172 and 170 nm. From the similar focused area, the total fringe lengths from the difference images are approximately the same. It might be expected that the carbon atom density of each image might be the same too because the images are also taken form the difference cross sections of soot primary particle

Although the carbon crystalline lengths measured from TEM is not the true length (since the TEM image is an image of a cross section in a 3-D dimension) the lengths might not much difference from the real because the crystalline contains many carbon atoms that means no matter where the TEM image taken in a three dimension, the crystalline length may not significantly difference because it is complex and distorted as shown in Figure 4.8.

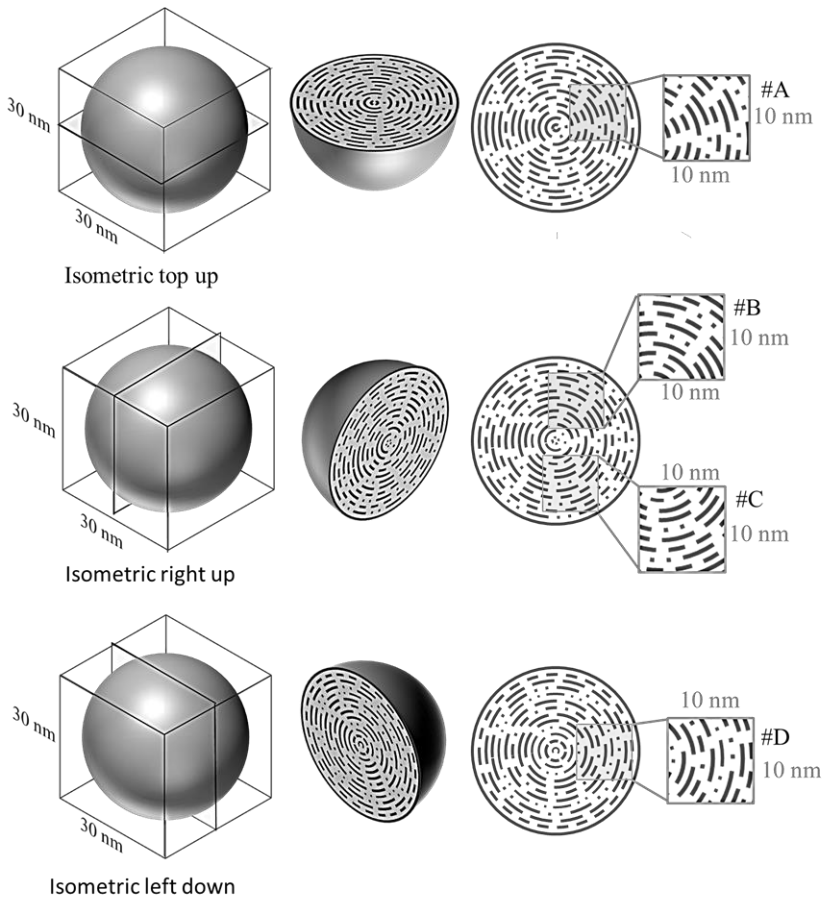

Figure 4. 8 The cross-section TEM models of CB N330 A-D.

Figure 4.9 shows the TEM micrographs of soot primary particle, 10 nm^2 focused area as well as black and white image of carbon black (CB) difference types including CB N220, N330, N550 and N550. From the TEM images, it can be seen that the soot particle consists of many carbon crystallites. The crystallites of each CB seem not significantly difference. The black and white image should have been change to skeletonize image in order to calculate carbon atom density. But it is clear seen from images that the carbon crystallite of each type is not significantly difference. Additionally, the hardness of difference types of CB might be between the hardness of Diesel (13 GPa.) and Biodiesel (12 GPa.) engine soot and it is higher than that of the steel ball (8.5 GPa.).

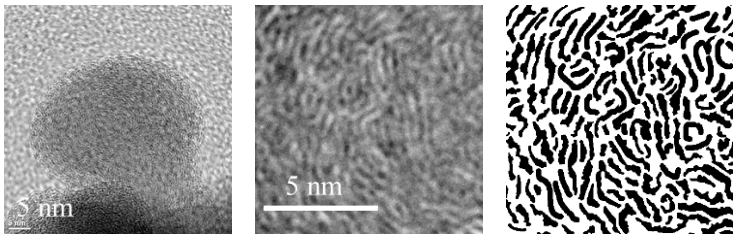

(a) Carbon black N220

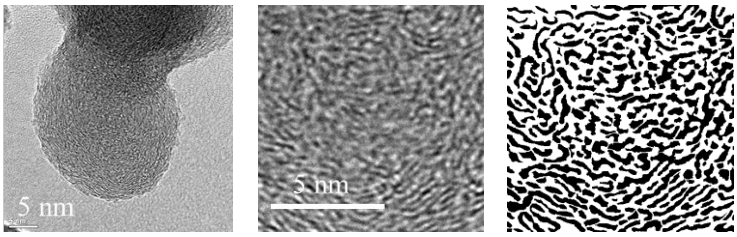

(b) Carbon black N330

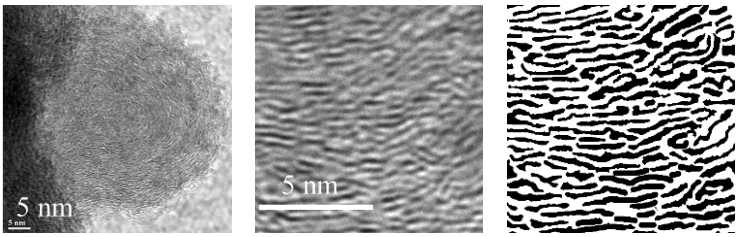

(c) Carbon black N550

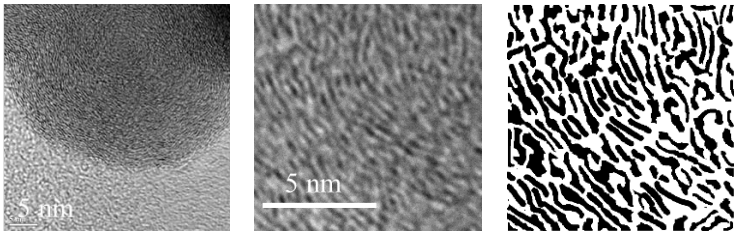

(d) Carbon black N660

Figure 4. 9 TEM micrographs , black and white and skelotonize image of CB difference types.

In order to clearly investigate the impact of soot hardness on metallic wear, it is necessary to create a relationship between carbon atom density and mechanical hardness. (This method is modified from Jao [25]). Table 4.4 shows the properties of various forms of carbon taken from Roberson [4]. Taking the literature values for the carbon atom density and hardness data of diamond and diamond like-carbon which are glassy carbon, amorphous carbon and diamond, we can create a plot which is shown in Figure 4.10. The black solid line is the best linear least square fit of all four data points. And the R square is 0.95. The plot is also represented in the log scale.

Table 4. 4 The properties of various forms of carbon [5].

	Density (g/cm^3)	Hardness (kg/mm^2)
Glassy carbon	1.43	250
Evaporated amorphus carbon (a-C:evap)	1.95	.50
Hydrogenated amorphus carbon (a-C:evap)	1.9	1,500
Daimond	3.52	10,000

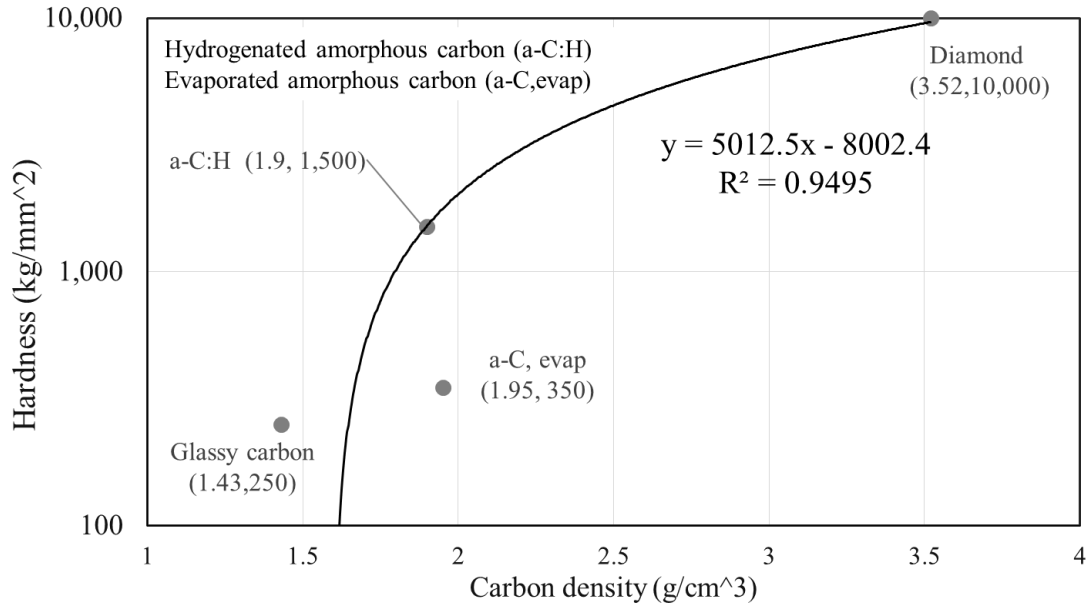

Figure 4. 10 Plots of carbon density and its hardness of diamond-like carbon and diamond [5].

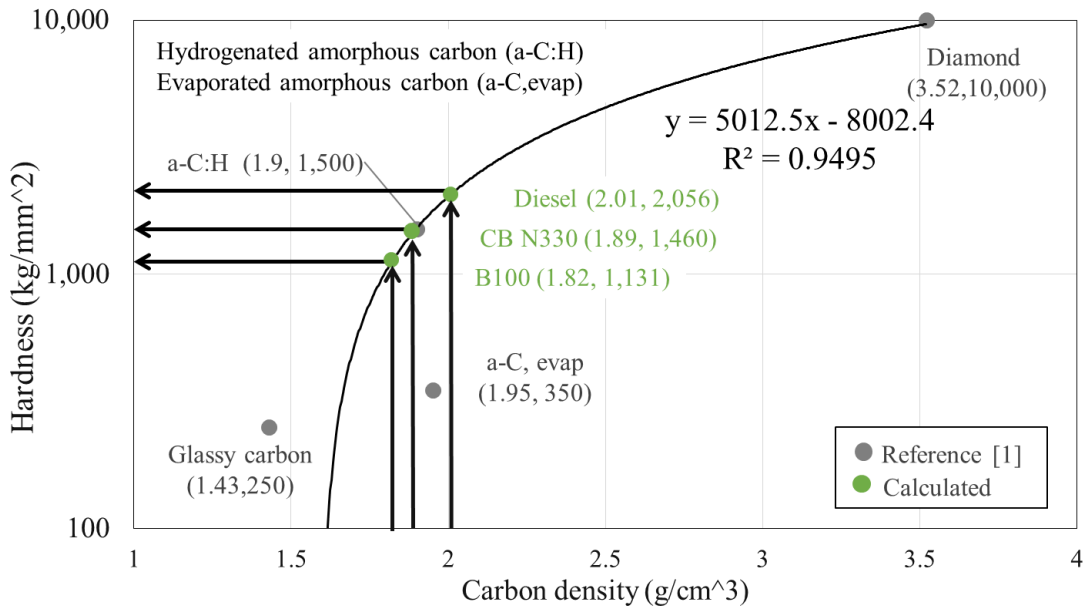

Figure 4. 11 Plots of carbon density and its hardness of diamond-like carbon and diamond [5].

Figure 4.11 allows us to calculate the hardness of individual soot particle. For example according to the best-fit scale, biodiesel soot with the carbon density of 1.82 g/cm^3 would have hardness of 1,334 kg/mm^2, while diesel soot with the density of 2.0 g/cm^3 would have hardness of 2,056 kg/mm^2. Additionally, carbon black with the density of 1.89 g/cm^3 would have the hardness of 1,460 kg/mm^2. Table 4.6 also shows the carbon density and mechanical hardness of the individual soot of this work and the data from the referees.

The other way to measure the carbon atom density is using low-loss electron energy-loss spectroscopy (EELS) which have been using by many researchers [25, 27, 28]. They measured the plasmon energy of the individual soot particle by EELS spectroscopy and then the plason energy is converted to the carbon atom density. Finally, the sot hardness is calculated by the relationship crated by Jao [25]. From the references, the density of Diesel soot reported by [25, 27] are in the range of 1.79 – 1.86 (g/cm^3) then their hardness are going to be in the range of 968.67 to 1,300 kg/mm^2. Additionally, the density of Biodiesel soot (B20) reported by [7] are in the range of 1.82 – 1.84 (g/cm^3) then their hardness are going to be in the range of 1,100 to 1,200 kg/mm^2. (From Devlin et al [7] they collected the soot of B20 from the difference engines).

Figure 4.12 shows the calculated carbon atom density and mechanical hardness and it also include the data from the references [25, 27, 28]. Using the correlation, we can compare the hardness of any individual soot particle with the hardness of steel ball [8]. The hardness of steel ball followed by the standard Four-ball wear test is about 799-867 kg/mm^2. It is clearly shows that the hardness of soot is much higher than that of the steel ball.

Table 4. 5 Carbon atom density and its hardness of soot primary particle from the references

	Source #	Method to measure carbon density?	Carbon density (g/cm^3)	Hardness (kg/mm^2)
B100	calculated	Qualitatively analysis from the TEM images	1.82	1,334
CB N330			1.89	1,460
Diesel			2.0	2,056
Diesel –A	Li et al [2]	Measuring the plasmon energy of the individual soot by using low-loss electron energy-loss spectroscopy (EELS)	1.86	1,330
Diesel-B	Jao et al [1]		1.84	1,200
Diesel-C	Li et al [2]		1.79	968.67
B20-A	Devlin et al [3]		1.84	1,200
B20-B	Devlin et al [3]		1.82	1,100

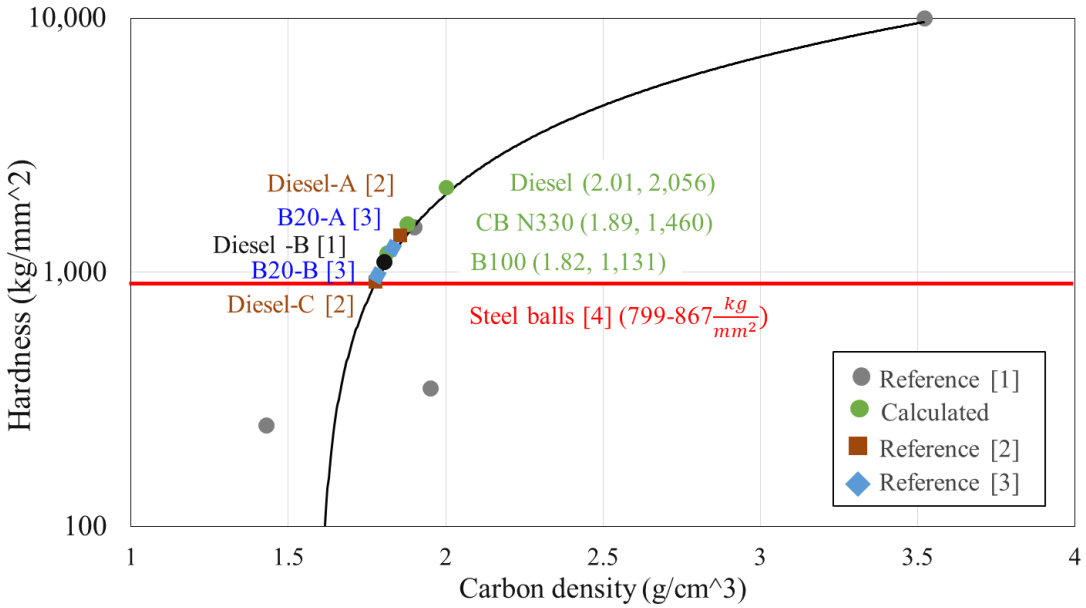

Figure 4. 12 Plots of carbon density and its hardness.

4.5 Impact of soot on metallic wear using four ball wear tester

In order to investigate the effect of soot Nano particle size on metallic wear, the four ball wear tester was used. In this study the commercial carbon black was used to simulate engine soot. The several types of commercial carbon blacks (CB) which have different primary particle size were mixed with the engine oil at 1% by weight per volume for simulating soot different primary particle size contaminated engine oil. After the four ball tests, the three lower balls used to measure wear scar diameter (WSD) using a high-resolution optical microscope (OM). Testing formulations were compared using average diameter of the wear scar diameter on the three lower balls. An average of 3 wear scars readings is reported as wear scar diameters. Moreover, the surface roughness was also measured using 3D rendering system of that OM.

Figure 4.13 shows microscopy image of wear scars and 3D-rendering image found on three lower balls and one upper ball after 60 min running time. Figure 4.14 shows the corresponding average wear scar diameter and surface roughness the engine oil without soot and engine oil containing 1% wt. of N220, N330, N550 and N660 Carbon Black. Base on four ball wear test, the 1% by weight of CB contamination (CB N220, N330, N550 and N660) shows 14% high average WSD compare to the pure SAE0W30 engine oil, but the surface roughness was 22 % lower than the engine oil alone. The results showed that the ball wear scar diameter of the new engine oil, and the engine oil containing carbon black N220 and N330 were not significantly difference. On the other hand, the wear scar diameter of the engine oil containing carbon black N550 and N660 were larger than the others. It might be expected that when soot primary particle was smaller than the oil film thickness, wear rate was not significantly difference, On the other hand, wear was accelerated when soot particle was larger than the oil film. Soot particle could be increase the rate of wear because it was large in comparison with the oil film and its hardness was higher than that of the steel ball. Moreover, in case of CB N660, soot particle was much larger than the oil film thickness. So, that it might be block the lubrication inlet to the contact, therefore resulting in unlubricated sliding wear which causes the largest wear scar diameter.

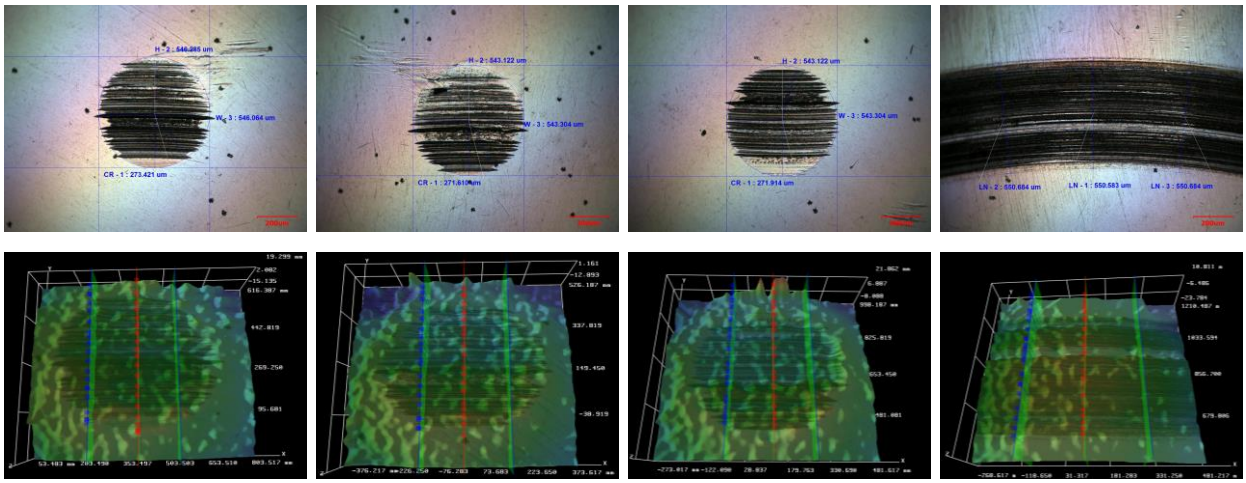

(a) Engine oil without CB

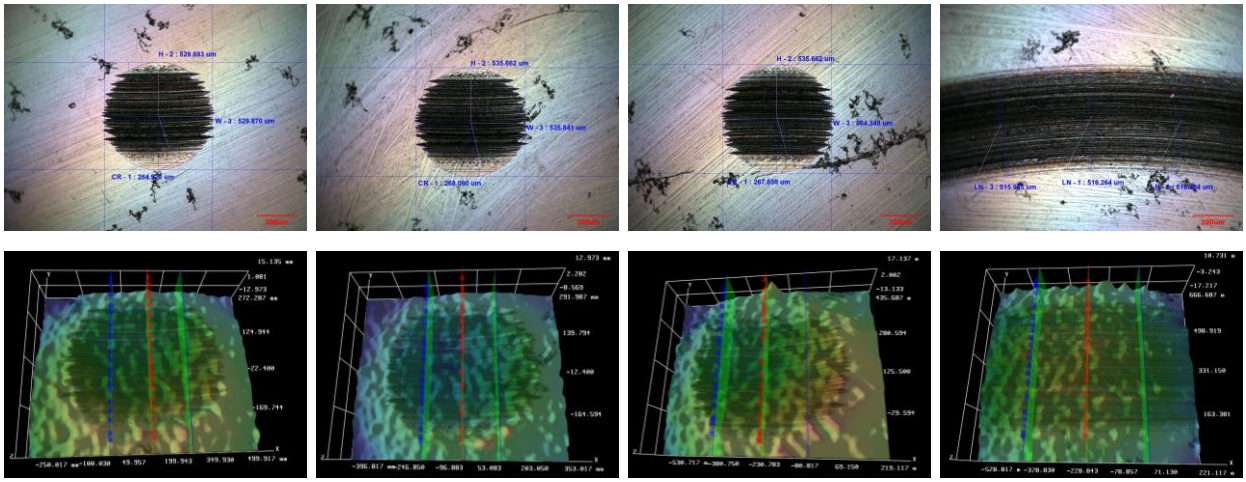

(b) Engine oil with CB N220

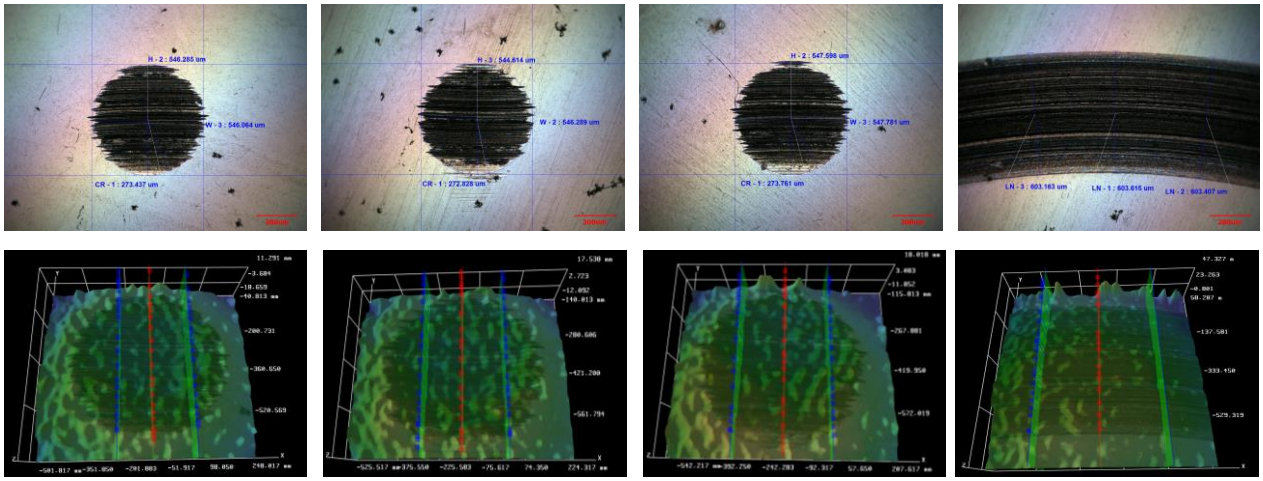

(c) Engine oil with CB N330

Figure 4. 13 Wear scar and surface roughness of the ball from (a) the engine oil without soot and the engine oil containing 1% wt. of (b) CB N 220, (c) CB N330, (d) CB N550 and (e) CB N660.

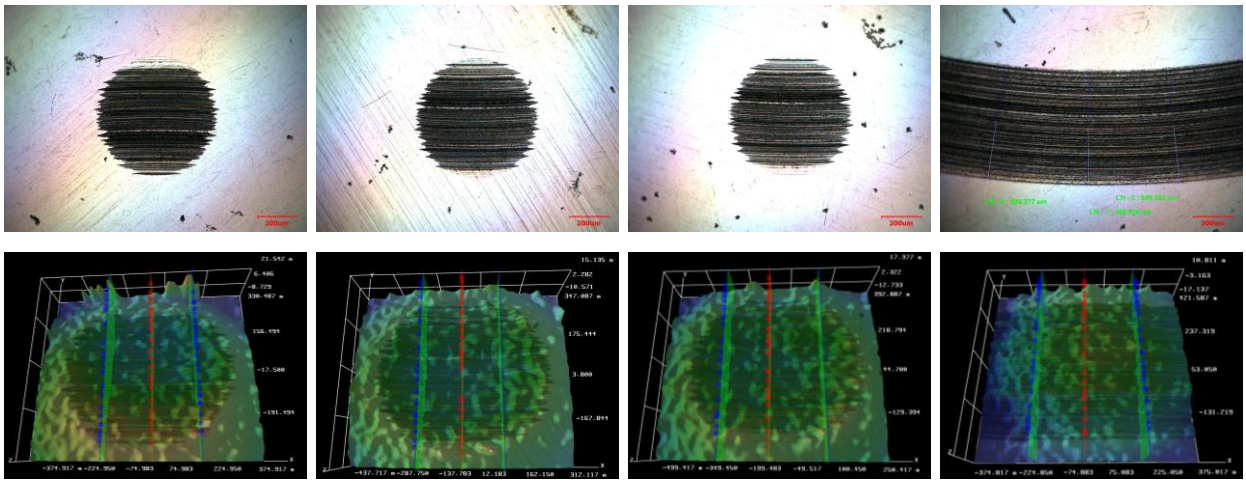

(d) Engine oil with CB N550

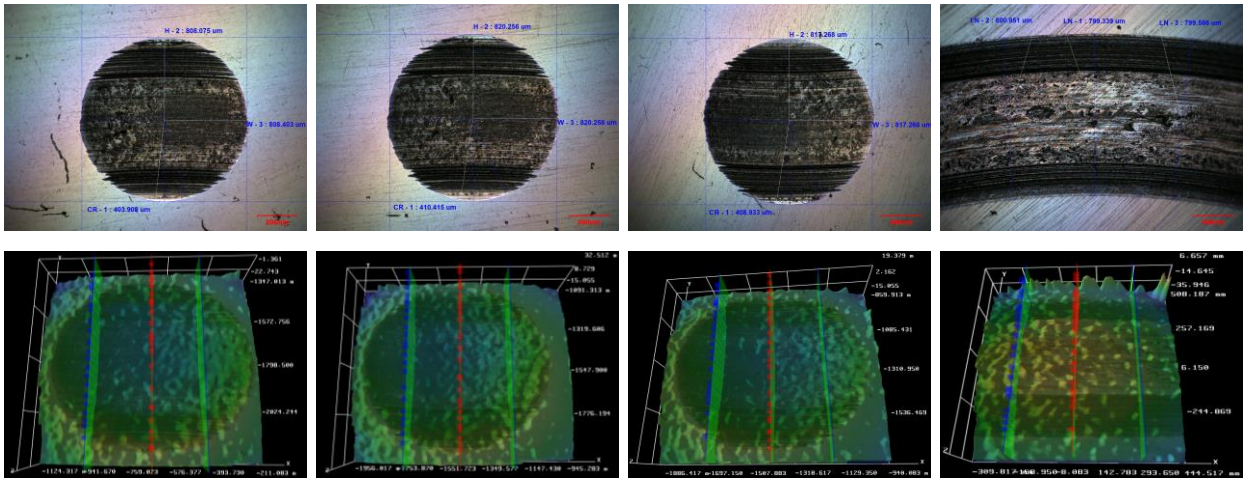

(e) Engine oil with CB N660

Figure 4.13 Wear scar and surface roughness of the tested balls (continuous).

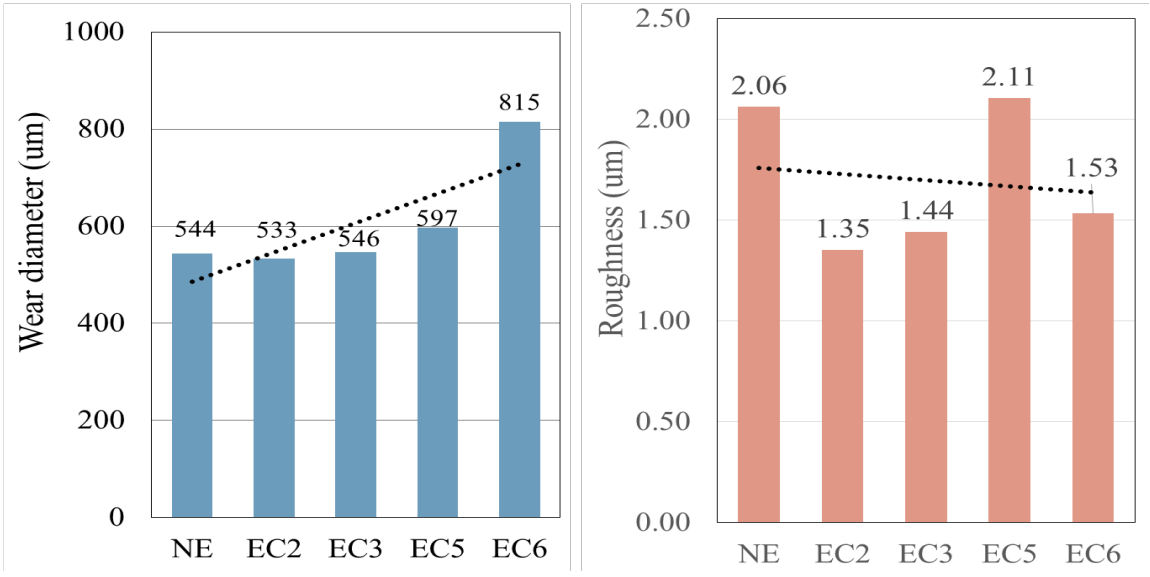

Figure 4. 14 Average wear scar diameter and surface roughness on lower balls.

4.6 Particle size distribution after wear test

After Four-ball wear test, the tested oils were also measured size distribution. They were the wear metal without CB and wear metal with CB N220, N330, N550 and N660. Figure 4.15 shows size distribution of particles inside the tested oils. They were in the range of 0.01 – 200 micron. The size of wear metal without CB was in the range of 1-100 microns. On the other hand, the size of wear metal with CB were in the range of 0.01 – 300 microns. It might be expected that the size of soot particle might be in the 0.01-300 microns. The small particle should be soot primary and agglomerate particles.

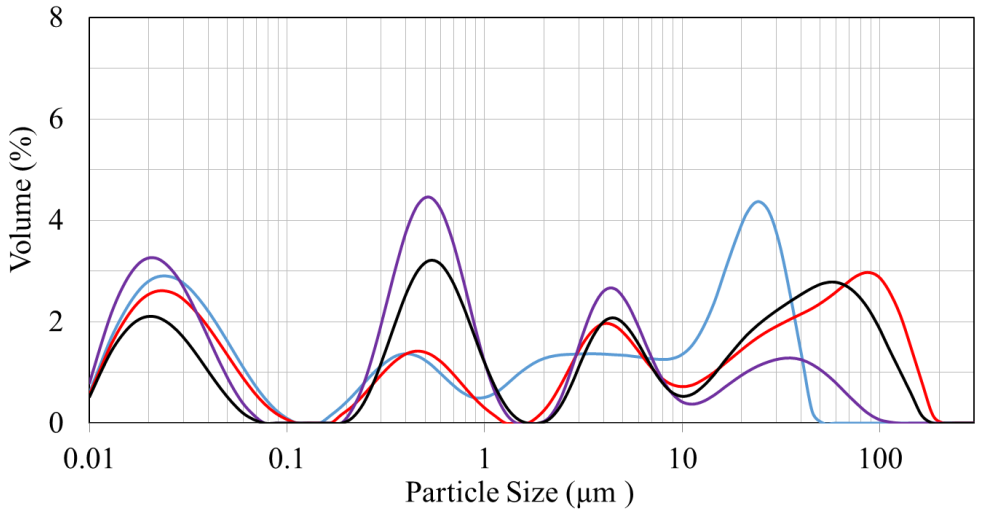

(a) Particle size distribution

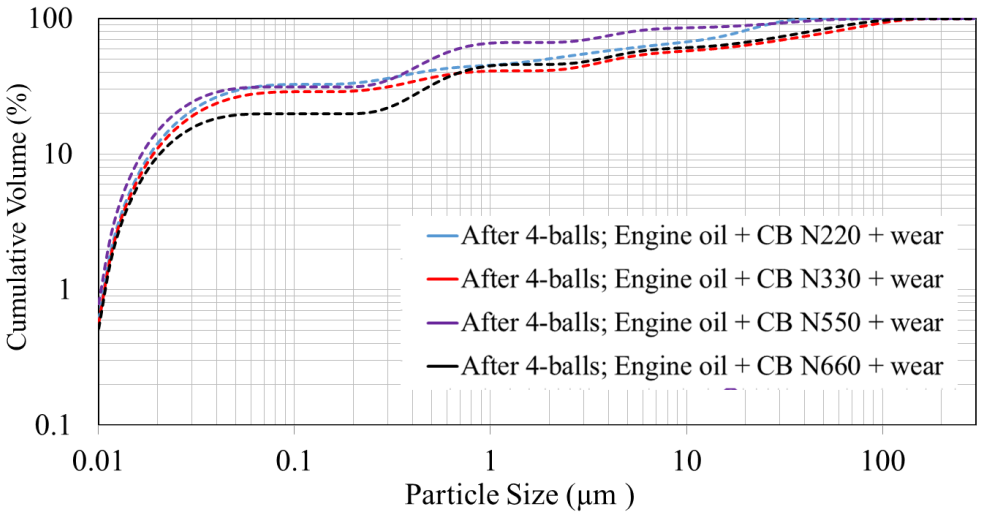

(b) Particle cumulative volume

Figure 4. 15 Carbon black (a) size distribution and (b) cumulative volume in lubricating oil before Four-ball wear test using Laser Particle Diffraction Spectroscopy.

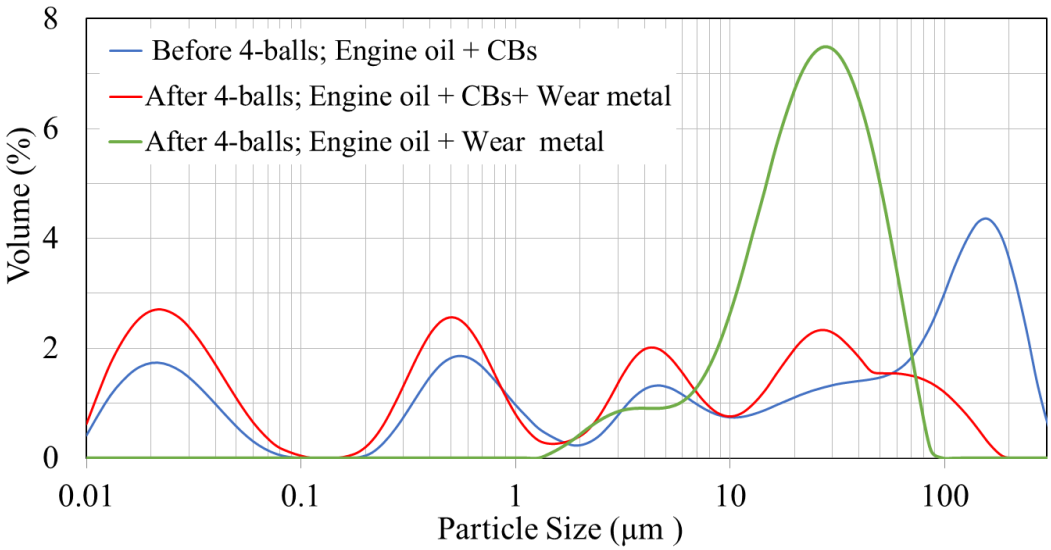

Figure 4. 16 Carbon black size distribution e in lubricating oil before Four-ball wear test using Laser Particle Diffraction Spectroscopy.

Moreover, the comparison between particle size distribution before and after Four-ball wear tests are shown in Figure 4.16. The average CB size distribution before Four-ball wear test of the 4 samples is represented by blue line. The wear metal without CB size distribution is represented by black dash line. In addition, the average wear metal with CB size distribution after Four-ball wear is represented by orange line with circle marker type. The average size distribution before Four- ball wear test were in the range of 0.01-300 microns. The average wear metal without CB and wear metal with CB particle size distribution after Four-ball wear test were in the range of 1-100 microns and 0.01-200 microns. From the results it might be expected that it should be No wear metal that have size lower than 1 microns and larger than 100 microns. That means the particle which have size in the range of 0.01-1 microns and 100 – 300 microns should be carbon black particle.

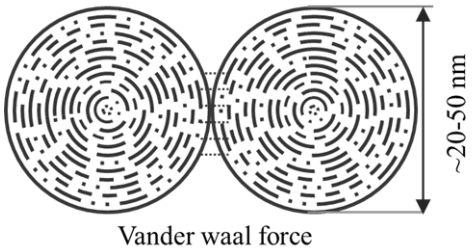

(a) Two soot particles which are hold together with Van der Waals force.

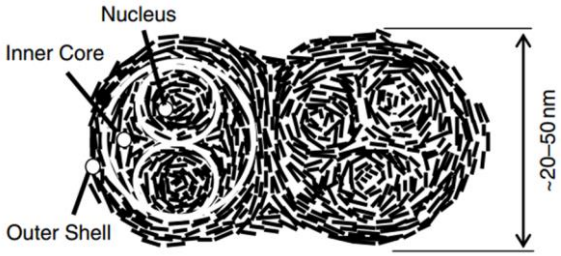

(b) Two complete spherules bonded via a shared outer layering of crystallites **[9]**.

Figure 4. 17 conceptual models of soot particle

Soot agglomerate particles might be sheared in to the single particle when the bonding between soot particles is Van der waals force. Kuo et al [4] used the Cummins M-11 to study the impact of soot on wear and they reported that "Aggregated soot particles, which are held together by weak Van Der Waals forces can be dissociated readily under a shearing force, which is believed to be occurring here as shown in Figure 4.17. On the other hand, Soot agglomerate particles might not be sheared in to the single particle when that particles are bonded by sharing the same carbon crystallites as shown in Figure 4.17.Because the force that hold it together might greater than that of the shearing force.

4.7 Analysis by SEM and EDX

4.7.1 Analysis of worn surfaces by SEM

Figure 4.18, 22, 26 and 30 show SEM micrographs at 150 magnification of the wear scar found on the ball of (a) the engine oil without soot and engine oil containing 1% wt. of (b) N220, (c) N330, (d) N550 and (e) N660 Carbon Black. This figure present the wear scar worn surface of the three stationary ball and one rotating ball under the same test conditions according to ASTM D4172. Figure 4.19, 23, 27 and 31 show the SEM micrographs at higher magnification. The wear scars on the stationary ball from the test with the new engine oil are shown in Figure 18, 22, 26 and 30 (a). The worn surface of uncontaminated oil was covered with several fine wear track parallel to the sliding direction, which suggests a mechanism of slight abrasive wear and it also shown some area of plastic deformation. It was reported that the plastically deformation of the worn surface which was larger than 20 microns was reflected to adhesive wear [5]. Moreover, some area of pitting and subsurface cracks were also found that was reported as fatigue wear [5]. Figures 18, 22, 26 and 30 (b) - (c) shows SEM micrographs of the wear scars of engine oil containing CB N220, N330 and N550. It is clearly seen that, When carbon black was added to the oils the wear behavior was slightly difference, It could be seen the many deep and wide wear track parallel to the sliding direction. The calculated soot hardness of CB N330 was about 14 GPa, which was much higher than the hardness of the steel ball (7GPa) used in this study. Therefore, the predominant wear mechanisms of the CB N220, N330 and N550 contaminated engine oil is expected as three body abrasive wear. In the oil with carbon black N660 as shown in Figure 18, 22, 26 and 30 (d), the wear mechanisms differs from the other. It could be seen the smooth worn surface which suggests a mechanisms of scuffing adhesive wear. This area could be the results of carbon black particle accumulating at the inlet zone leading to the partial oil starvation. The oil film thickness could be reduced and leads to boundary lubrication. The metal to metal contract could increase the wear rate and adhesive material transfer. In order to qualitatively analysis of wear mechanisms, the 24 X 18 blocks were created as shown in Figure 4.21, 25, 29 and 33. The size of each block was 10.66 microns. The wear mechanisms could be .characteristic as follows: The fine wear track or grove along with the sliding direction which was defined by a blue color was reflected to abrasive wear [5]. The plastically deformation which was larger than 20 microns defined by a red color was reflected to adhesive wear [5]. Moreover, the pitting and subsurface crack which was defined by a green color was reflected to fatigue wear.

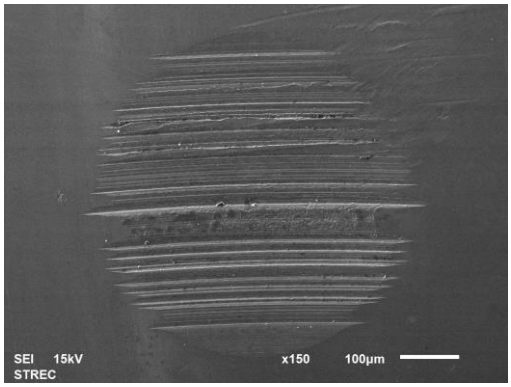

(a) The engine oil without soot

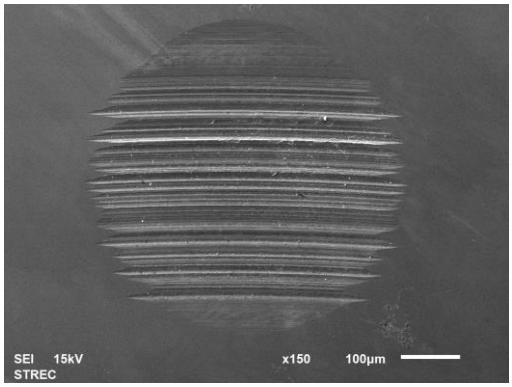

(b) The engine oil containing CB N220.

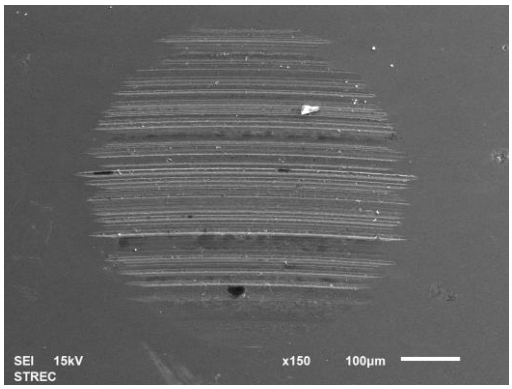

(c) The engine oil containing CB N330.

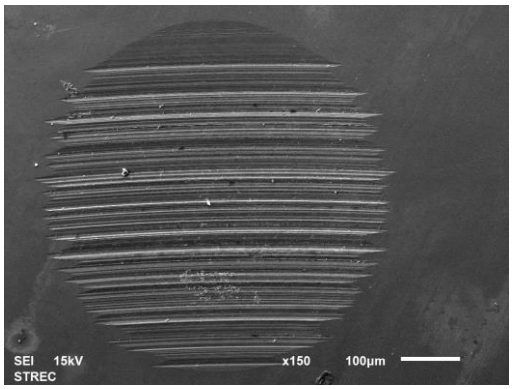

(d) The engine oil containing CB N550.

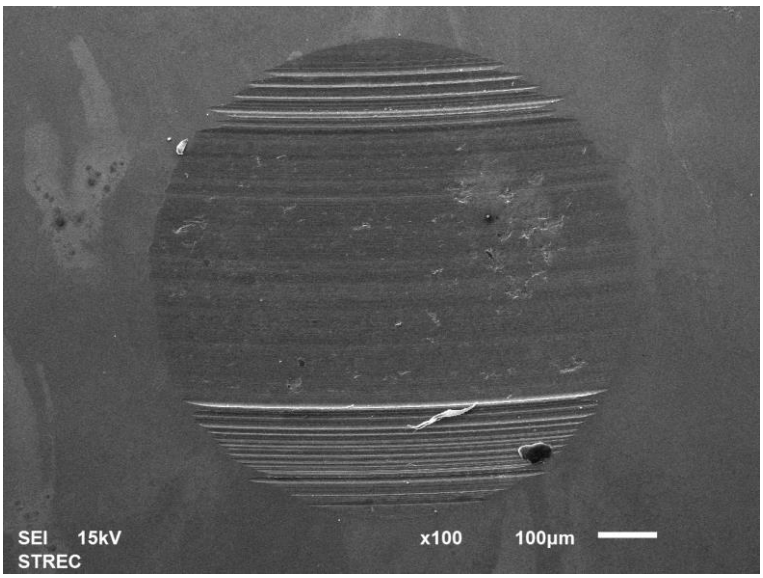

(e) The engine oil containing CB N660.

Figure 4. 18 SEM micrographs of the first lower balls at 100\150 magnification.

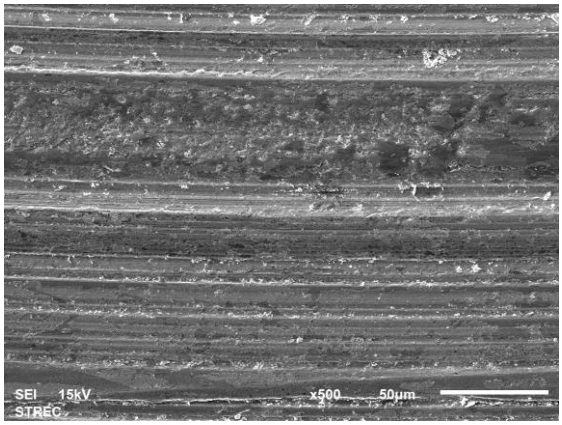

(a) The engine oil without soot

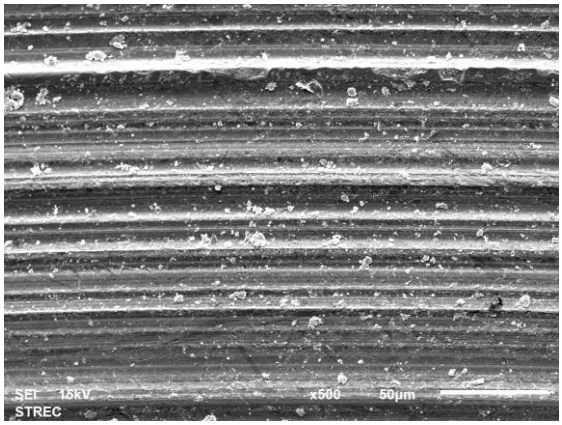

(b) The engine oil containing CB N220.

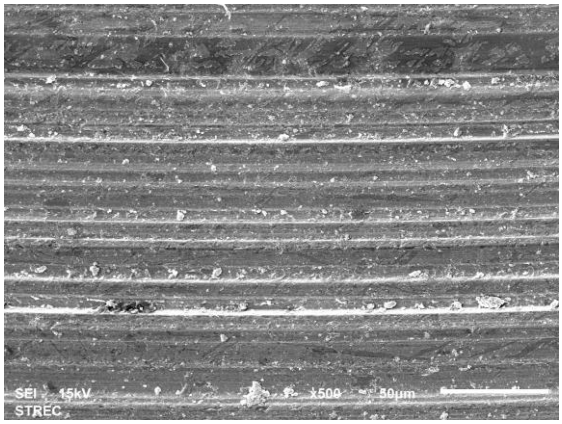

(c) The engine oil containing CB N330.

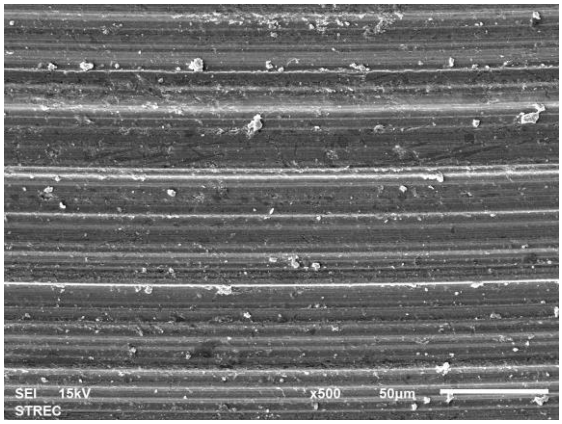

(d) The engine oil containing CB N550.

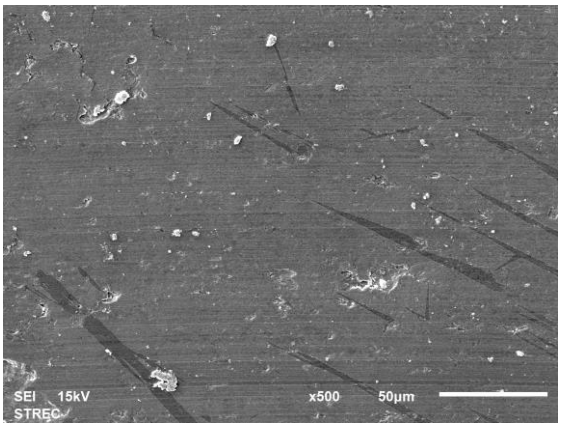

(e) The engine oil containing CB N660.

Figure 4. 19 SEM micrographs of the first lower balls at 500 magnification.

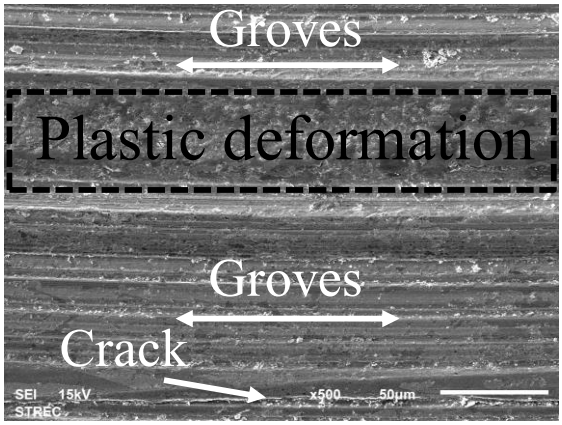

(a) The engine oil without soot

(b) The engine oil containing CB N220.

(c) The engine oil containing CB N330.

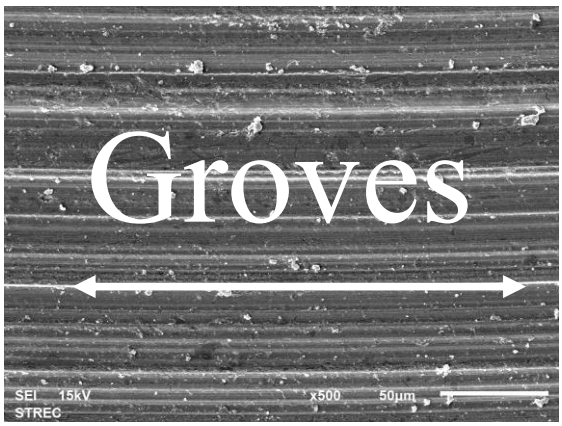

(d) The engine oil containing CB N550.

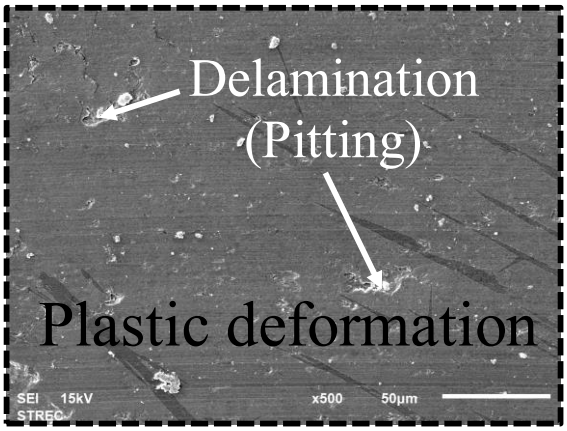

(e) The engine oil containing CB N660.

Figure 4. 20 SEM micrographs of the first lower balls with wear description.

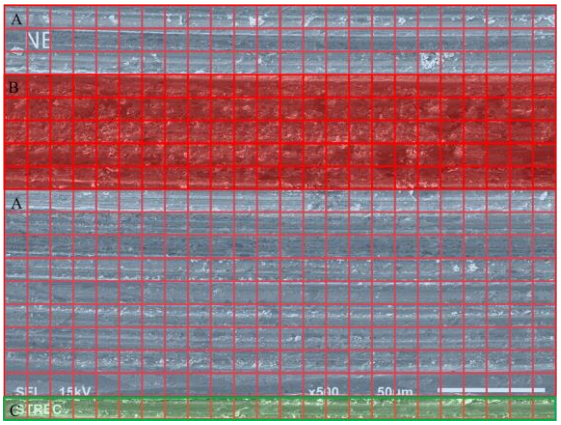

(a) The engine oil without soot

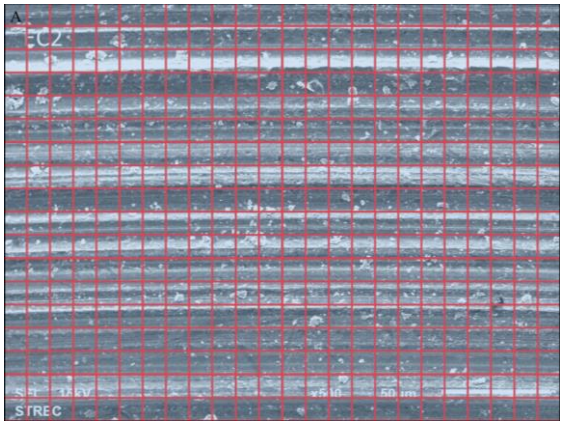

(b) The engine oil containing CB N220.

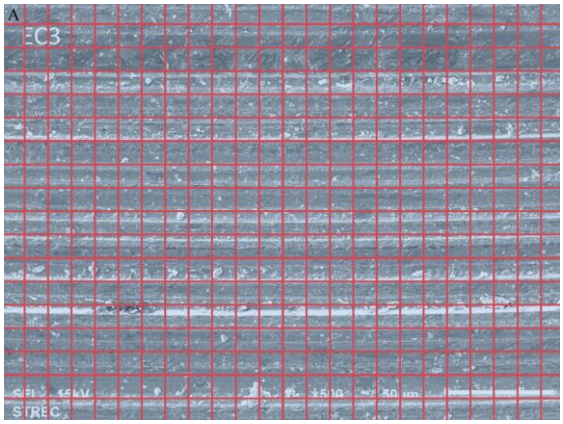

(c) The engine oil containing CB N330.

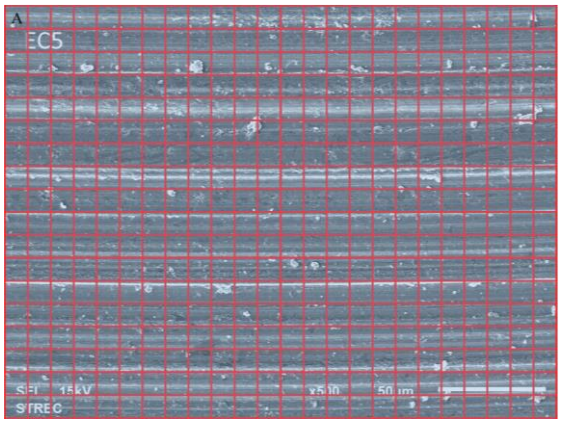

(d) The engine oil containing CB N550.

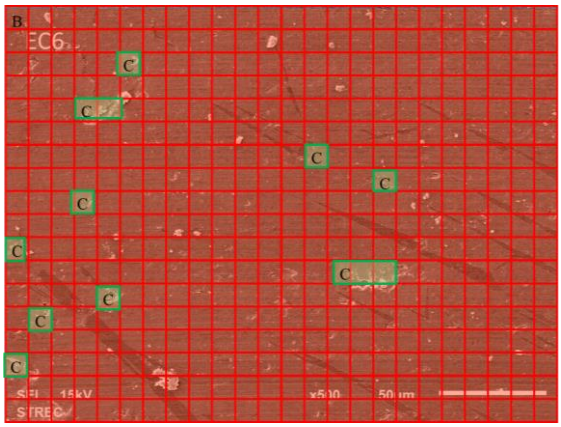

(e) The engine oil containing CB N660.

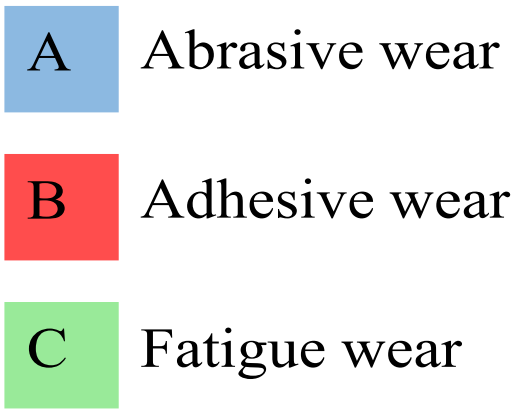

Figure 4. 21 SEM micrographs of the first lower balls with colored wear analysis.

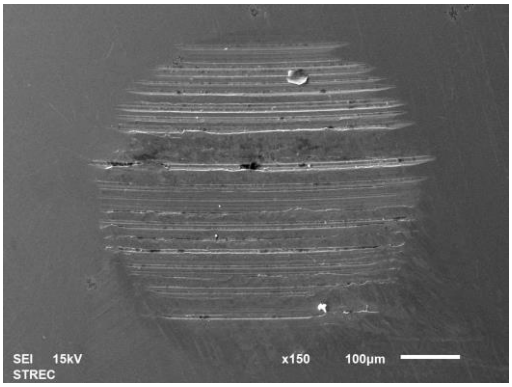

(a) The engine oil without soot

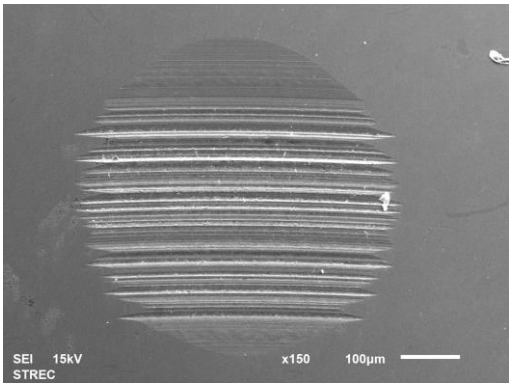

(b) The engine oil containing CB N220.

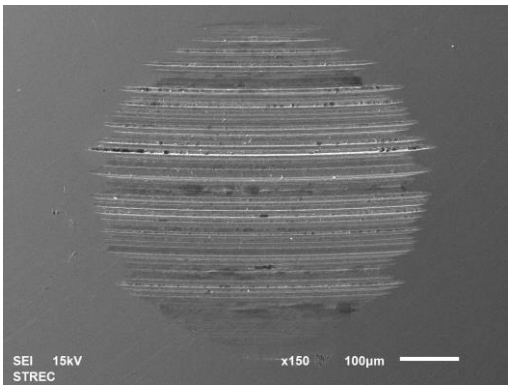

(c) The engine oil containing CB N330.

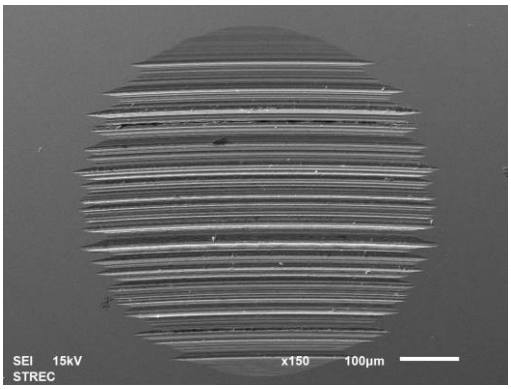

(d) The engine oil containing CB N550.

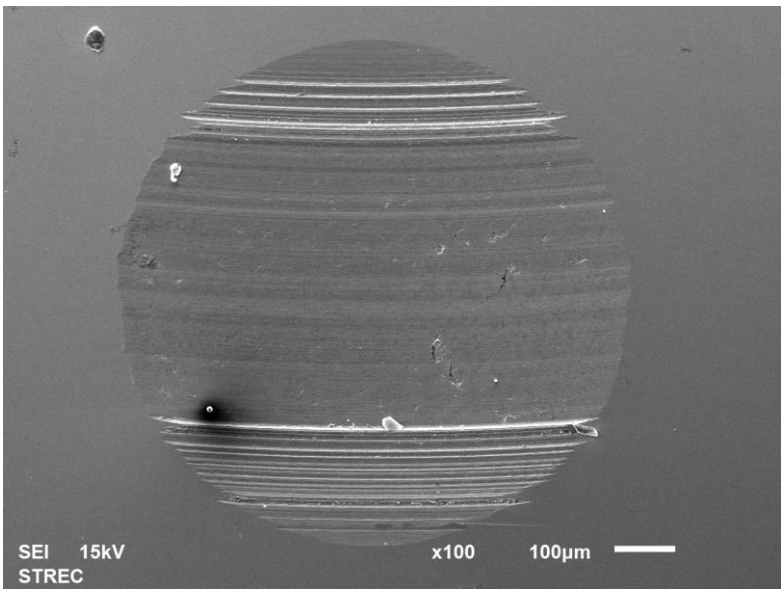

(e) The engine oil containing CB N660.

Figure 4. 22 SEM micrographs of the second lower balls at 100\150 magnification.

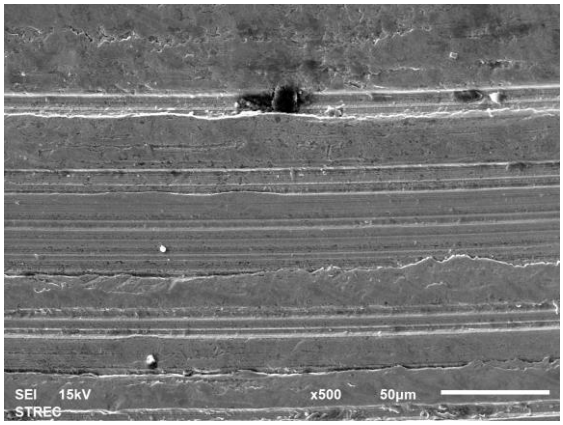

(a) The engine oil without soot

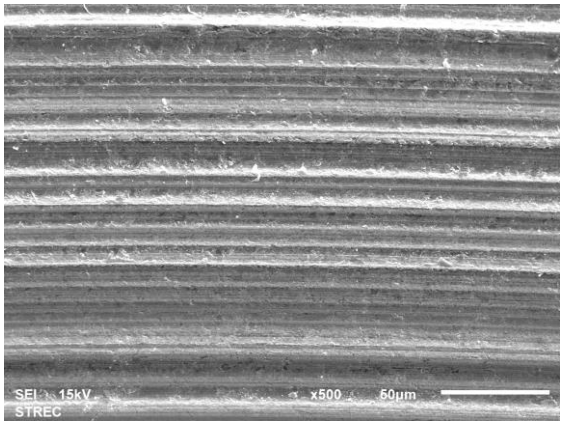

(b) The engine oil containing CB N220.

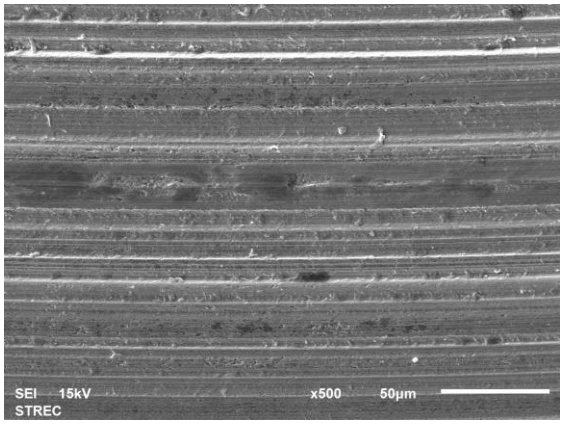

(c) The engine oil containing CB N330.

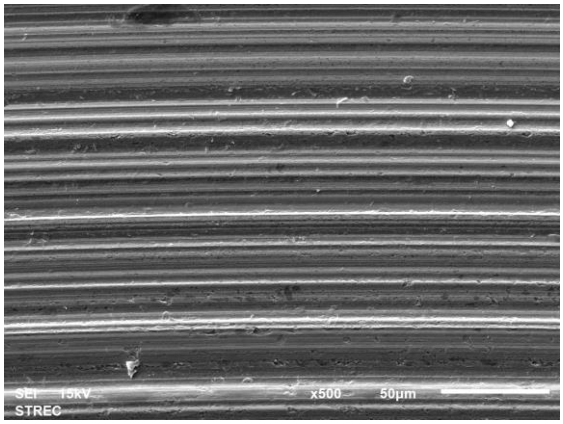

(d) The engine oil containing CB N550.

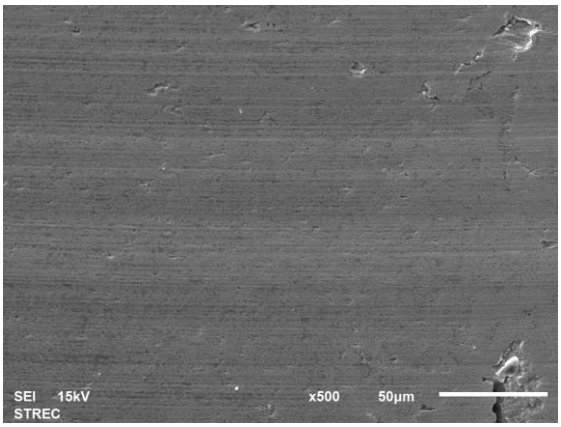

(e) The engine oil containing CB N660.

Figure 4. 23 SEM micrographs of the second lower balls at 500 magnification.

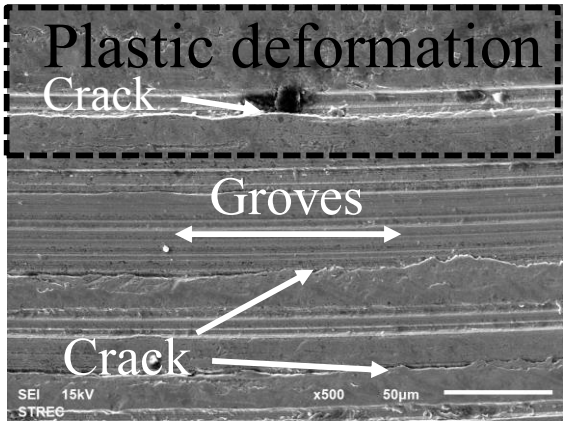

(a) The engine oil without soot

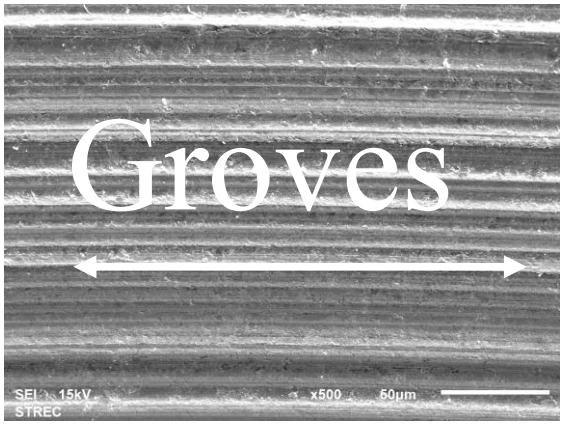

(b) The engine oil containing CB N220.

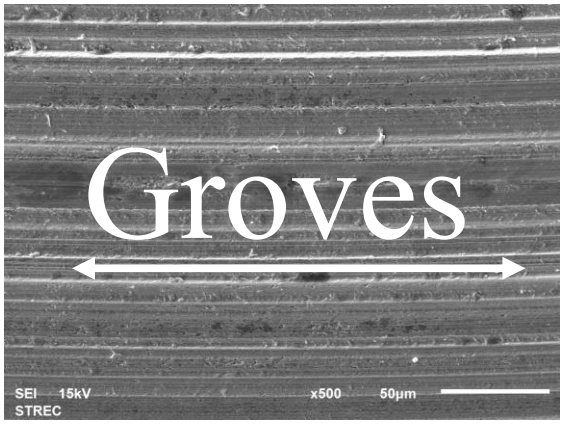

(c) The engine oil containing CB N330.

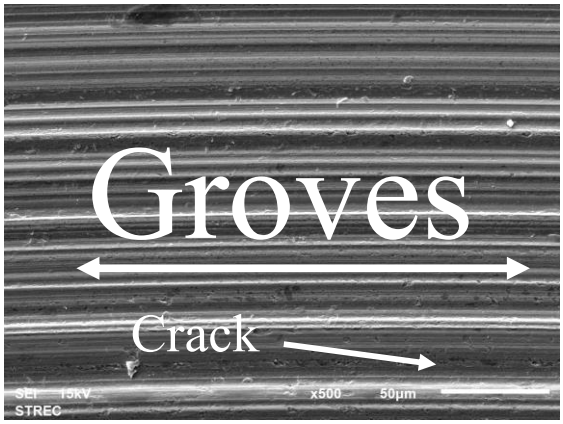

(d) The engine oil containing CB N550.

(e) The engine oil containing CB N660.

Figure 4. 24 SEM micrographs of the secound lower balls with wear description.

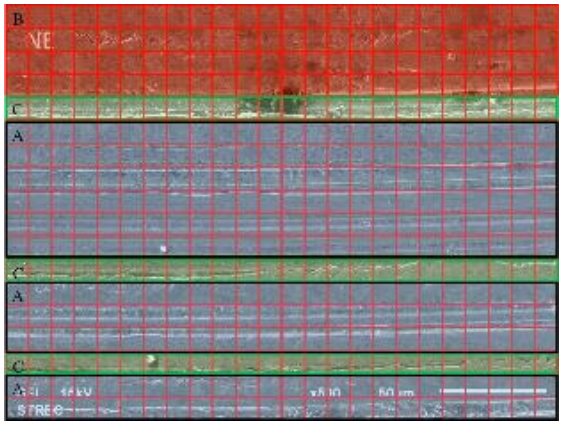

(a) The engine oil without soot

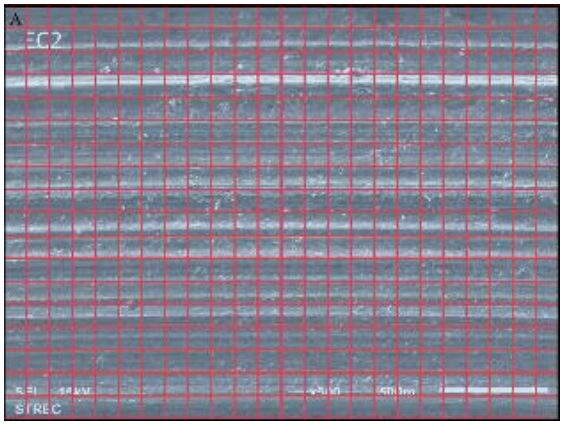

(b) The engine oil containing CB N220.

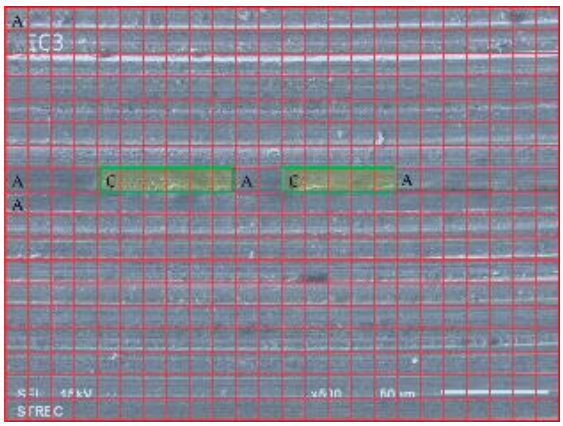

(c) The engine oil containing CB N330.

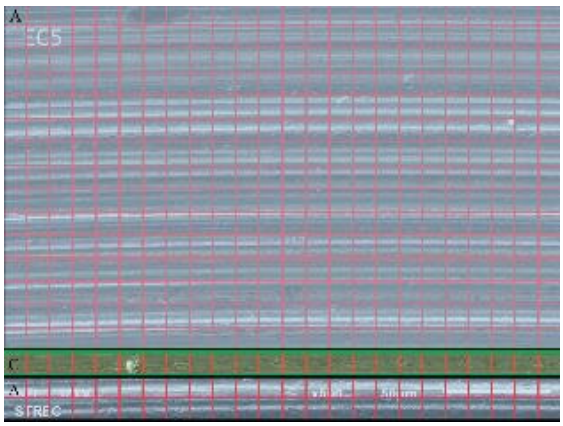

(d) The engine oil containing CB N550.

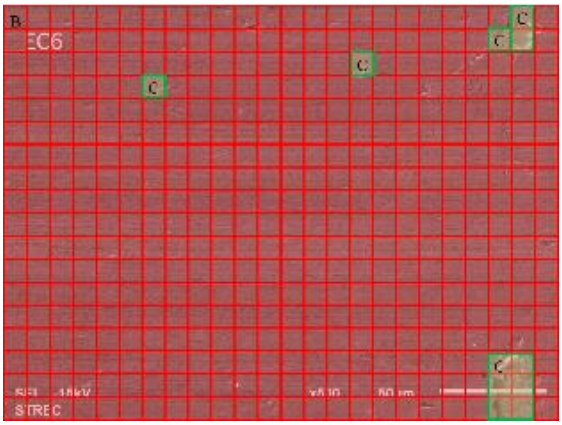

(e) The engine oil containing CB N660.

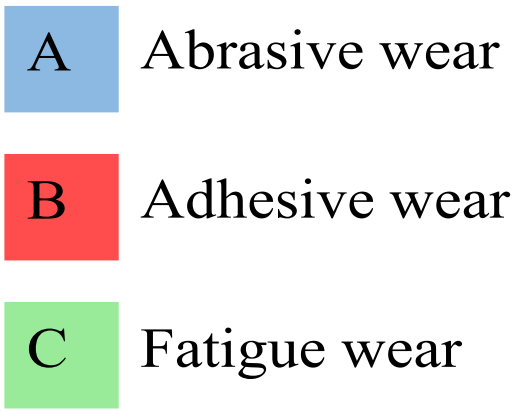

Figure 4. 25 SEM micrographs of the first lower balls with colored wear analysis.

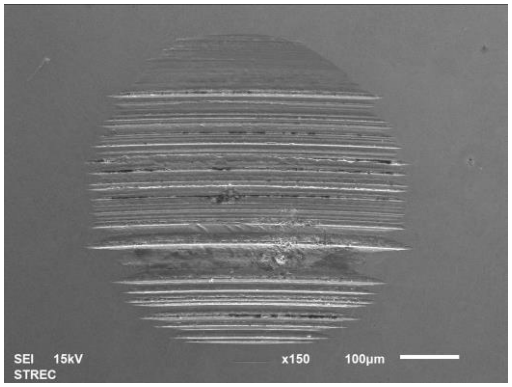

(a) The engine oil without soot

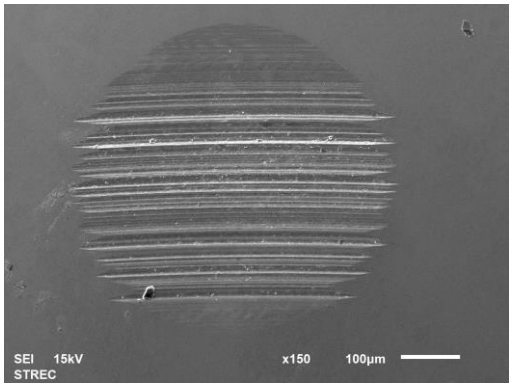

(b) The engine oil containing CB N220.

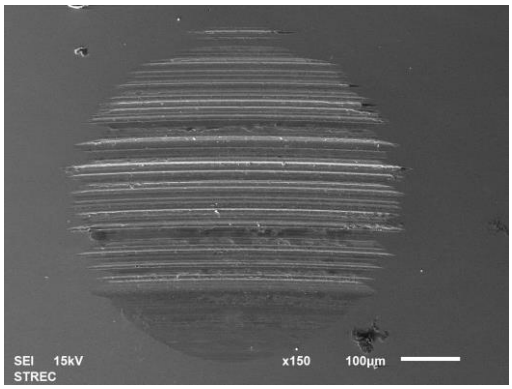

(c) The engine oil containing CB N330.

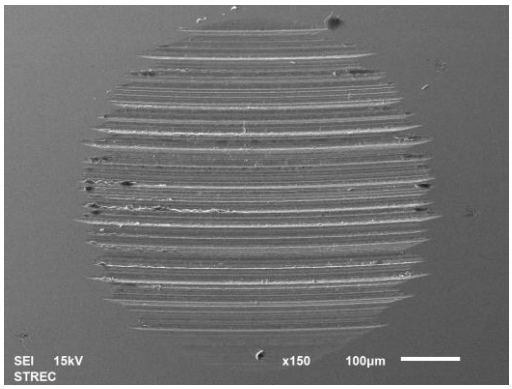

(d) The engine oil containing CB N550.

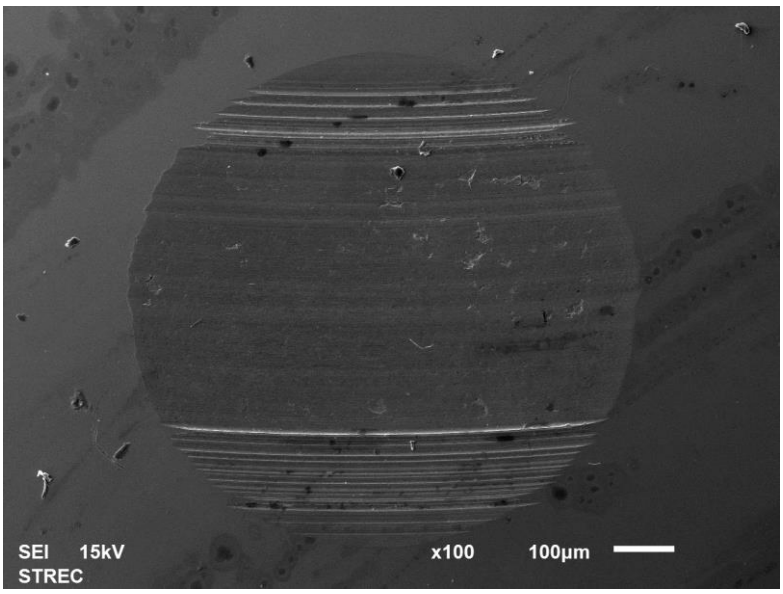

(e) The engine oil containing CB N660.

Figure 4. 26 SEM micrographs of the third lower balls at 100\150 magnification.

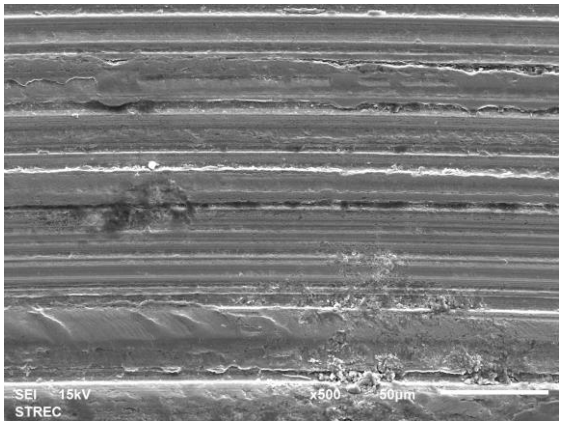

(a) The engine oil without soot

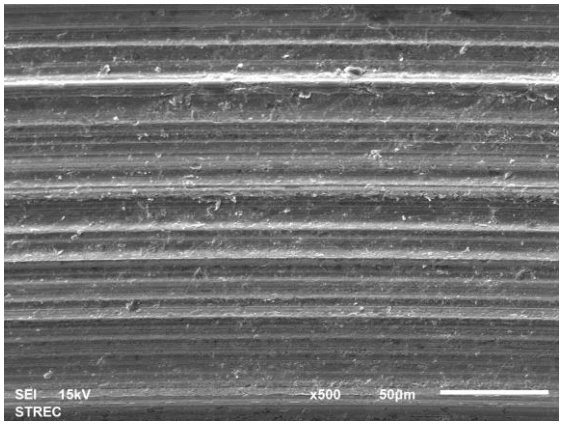

(b) The engine oil containing CB N220.

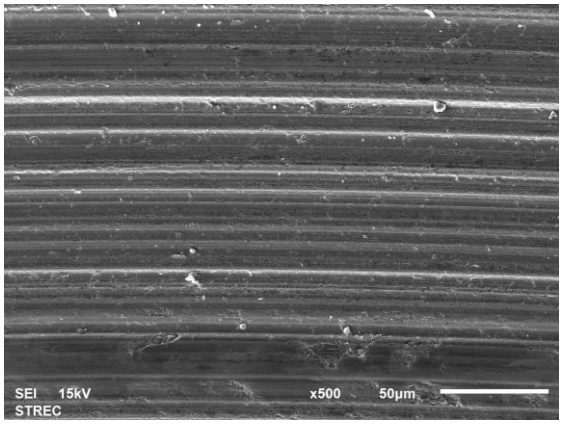

(c) The engine oil containing CB N330.

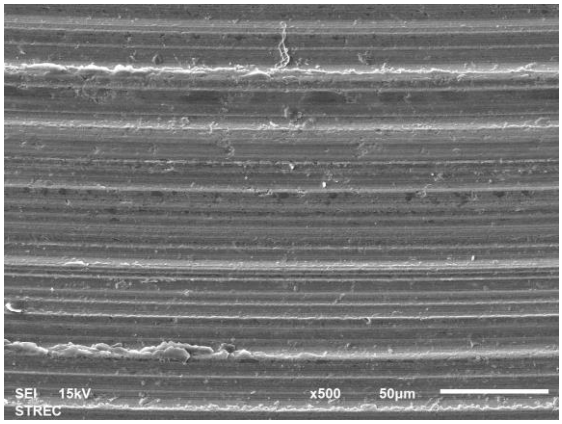

(d) The engine oil containing CB N550.

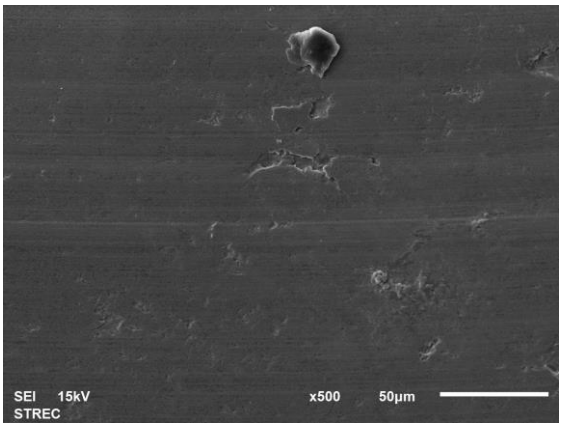

(e) The engine oil containing CB N660.

Figure 4. 27 SEM micrographs of the third lower balls at 500 magnification.

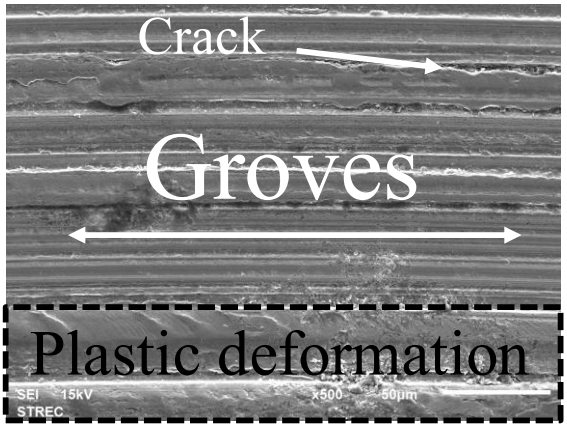

(a) The engine oil without soot

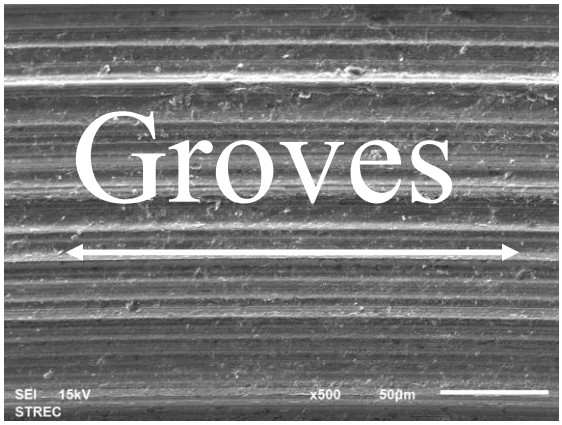

(b) The engine oil containing CB N220.

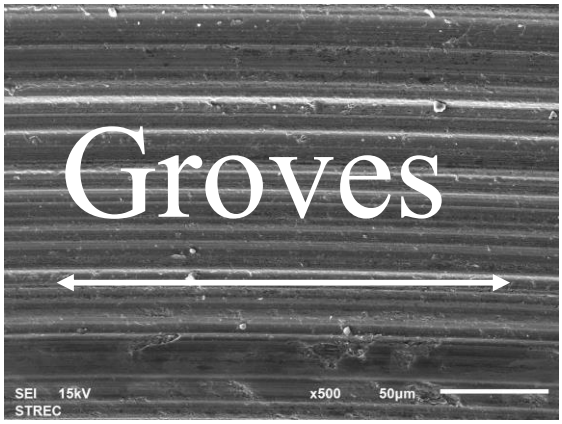

(c) The engine oil containing CB N330.

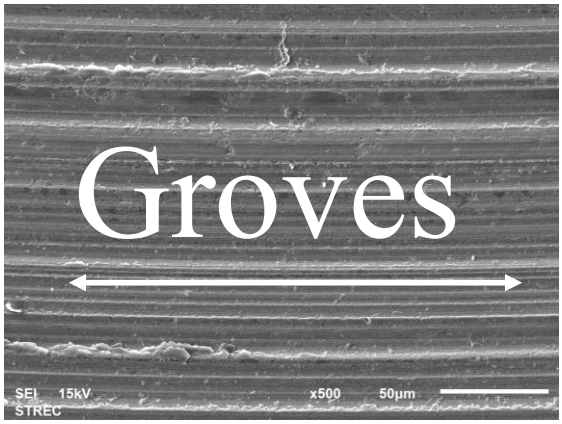

(d) The engine oil containing CB N550.

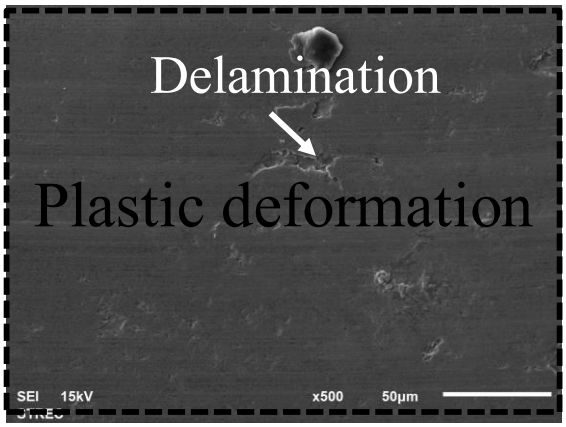

(e) The engine oil containing CB N660.

Figure 4. 28 SEM micrographs of the third lower balls with wear description.

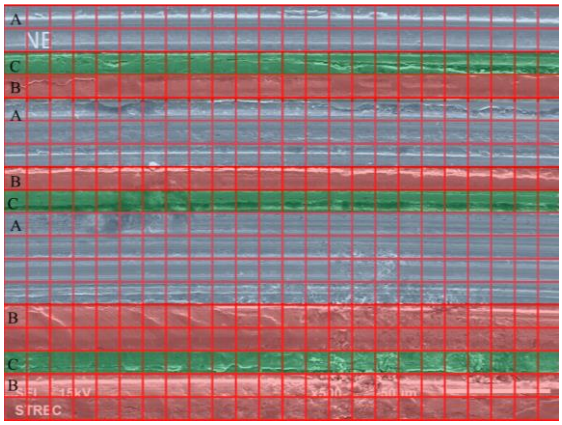

(a) The engine oil without soot

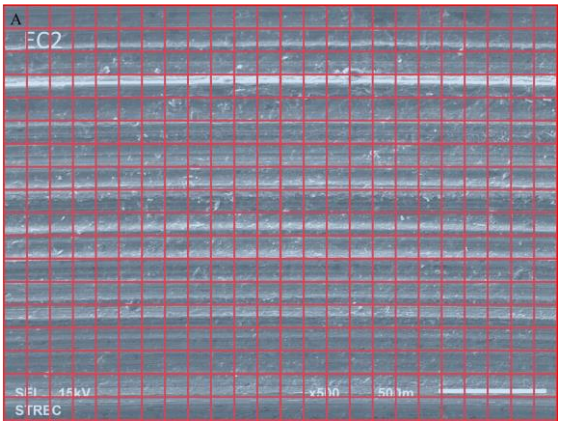

(b) The engine oil containing CB N220.

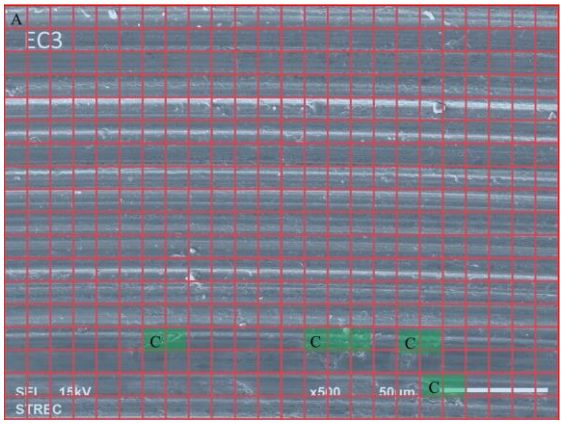

(c) The engine oil containing CB N330.

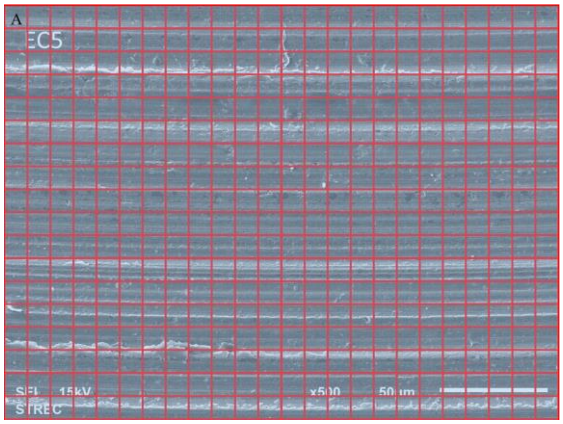

(d) The engine oil containing CB N550.

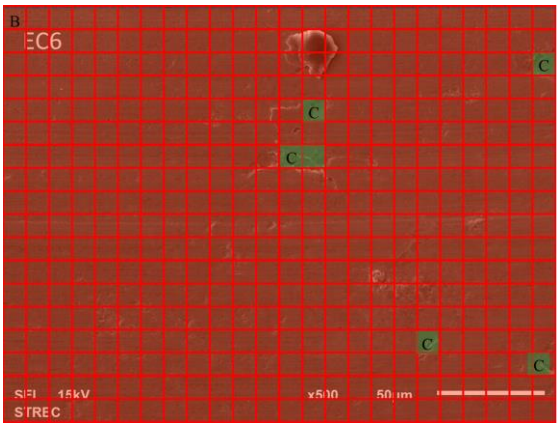

(e) The engine oil containing CB N660.

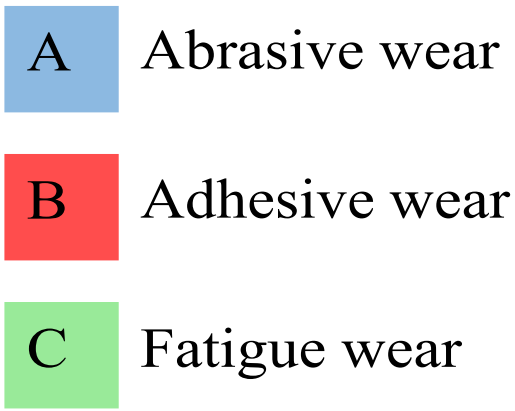

Figure 4. 29 SEM micrographs of the first lower balls with colored wear analysis.

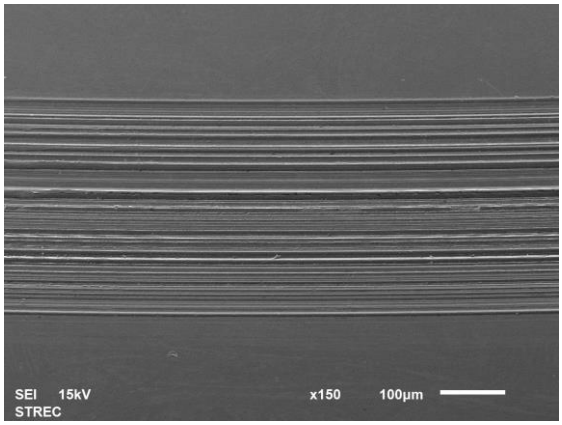

(a) The engine oil without soot

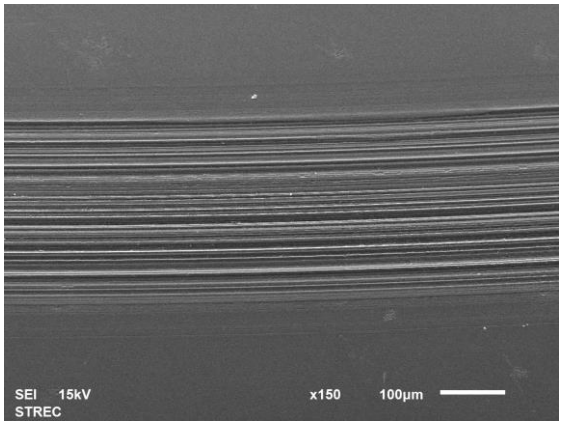

(b) The engine oil containing CB N220.

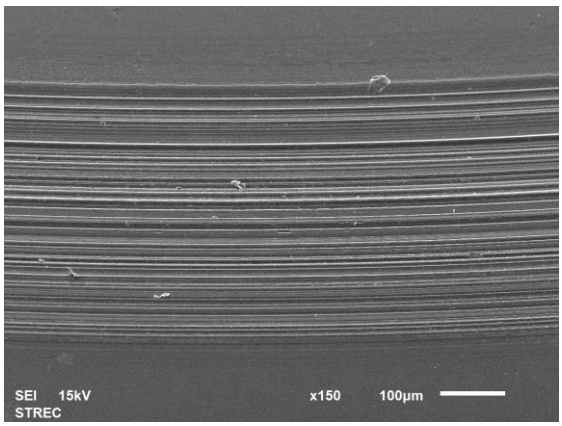

(c) The engine oil containing CB N330.

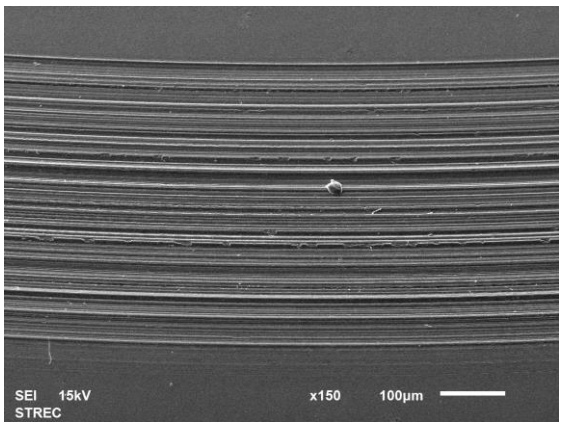

(d) The engine oil containing CB N550.

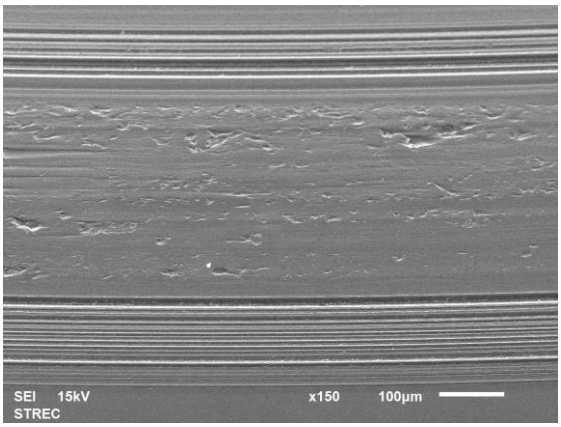

(e) The engine oil containing CB N660.

Figure 4. 30 SEM micrographs of the fourth upper balls at 150 magnification.

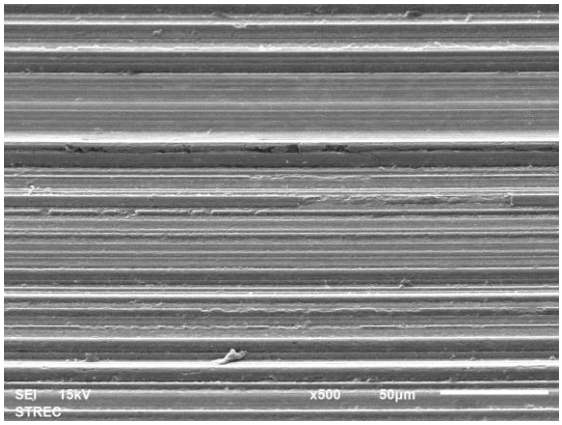

(a) The engine oil without soot

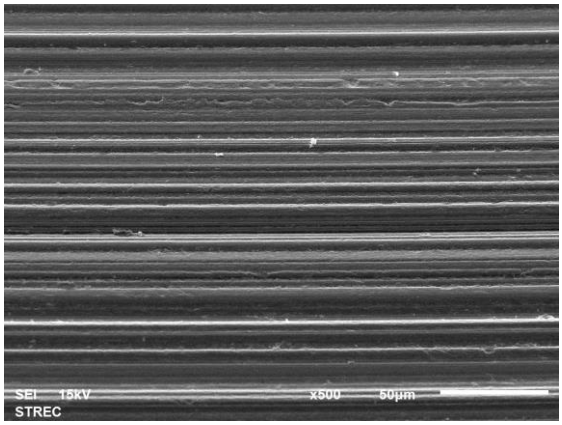

(b) The engine oil containing CB N220.

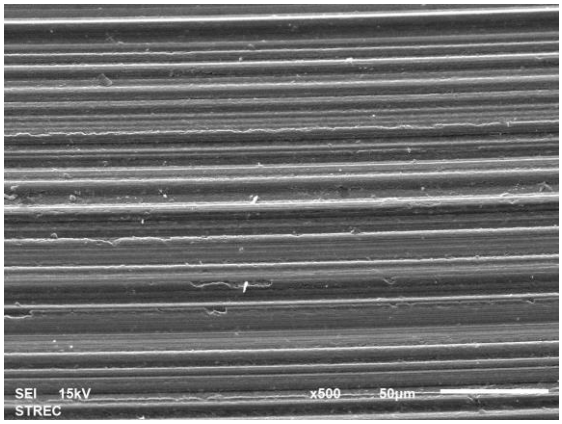

(c) The engine oil containing CB N330.

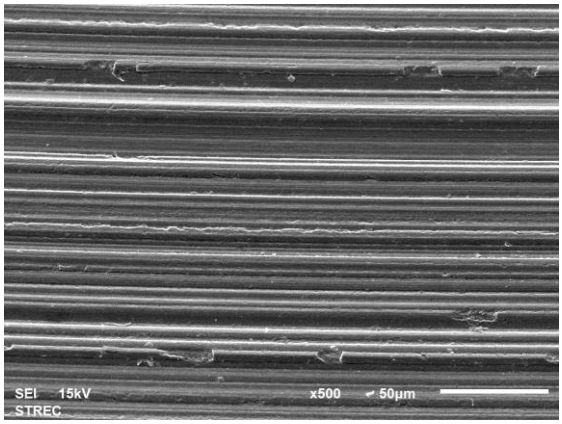

(d) The engine oil containing CB N550.

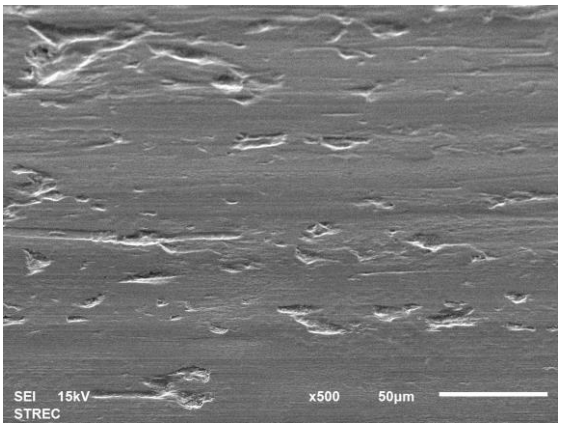

(e) The engine oil containing CB N660.

Figure 4. 31 SEM micrographs of the fourth upper balls at 500 magnification.

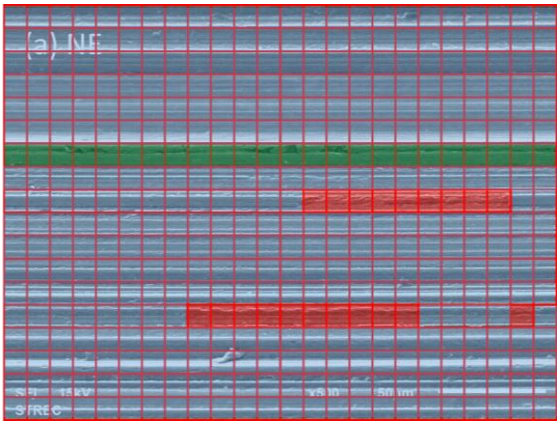

(a) The engine oil without soot

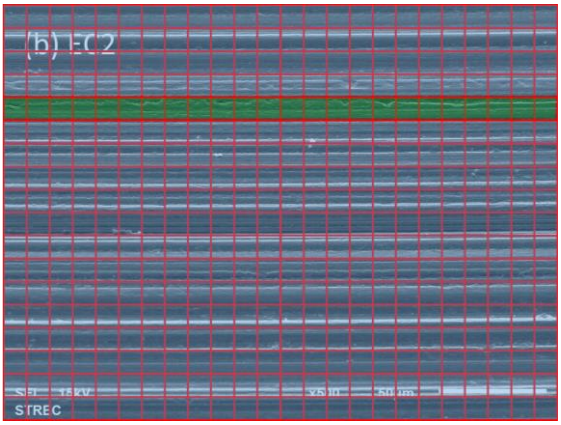

(b) The engine oil containing CB N220.

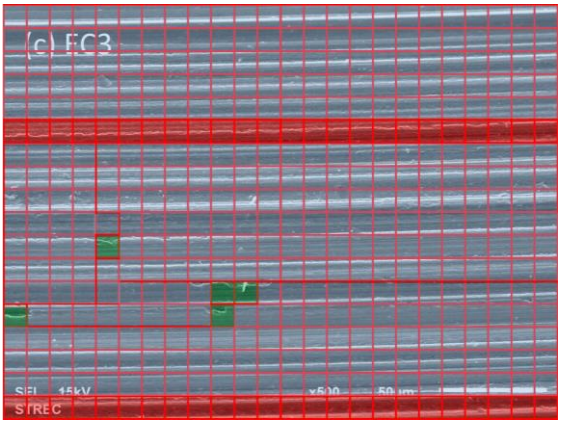

(c) The engine oil containing CB N330.

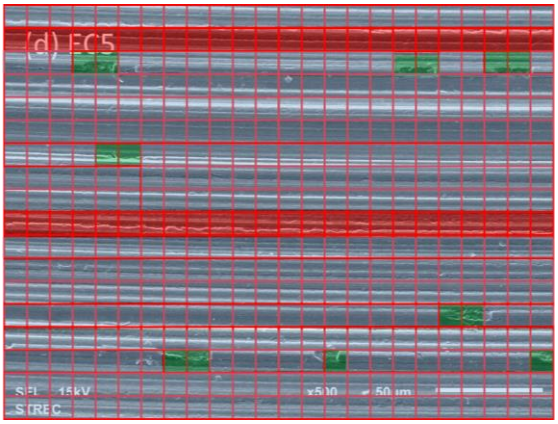

(d) The engine oil containing CB N550.

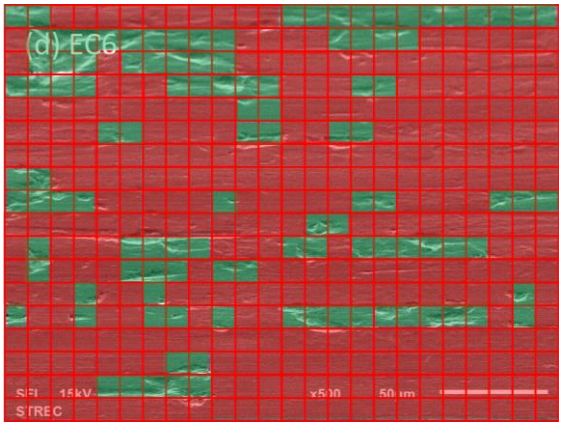

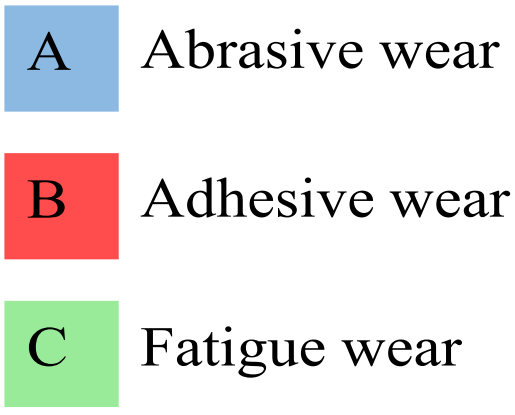

(e) The engine oil containing CB N660.

Figure 4. 32 SEM micrographs of the first lower balls with colored wear analysis.

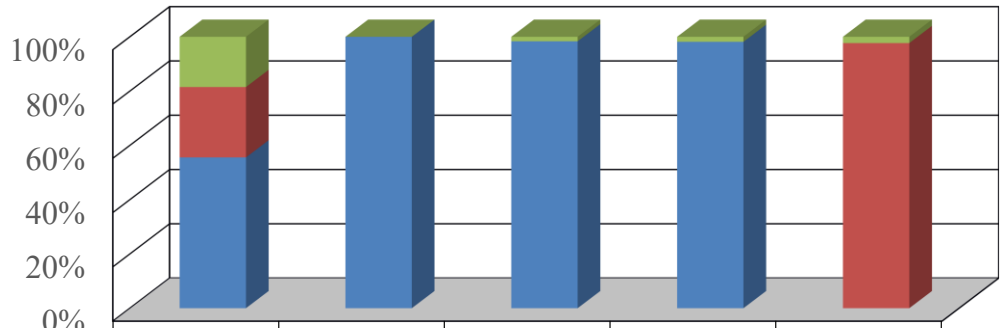

	NE	EC2	EC3	EC5	EC6
Fratigue	19	0	2	2	2
Adhesive	26	0	0	0	98
Abrasive	56	100	98	98	0

(a) Average wear mechanisms of the three stationary ball

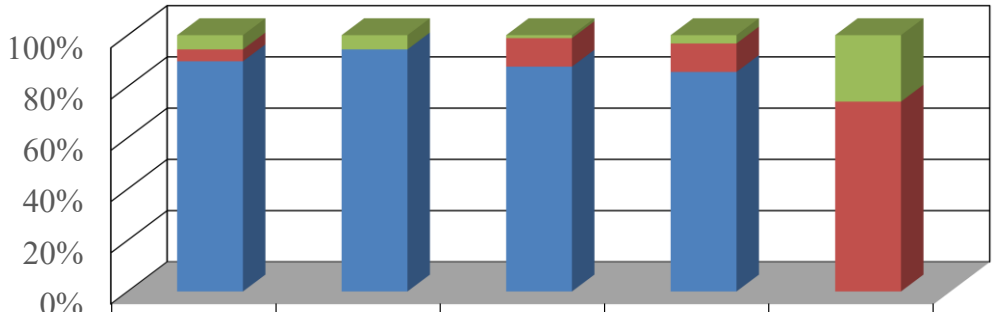

	NE	EC2	EC3	EC5	EC6
Fratigue	6	6	1	3	26
Adhesive	5	0	11	11	74
Abrasive	90	94	88	86	0

(b) Wear mechanisms of the rotating ball

Figure 4. 33 Wear mechanisms qualitatively analysis of (a) the three stationary balls and (b) the rotating ball.

Figure 4.33 show Wear mechanisms qualitatively analysis found on (a) the three stationary balls and (b) the rotating ball of the engine oil without soot and engine oil containing 1% wt. of N220, N330, N550 and N660 Carbon Black. The predominant wear mode of soot contaminated engine oil was abrasive wear. In the test oil with the highest soot primary particle size (CB N660), wear also occurred by a scuffing mechanism in addition to the adhesive wear mechanism.

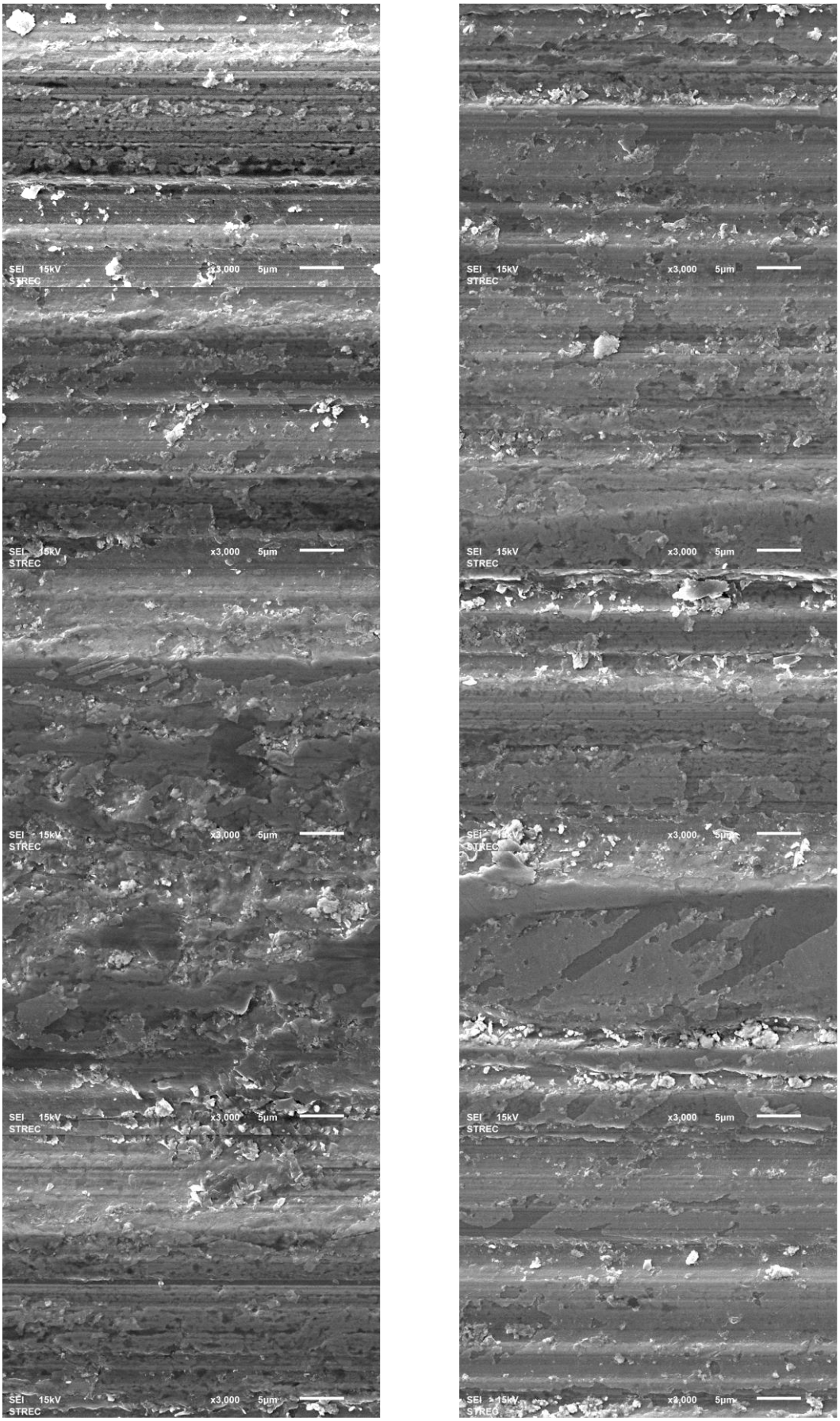

Figure 4. 34 SEM micrographs at 3,000 magnification of the NE.

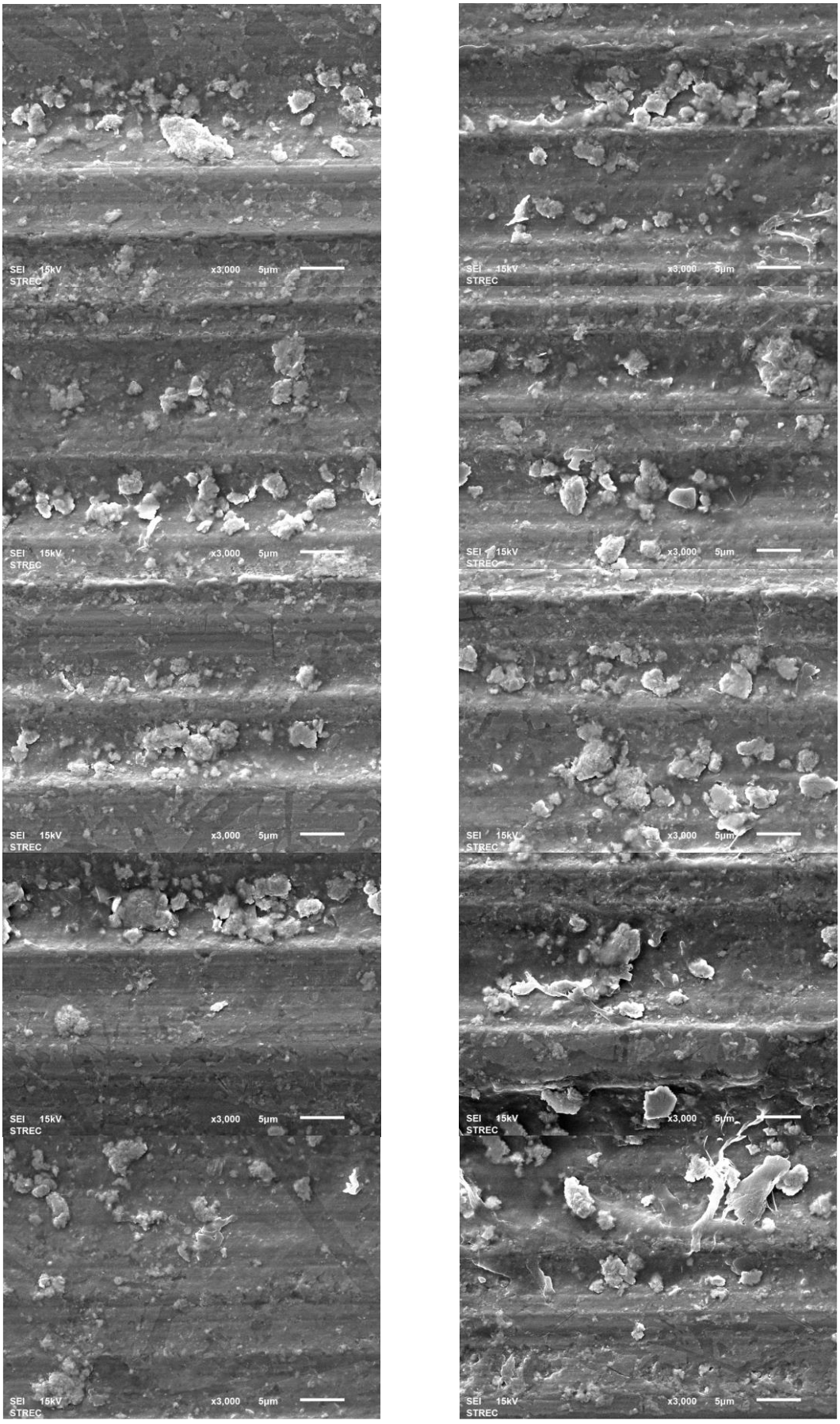

Figure 4. 35 SEM micrographs at 3,000 magnification of the EC2.

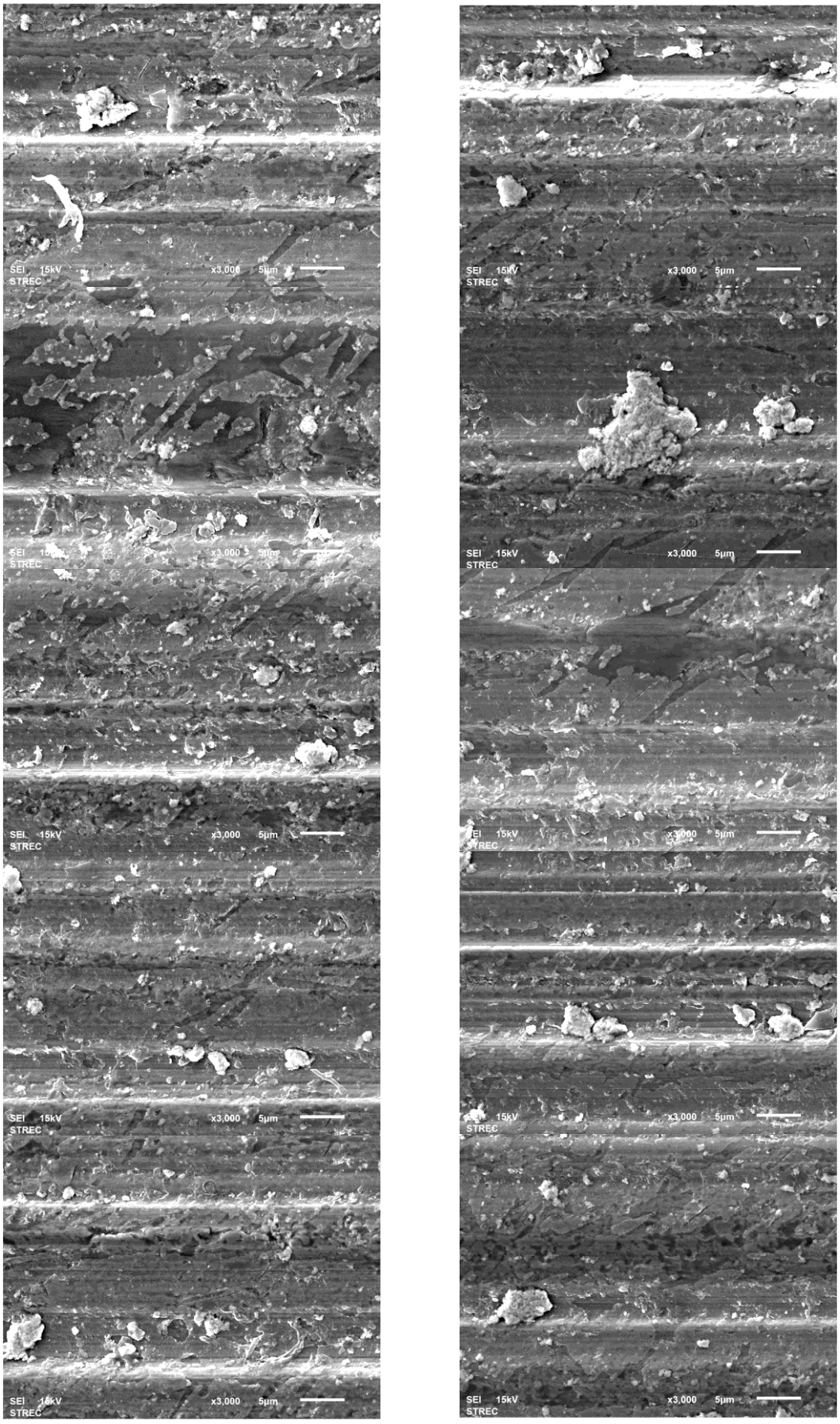

Figure 4. 36 SEM micrographs at 3,000 magnification of the EC3.

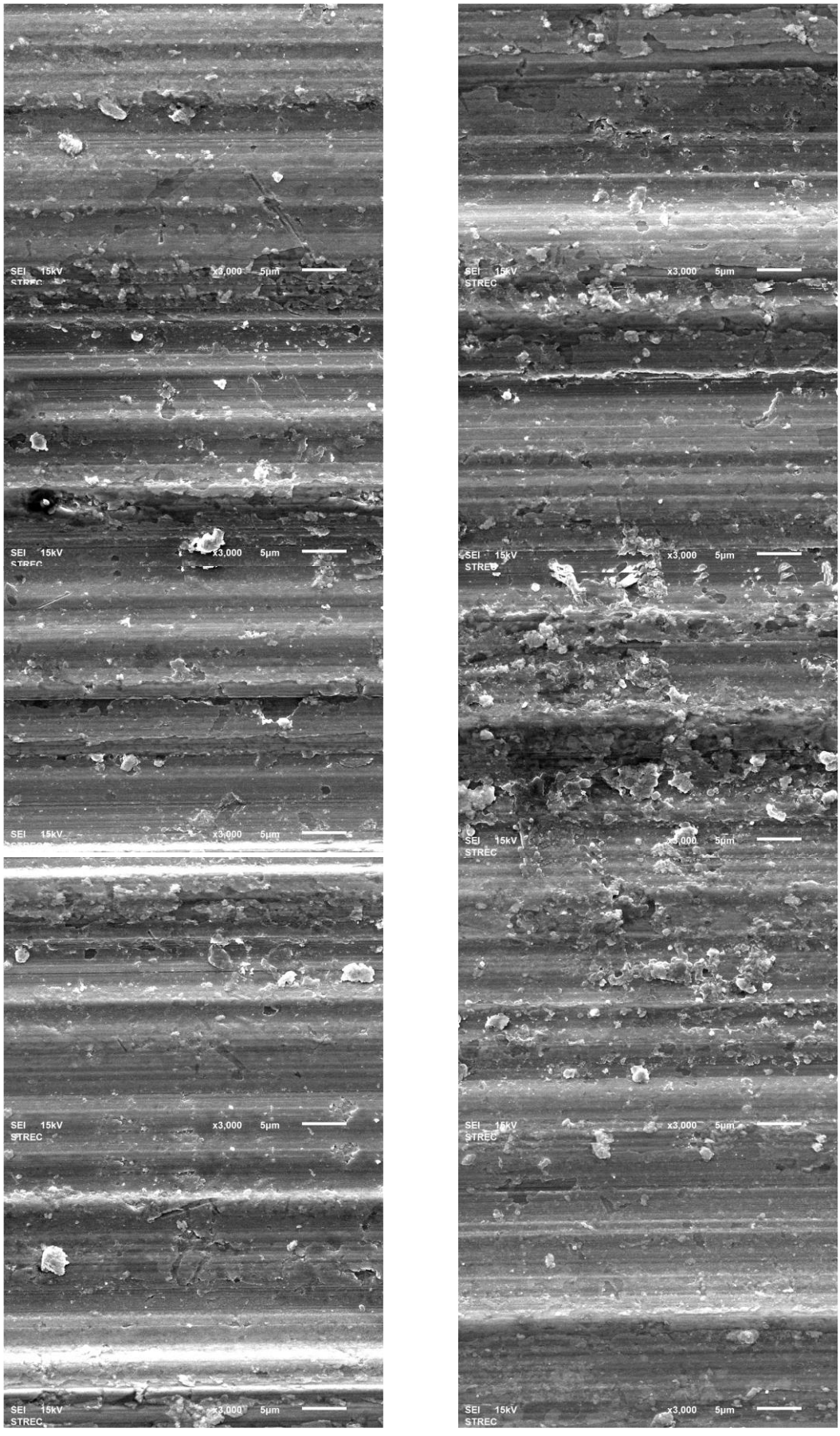

Figure 4. 37 SEM micrographs at 3,000 magnification of the EC5..

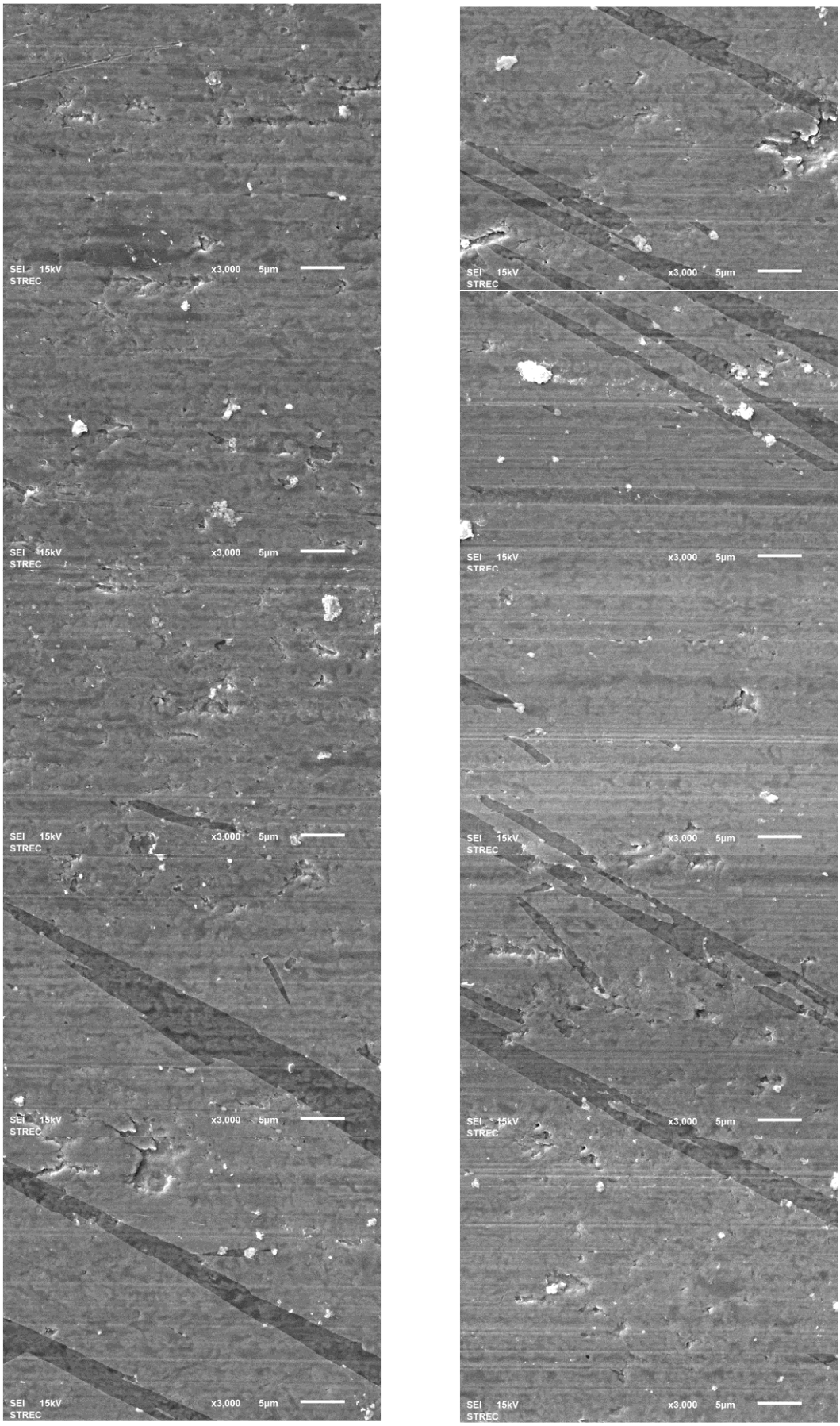

Figure 4. 38 SEM micrographs at 3,000 magnification of the EC6.

4.7.2 Analysis of worn surfaces by EDX

The surface morphologies of the wear zones of steel test samples were observed with SEM/EDX system to determine whether the simulated soot particulates would promote the wear. Figure 4.35-39 show SEM micrographs and EDX mapping at 500 magnification of the wear scar found on the ball of the engine oil without soot and engine oil containing 1% wt. of N220, N330, N550 and N660 Carbon Black, espectively. Moreover, Figure 4.40, shows SEM micrographs and EDX spectra of each oil samples. The results of the qualitative EDX analysis are shown in bar chart as shown in Figure 4.41. Elements on the ball surfaces are iron, carbon and chromium. The element of the NE clearly shows the oil deposit and additives element which are carbon, Zinc, calcium, and sulphur. When carbon black is added to the oil, it is clearly seen the carbon and sulphur on the ball worn surfaces. The carbon content on the EC2 shows the highest value and it decrease as the size of the carbon black increases. Soot small particle can easy get into the contact and deposit on ball surface. On the other hand, It is very difficult for Soot with larger particle to get into that contact then the carbon content on the surface decrees.

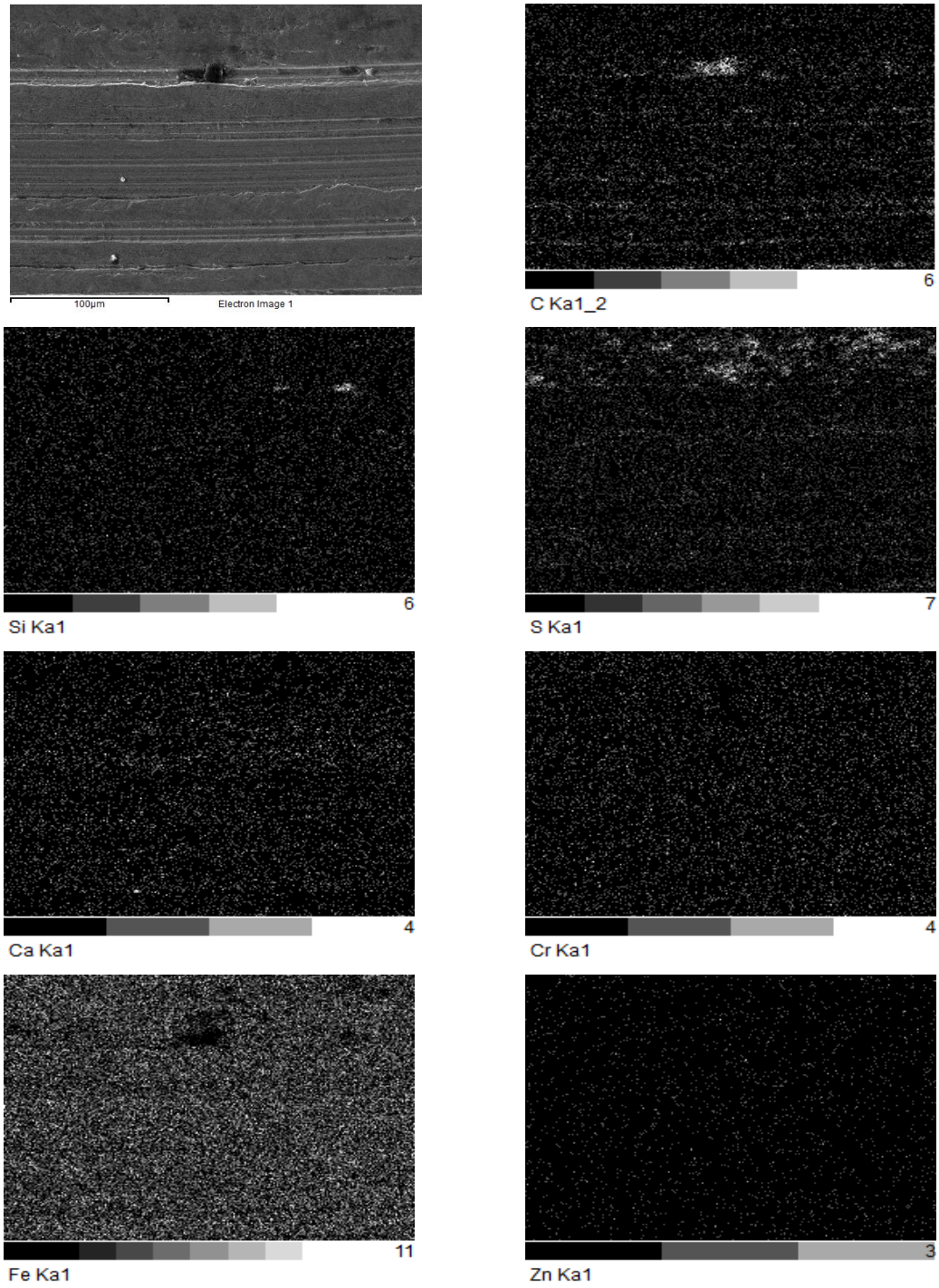

Figure 4. 39 SEM micrographs and EDX mapping at 500 magnification of the wear scar found on the ball of the engine oil without soot.

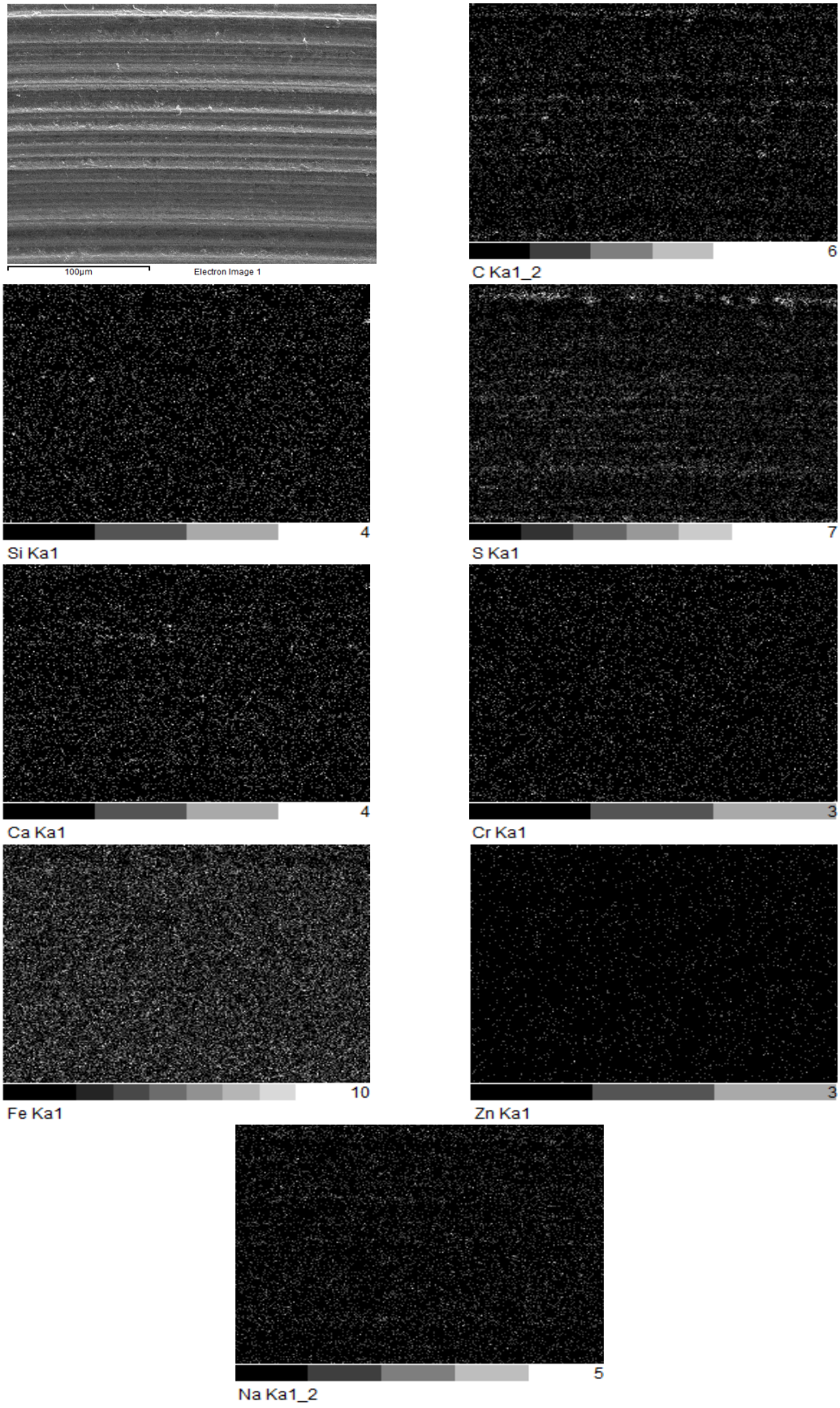

Figure 4. 40 SEM micrographs and EDX mapping at 500 magnification of the wear scar found on the ball of the engine oil containing 1% wt. of CB N220.

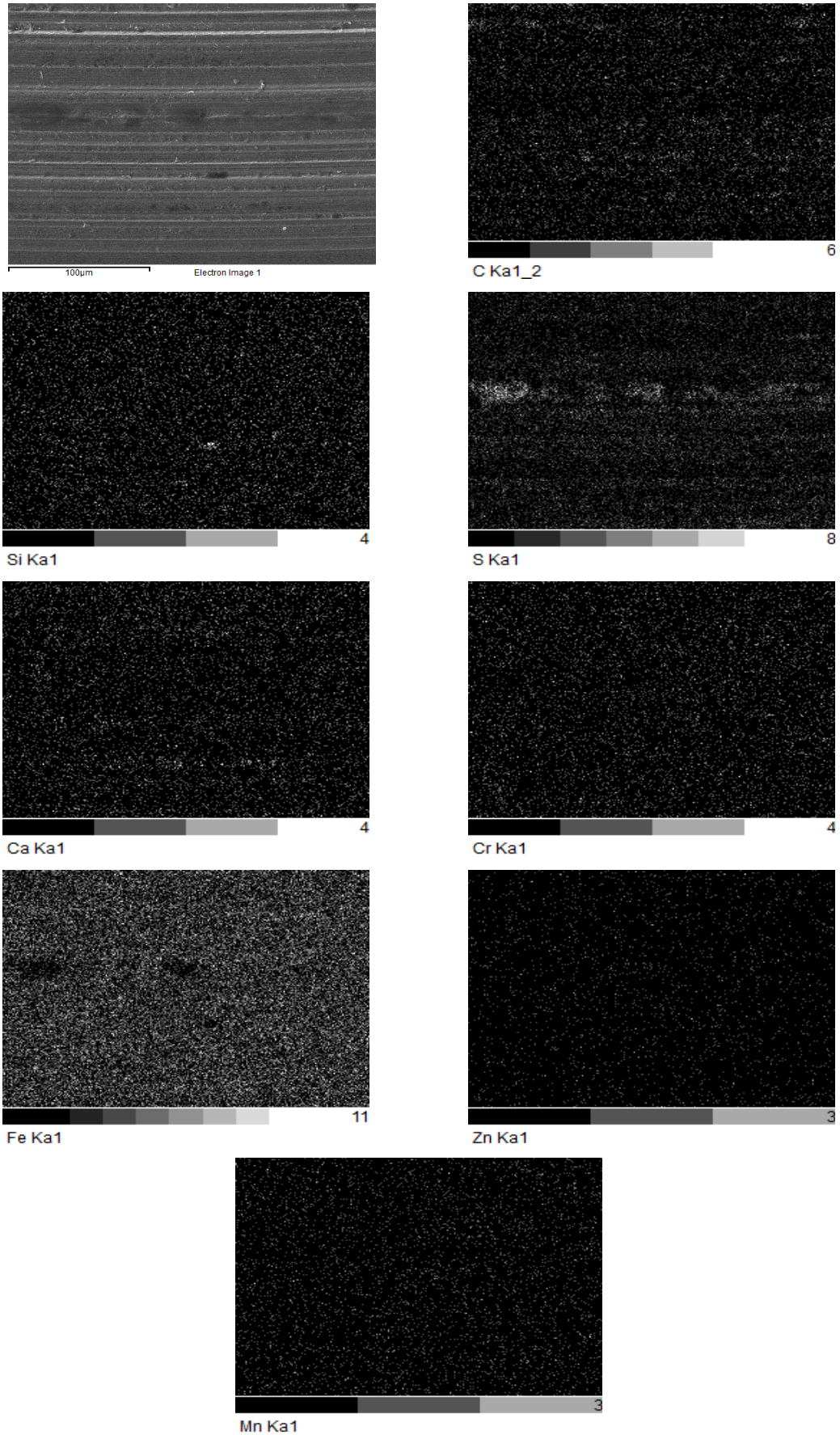

Figure 4. 41 SEM micrographs and EDX mapping at 500 magnification of the wear scar found on the ball of the engine oil containing 1% wt. of CB N330.

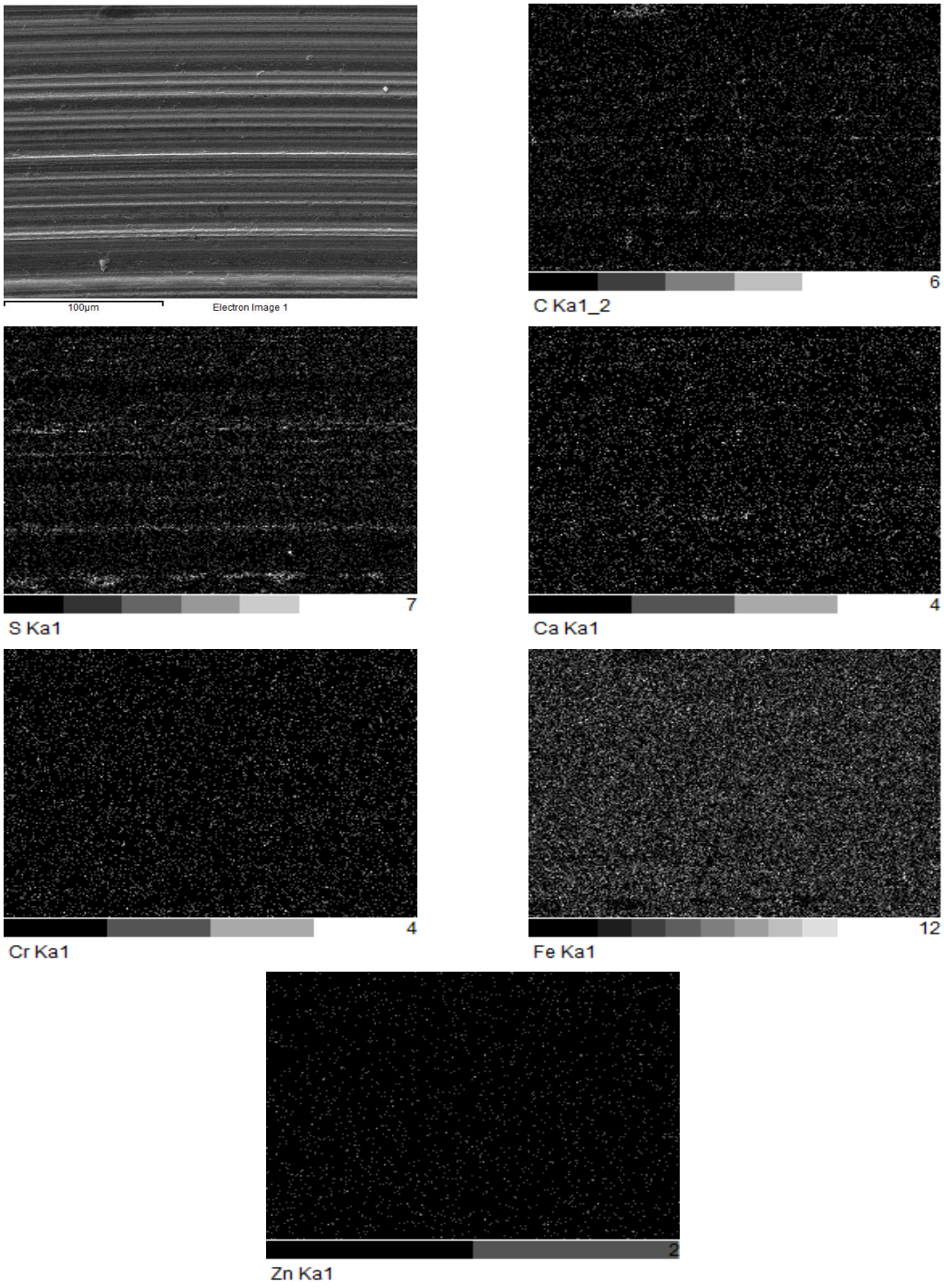

Figure 4. 42 SEM micrographs and EDX mapping at 500 magnification of the wear scar found on the ball of the engine oil containing 1% wt. of CB N550.

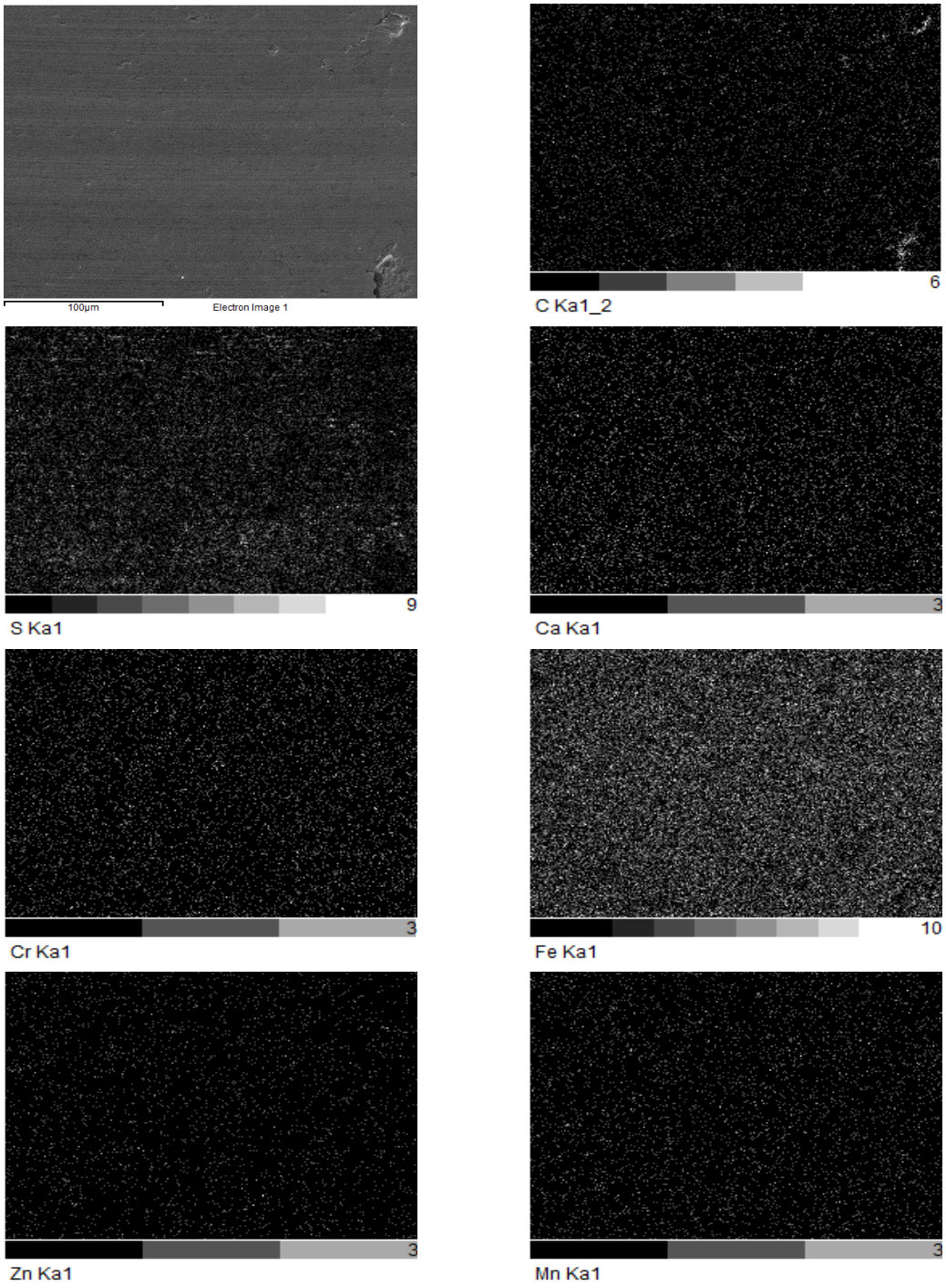

Figure 4. 43 SEM micrographs and EDX mapping at 500 magnification of the wear scar found on the ball of the engine oil containing 1% wt. of CB N660.

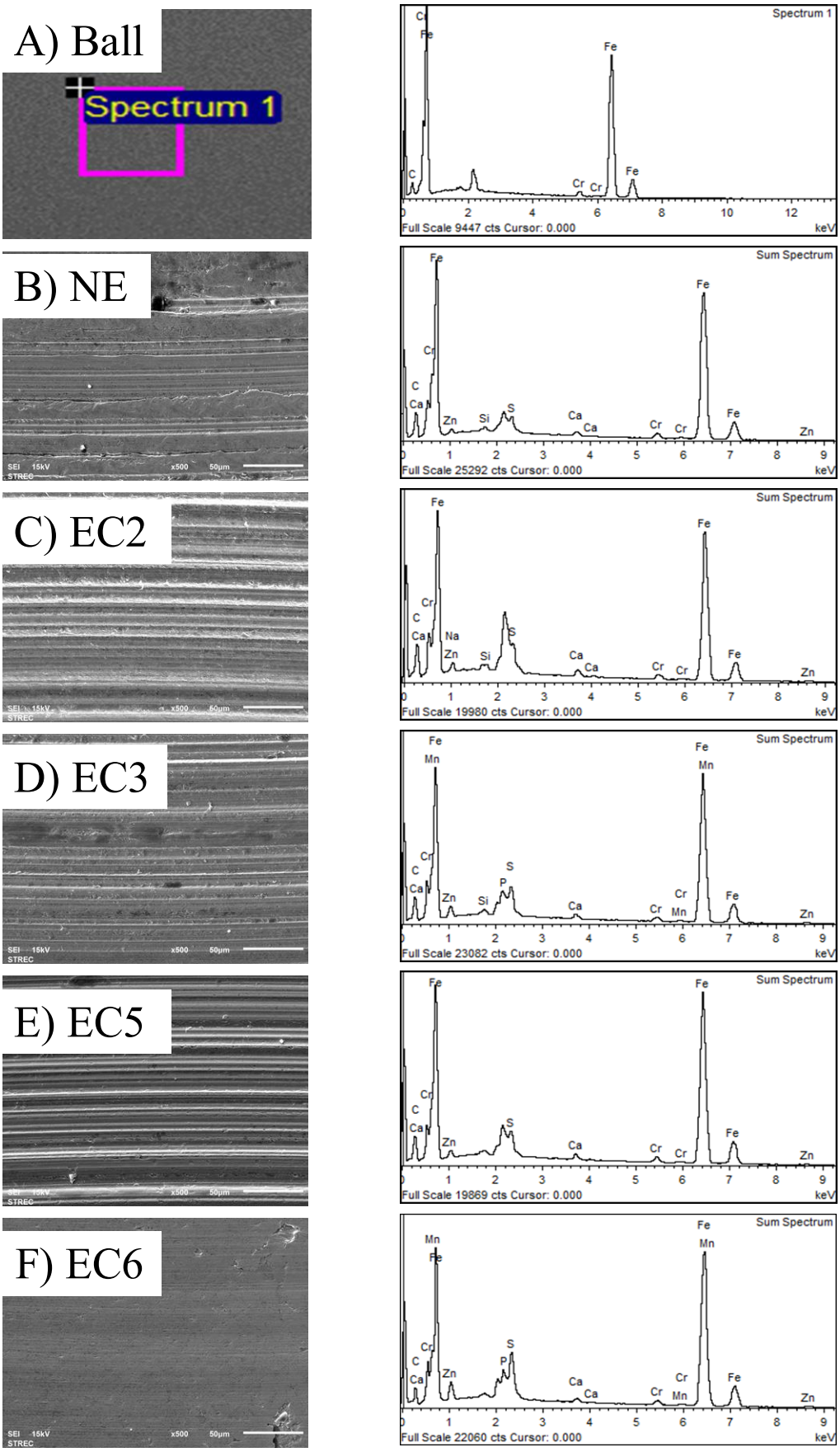

Figure 4. 44 SEM micrographs and EDX spectra of (a) ball surface and (b) the engine oil without soot and the engine oil containing 1% wt. of (c) CB N 220, (d) CB N330, (e) CB N550 and (f) CB N660.

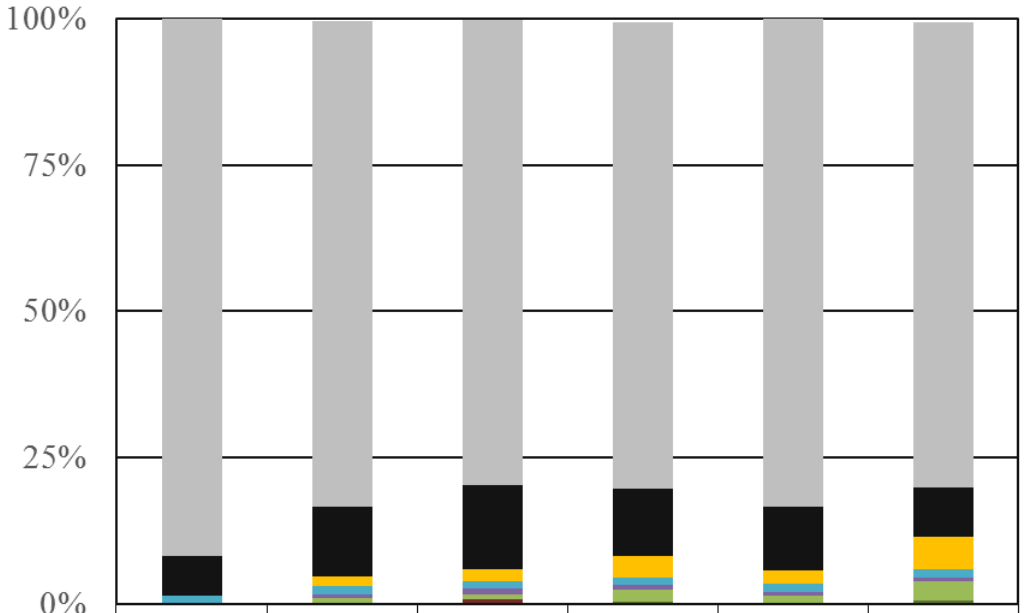

	Ball surface	NE	EC2	EC3	EC5	EC6
Fe	91.81%	83.12%	79.43%	79.79%	83.52%	79.50%
C	6.79%	11.75%	14.37%	11.52%	10.77%	8.34%
Zn	0.00%	1.77%	2.08%	3.75%	2.22%	5.66%
Cr	1.41%	1.43%	1.29%	1.25%	1.43%	1.29%
Ca	0.00%	0.63%	0.96%	0.68%	0.75%	0.57%
S	0.00%	0.92%	0.86%	2.05%	1.31%	3.48%
Na	0.00%	0.00%	0.73%	0.00%	0.00%	0.00%
Mn	0.00%	0.00%	0.00%	0.42%	0.00%	0.45%

Figure 4. 45 Qualitative EDX analysis of ball surface and the engine oil without soot and the engine oil containing 1% wt. of CB N 220, CB N330, CB N550 and CB N660.

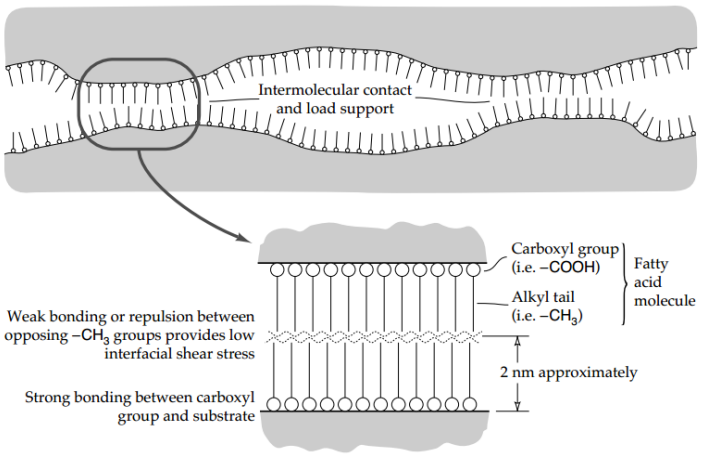

Figure 4. 46 Model of boundary film lubrication [5].

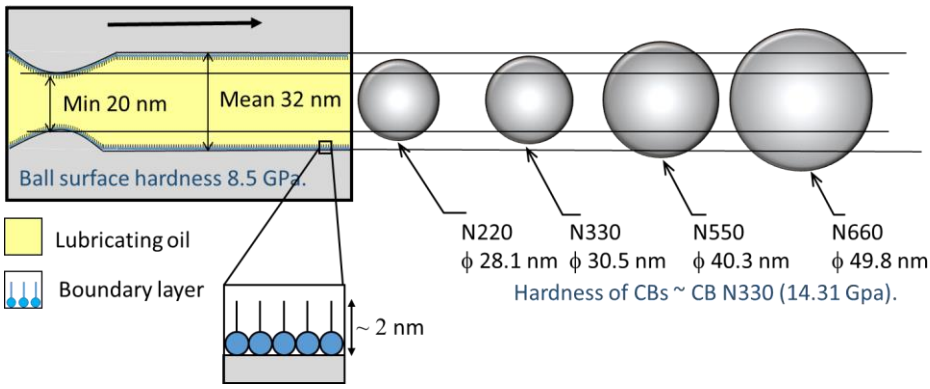

Figure 4. 47 Model description of soot primary nanoparticles induces metallic wear.

Figure 4.46 shows the model of boundary lubrication by oiliness additive [1]. From the Engineering Tribology [1] , boundary lubrication is defined as the formation of low friction protective layer on the wearing surfaces. These mechanisms are usually controlled by additive present in the oil. The best boundary lubricant are long chain molecules with an active end group typically fatty acids. These consist if hydrocarbon backbone of carbon atoms and active end group. Additionally, the length of the boundary lubrication is approximately 2 nm.

Figure4 . 4 7 shows the Model according to the theory of EHL as well as the boundary layer lubrication. The minimum and mean oil film thickness of the test engine oil under 75 ℃ are 32 and 20 nm, respectively. The typical length of boundary layer is approximately 2 nm. The average size of carbon black N220, N330, N550 and N660 measured by TEM are 28, 30, 40 and 50 nm, respectively. The calculated soot hardness of N330 by image processing is about 14 GPa which is much higher than that of steel ball. Soot particle can increase the rate of wear because it is large in comparison with the oil film and its hardness is much higher than that of the steal ball. When the size of CB is much higher than the oil film it might block the lubricant into the contract which lead to the breakdown of the oil film thickness. The direct metal to metal contact generates the strong adhesive fore that may smoothen or roughen the worn surfaces.

CHAPTER 5
CONCLUSION

In order to investigate the effect of soot Nano particle sizes on metallic wear. The different types of commercial carbon blacks (CB) which have different primary particle sizes were mixed with the engine oil at 1% by weight per volume. There were CB N220, N330, N550 and N660. Theirs primary particle size measured by TEM were 28, 30, 40, 50 nanometers, respectively. From the previous study, the primary particle size of the diesel and biodiesel are 27 and 30 nm, respectively. That means in this research the CN N220 is used to represent Biodiesel soot on the other hand N 330 is used to represent diesel soot.

The high resolution TEM image is used to calculated carbon atom density by image processing method. The concept of estimation is that “The molecules of carbon-six is the possible smallest size. Such molecules are agglomerate to be the large ring and then become carbon platelet “. After that, the carbon atom density is used to calculate the soot hardness by using the relationship between the carbon atom density and mechanical hardness of the diamond like carbon and diamond. The results show that the hardness of the Biodiesel, CB and Diesel are above 1,000 kilogram per square millimeter which are much higher than that the steel ball (8.5 GPa.). The lubricant oil film is calculated using EHL equation. The calculated mean oil film thickness is about 32 nm and it is 20 nm for minimum oil film thickness.

Base on four ball wear test, the 1% by weight of CB contamination (CB N220, N330, N550 and N660) shows 14% high average WSD compare to the pure SAE0W30 engine oil, but the surface roughness was 22 % lower than the engine oil alone. Soot particle could be increase the rate of wear because it was large in comparison with the oil film and its hardness was higher than that of the steel ball. Soot wear mechanisms might be expected as three body abrasive wear. Moreover, in case of CB N660, soot particle was much larger than the oil film thickness. So, that it might be block the lubrication inlet to the contact, therefore resulting in unlubricated sliding wear which causes the largest wear scar diameter. Analysis of wear echanisms shows that CB contamination generates abrasive wear, although when CB N660 is added to the oil, there is an evidence of the lubricating oil starvation which is the cause of adhesive scuffing wear.

REFERENCES

[1] M. Torbacke, Å. K. Rudolphi and E. Kassfeldt, Lubricants: Introduction to Properties and Performance, United Kingdom: John Wiley & Sons Ltd, 2014.

[2] D. A. Green and R. Lewis, "The effects of soot-contaminated engine oil on wear and," *IMechE,* vol. 222, 2008.

[3] T. C. Jao, S. Li, K. Yatsunami, S. J. Chen, A. A. Csontos and J. M. Howe, "Soot Characterisation and Diesel engine wear," in *Proceedings International Tribology*, 2004.

[4] S. N. Nayak and P. A. Lakshminarayanan, Critical Component Wear in Heavy Duty Engine, John Wiley & Sons (Asia) Pte Ltd, 2011.

[5] G. W. Stachowiak and A. W. Batchelor, ENGINEERING TRIBOLOGY, ELSEVIER, 1993.

[6] K. G. Budinski, Friction, wear, and erosion atlas, CRC Press, 2014.

[7] W. Tuszynski and M. Szczerek, "Qualitative discrimination between API GL performance levels of manual transmission fluids by comparing their EP properties determined in a new four-ball scuffing test," *Tribology International,* pp. 57-73, 2013.

[8] S. Q. A. Rizvi, A Comprehensive Review of Lubricant Chemistry, Technology, Selection, and Design, Baltimore: ASTM stock number: MNL59, 2009.

[9] T. Corporation, "Typical ferrographic wear particles," 2017. [Online]. Available: https://www.tricocorp.com. [Accessed 2017].

[10] Focuslab, "Oil Analysis-level 2," 2016.

[11] "Schematics of scanning electron microscopy operation," [Online]. Available: http://li155-94.members.linode.com/myscope/sem/practice/principles/layout.php. [Accessed 2017].

[12] " Particle Analytical, Laser diffraction theory," http://particle.dk/methods-analytical-laboratory/particle-size-by-laserdiffraction/laser-diffraction-theory, 2017.

[13] M. Maricq, "Review Chemical Characterization of particulate emissions from," *Journal of Aerosal Science,* 2007.

[14] K. Siricholathum, P. Karin, C. Charoenphonphanich, K. Hanamura and N. Chollacoop, The impact of biodiesel particulate matter morphology and oxidation kinetic on filter trapping and regeneration mechanism, Master degree thesis KMITL, 2015.

[15] P. Watanawongskorn, P. Karin, K. Hanamura and N. Chollacoop, Impact of morphology and nanostructure on particulate matter's oxidation kinetics from biofuel combustion, Master degree thesis KMITL, 2017.

[16] C. Supanamok, P. Karin, C. Benyajati and K. Hanamura, impact of soot contamination on metal wear and oil properties using four-ball tribology test, Master degree thesis KMITL, 2015.

[17] P. Kamsrisuk, P. Karin, K. Sriprapha and H. Kosaka, An Investigation on Physical and Chemical Properties in Used Lubricating Oil of Diesel Engine, Master degree thesis KMITL, 2016.

[18] F. G. Round, "Carbon: Cause of diesel engine wear?," *SAE Technical Paper,* 1977.

[19] P. R. Ryason, I. Y. CHAN and J. T. GILMORE, "Polishing wear by soot," *Symposium on Selective Catalytic Oxidation of Hydrocarbons,* 1990.

[20] M. Gautam, K. Chitoor, M. Durbha and J. C. Summers, "Effect of diesel soot contaminated oil on engine wear — investigation of novel oil formulations," *Tribology International 32,* 1999.

[21] H. Sato, N. Tokuoka, H. Yamamoto and M. Sasaki, "Study on Wear Mechanism by Soot Contaminated in Engine Oil (First Report: Relation Between Characteristics of Used Oil and Wear)," *SAE TECHNICAL PAPER SERIES 1999-01-3573,* 1999.

[22] S. Aldajah, O. O. Ajayi, G. R. Fenske and I. L. Goldblatt, "Effect of exhaust gas recirculation (EGR) contamination of diesel engine oil on wear," *Wear 263 ,* 2007.

[23] N. DATABASE, "Carbon Black," 2016. [Online]. Available: http://web.eng.nu.ac.th/eng2012/ceri/nanodatabase/info_index.php?cat_id=13.

[24] A. D. −. 94, "Standard Test Method for Wear Preventive Characteristics of Lubricating Fluid," 2016.

[25] "Schematics of transmission electron microscopy operation," [Online]. Available: http://www.hkphy.org/atomic_world/tem/tem02_e.html. [Accessed 2017].

[26] D. B. Kittelson, "Engines and nanoparticles: A review," *Aerosol Science,* vol. 29, 1998.

[27] P. Karin, j. Boonsakda, k. Siricholathum, e. Saenkhumvong, c. Charoenphonphanich, n. Chollacoop and k. Hanamura, "Morphology and Oxidation Kinetics of CI Engine's Biodiesel Particulate Matters on Cordierite Diesel Particulate Filters using TGA," *International Journal of Automotive Technology.*

[28] P. KARIN, M. BORHANIPOUR, Y. SONGSAENGCHAN, S. LAOSUWAN, C. CHAROENPHONPHANICH, N. CHOLLACOOP and K. HANAMURA, "oxidation kinetics of small ci engine's biodiesel particulate matter," *International Journal of Automotive Technology,* vol. 16, no. 2, p. 211−219, 2015.

APPENDIX A
FOUR BALL REPORTS

InS Thai Ltd.
Thai-French Innovation Institute (8th Floor),
King Mongkut's University of Technology North Bangkok,
1518 Pracharat 1 Rd., Wongsawang, Bangsue, Bangkok 10800, Thailand.
Tel: +66 (0)2 585 9946, +66 (0)2 585 9964, +66 (0)2 585 9982, Fax: +66 (0)2 585 9951
www.ins-thai.com

ANALYSIS REPORT:
King Mongkut's Institute of Technology Ladkrabang
Four ball – Wear resistance according to ASTM D4172

Sample description	Lubricants
Customer Sample Reference	See table 1
Internal Sample Reference	See table 1
Date of Receipt	12/01/2017
Date of Analysis	12/01/2017-03/02/2017
Analysis Report Reference	R1701204KMI

TESTS & SAMPLES

TEST	STANDARD	CONDITIONS	CUSTOMER SAMPLE REF.	INTERNAL SAMPLE REF.
4-Ball Method	ASTM D4172	– *Rotational speed: 1200±10 rpm* – *Load: 392±2 N (40±2 kgf)* – *Duration per load: 60±1 min* – *Temperature: 75±2 °C*	See Table 1	See Table 1

Table 1: List of samples reference

Customer Reference	InS Thai Reference
SAEOW3O	S1701204KMI-01
N220	S1701204KMI-02
N330	S1701204KMI-03
N660	S1701204KMI-04
N550	S1701204KMI-05

InS Thai Ltd.
Thai-French Innovation Institute (8th Floor),
King Mongkut's University of Technology North Bangkok,
1518 Pracharat 1 Rd., Wongsawang, Bangsue, Bangkok 10800, Thailand.
Tel: +66 (0)2 585 9946, +66 (0)2 585 9964, +66 (0)2 585 9982, Fax: +66 (0)2 585 9951
www.ins-thai.com

SAMPLE PREPARATION & TESTING

According to the four balls testing standard (ASTM D4172), the samples are tested at 75°C. The normal load applied is 392 N. Running time is 60 minutes.

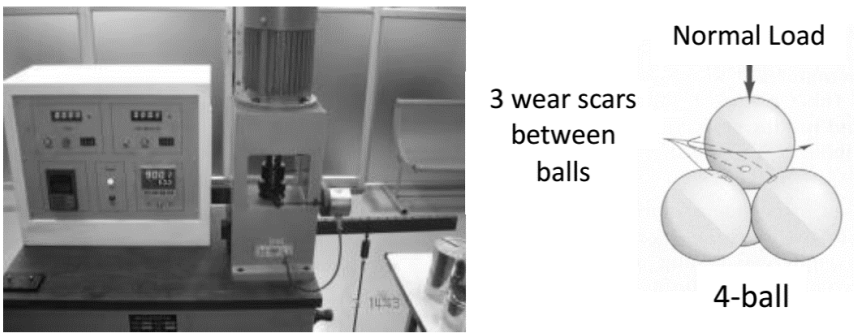

Figure 1: Four balls testing machine and direction of applied load

Figure 2: samples images received from the customer

After the test, the diameter of wear scar is measured by optical microscope at ×100 and ×200 magnifications. The wear scar diameters of the three lower balls are measured and the average values are calculated. The friction torque during the test is recorded every 5 minute and reported also.

RESULTS

Table 2 presents the wear scars diameter measured on the three lower balls. The variation of wear scar diameter is small indicating a good sample installation. Figure 3 shows the comparison of wear scar size between different samples.

Table 2: Wear scars diameter measured by microscope

Sample	Ball 1		Ball 2		Ball 3		Average (µm)	Ball 4			Average (µm)
	d_1 (µm)	d_2 (µm)	d_1 (µm)	d_2 (µm)	d_1 (µm)	d_2 (µm)		d_1 (µm)	d_2 (µm)	d_3 (µm)	
SAEOW30	546.29	546.06	543.12	543.30	543.12	543.30	**544.20**	550.58	550.68	550.68	**550.65**
N220	529.69	529.87	535.66	535.84	535.66	534.35	**533.51**	516.26	516.40	515.99	**516.22**
N330	546.29	546.06	546.29	544.61	547.60	547.78	**546.44**	603.62	603.41	603.16	**603.40**
N660	808.08	808.40	820.26	820.26	817.27	817.27	**815.25**	799.34	800.95	799.57	**799.95**
N550	582.73	596.14	606.60	579.63	599.13	605.14	**579.90**	573.73	573.38	569.89	**572.34**

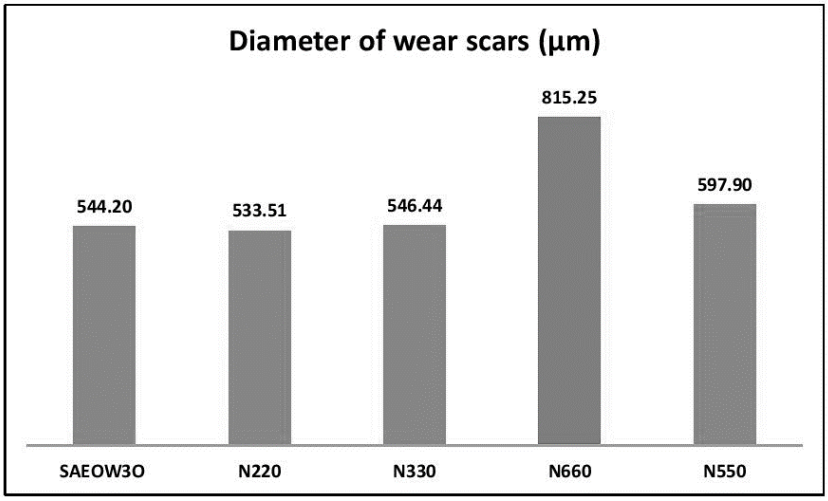

Figure 3: Average wear scar size of three lower balls after testing

InS Thai Ltd.
Thai-French Innovation Institute (8th Floor),
King Mongkut's University of Technology North Bangkok,
1518 Pracharat 1 Rd., Wongsawang, Bangsue, Bangkok 10800, Thailand.
Tel: +66 (0)2 585 9946, +66 (0)2 585 9964, +66 (0)2 585 9982, Fax: +66 (0)2 585 9951
www.ins-thai.com

Table 3 showed the mass loss of each ball after testing of all lubricant samples.

Table 3: Mass loss measured by high precision balance (4 digit)

Sample	Customer Reference		Weight (g)		
			Before	After	Weight loss (g)
Sample 1	SEAOW30	Ball 1	8.3506	8.3506	0.0000
		Ball 2	8.3550	8.3549	0.0001
		Ball 3	8.3530	8.3528	0.0002
		Ball 4	8.3524	8.3522	0.0002
Sample 2	N220	Ball 1	8.3548	8.3548	0.0000
		Ball 2	8.3508	8.3508	0.0000
		Ball 3	8.3533	8.3532	0.0001
		Ball 4	8.3543	8.3542	0.0001
Sample 3	N330	Ball 1	8.3540	8.3539	0.0001
		Ball 2	8.3521	8.3520	0.0001
		Ball 3	8.3549	8.3548	0.0001
		Ball 4	8.3542	8.3540	0.0002
Sample 4	N660	Ball 1	8.3546	8.3545	0.0001
		Ball 2	8.3522	8.3521	0.0001
		Ball 3	8.3546	8.3545	0.0001
		Ball 4	8.3535	8.3533	0.0002
Sample 5	N550	Ball 1	8.3515	8.3514	0.0001
		Ball 2	8.3536	8.3535	0.0001
		Ball 3	8.3512	8.3511	0.0001
		Ball 4	8.3525	8.3524	0.0001

General conclusion:

- The lowest and highest wear scar diameters were found on N220 and N660, respectively.
- The mass loss of each ball for all samples were less than or equal to 0.0002 g.

Prepared by:
Mr.Panumas Songvut
Miss. Alisa Jukra
R&D Scientist
Panumas Songvut
Alisa Jukra
2017-02-03

Approved by:
Dr. Pornsit Lorkit
Project Leader, Material Science Laboratory
Pornsit L.
2017-02-03

APPENDIX B
X-RAY FLUORESCENCE SPECTRA

Eval2 V2.5.500 Admin 3/16/2017 4:28:44 PM
Sample: 601503-9876-Mazda sae0w30
Measured on 3/15/2017 2:18:03 PM
Sample measured by Admin
Measurement method: Best Detection-He34mm

Sum	S	Ca	Zn	P	Mo	K
0.60 %	0.214 %	0.166 %	847 PPM	779 PPM	454 PPM	74.0 PPM

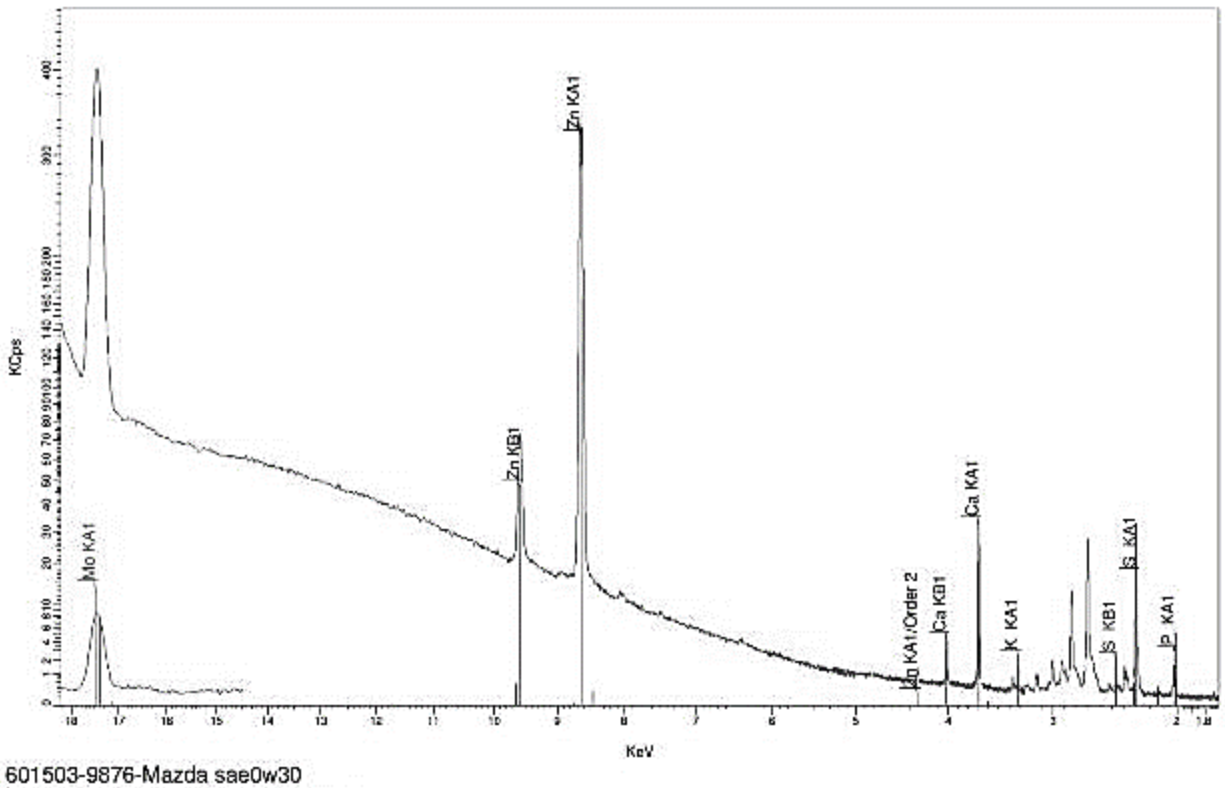

601503-9876-Mazda sae0w30
Eval2 V2.5.500 Admin 3/16/2017 4:28:02 PM

APPENDIX C
PARTICLE SIZE DISTRIBUTION

ศูนย์เครื่องมือวิจัยวิทยาศาสตร์และเทคโนโลยี จุฬาลงกรณ์มหาวิทยาลัย
อาคารสยามกัมมาจล ชั้น 3 ซอย 62 ถนนพญาไท เขตปทุมวัน กรุงเทพฯ 10330 โทร. (662) 218-8101, 218-8033 โทรสาร (662) 218-8101, 254-6911
SCIENTIFIC AND TECHNOLOGICAL RESEARCH EQUIPMENT CENTRE CHULALONGKORN UNIVERSITY
CHULALONGKORN SOI 62 PHAYA-THAI ROAD PHATUMWAN BANGKOK 10330 THAILAND TEL (662) 218-8101, 218-8033 FAX (662) 218-8101, 254-6911

Report No. 601601-3766 Page 1/1

Analysis Report

Sample: Carbon black
Sample owner: Warawut Amornprapa
International College King Mongkut's Institute of Technology Ladkrabang
Objective: To determine particle size distribution
Instrument: Laser Particle Size Analyzer (Mastersizer 3000)
Analysis date: February 6, 2017

Results (Refer also to data in the attached statistical results)

Sample name	Particle size (Micron)					
	Particle size distribution	Measured values			Mean	SD
		#1	#2	#3		
II	10 percentile, D(v,0.1)	0.2280	0.3640	0.4870	0.3597	0.1296
	50 percentile, D(v,0.5)	2.8100	3.0000	3.1200	2.9767	0.1563
	90 percentile, D(v,0.9)	8.5500	8.5900	8.3800	8.5067	0.1115
	Average D[4,3]	6.7600	6.9800	6.6500	6.7967	0.1680
III	10 percentile, D(v,0.1)	0.0184	0.0186	0.0190	0.0187	0.0003
	50 percentile, D(v,0.5)	0.3200	0.3500	0.3850	0.3517	0.0325
	90 percentile, D(v,0.9)	2.7200	2.9600	3.2000	2.9600	0.2400
	Average D[4,3]	0.8680	0.9620	1.0600	0.9633	0.0960
V	10 percentile, D(v,0.1)	0.0245	0.0255	0.0268	0.0256	0.0012
	50 percentile, D(v,0.5)	0.7620	0.8860	1.0400	0.8960	0.1393
	90 percentile, D(v,0.9)	10.4000	10.3000	10.1000	10.2667	0.1528
	Average D[4,3]	3.4000	3.4100	3.3800	3.3967	0.0153
VI	10 percentile, D(v,0.1)	0.0207	0.0215	0.0222	0.0215	0.0008
	50 percentile, D(v,0.5)	0.5020	0.5650	0.6400	0.5690	0.0691
	90 percentile, D(v,0.9)	4.8200	5.0800	5.2500	5.0500	0.2166
	Average D[4,3]	1.9400	1.9700	2.0400	1.9833	0.0513

(Miss Kaew Kajornchaiyakul) Analyst
(Mrs. Sunan Rangseekansong) Chief Scientist
(Assoc. Prof. Dr. Amorn Petsom) Director

ศูนย์เครื่องมือวิจัยวิทยาศาสตร์และเทคโนโลยี จุฬาลงกรณ์มหาวิทยาลัย
อาคารสยามบรมราชกุมารี ชั้น 3 ซอยจุฬาลงกรณ์ 62 ถนนพญาไท เขตปทุมวัน กรุงเทพฯ 10330 โทร. (662) 218-8101, 218-8023 โทรสาร (662) 218-8101, 254-0211
SCIENTIFIC AND TECHNOLOGICAL RESEARCH EQUIPMENT CENTRE CHULALONGKORN UNIVERSITY
CHULALONGKORN SOI 62 PHAYA THAI ROAD PATHUMWAN BANGKOK 10330 THAILAND TEL. (662) 218-8101, 218-8023 FAX : (662) 218-8101, 254-0211

Report No. 600902-1263

Analysis Report

Sample: Carbon blacks mixed with new sae0w30 engine oil
Sample owner: Warawut Amornprapa
International College King Mongkut's institute of technology ladkrabang
Objective: To determine particle size distribution
Instrument: Laser Particle Size Analyzer (Mastersizer 3000)
Analysis date: March 2-3, 2017

Result: (Refer also to data in the attached statistical results)

Sample name	Particle size (Micron)					
	Particle size distribution	Measured values #1	#2	#3	Mean	SD
Sample 1	No result of particle size distribution because the samples amount was not enough for the measurement.					
Sample 2	10 percentile, D(v,0.1)	0.6180	0.5060	0.5180	0.5473	0.0615
	50 percentile, D(v,0.5)	79.4000	75.9000	74.4000	76.5667	2.5658
	90 percentile, D(v,0.9)	218.0000	214.0000	217.0000	216.3333	2.0817
	Average D[4,3]	95.5000	92.8000	93.4000	93.9000	1.4177
Sample 3	10 percentile, D(v,0.1)	0.0288	0.0282	0.0282	0.0284	0.0003
	50 percentile, D(v,0.5)	33.4000	29.6000	29.3000	30.7667	2.2855
	90 percentile, D(v,0.9)	232.0000	217.0000	217.0000	222.0000	8.6603
	Average D[4,3]	83.6000	76.3000	77.2000	79.0333	3.9801
Sample 4	10 percentile, D(v,0.1)	0.0224	0.0226	0.0227	0.0226	0.0002
	50 percentile, D(v,0.5)	2.1300	2.8000	3.0800	2.6700	0.4882
	90 percentile, D(v,0.9)	163.0000	159.0000	161.0000	161.0000	2.0000
	Average D[4,3]	44.9000	44.3000	45.6000	44.9333	0.6506
Sample 5	10 percentile, D(v,0.1)	0.0215	0.0216	0.0223	0.0218	0.0004
	50 percentile, D(v,0.5)	1.2000	1.3800	3.3200	1.9667	1.1755
	90 percentile, D(v,0.9)	150.0000	156.0000	169.0000	158.3333	9.7125
	Average D[4,3]	39.4000	40.9000	47.9000	42.7333	4.5369

Sample name	Particle size (Micron)					
	Particle size distribution	Measured values			Mean	SD
		#1	#2	#3		
Sample 1A	10 percentile, D(v,0.1)	8.3800	7.9500	7.9300	8.0867	0.2542
	50 percentile, D(v,0.5)	26.2000	25.1000	25.4000	25.5667	0.5686
	90 percentile, D(v,0.9)	55.6000	52.6000	55.4000	54.5333	1.6773
	Average D[4,3]	29.5000	28.1000	28.9000	28.8333	0.7024
Sample 2A	10 percentile, D(v,0.1)	0.0207	0.0207	0.0207	0.0207	0.0000
	50 percentile, D(v,0.5)	2.0300	2.1600	2.1900	2.1267	0.0850
	90 percentile, D(v,0.9)	27.9000	29.2000	29.6000	28.9000	0.8888
	Average D[4,3]	8.9100	9.2900	9.4400	9.2133	0.2732
Sample 3A	10 percentile, D(v,0.1)	0.0217	0.0215	0.0217	0.0216	0.0001
	50 percentile, D(v,0.5)	5.0700	4.7000	4.9200	4.8967	0.1861
	90 percentile, D(v,0.9)	99.1000	97.5000	99.0000	98.5333	0.8963
	Average D[4,3]	30.1000	29.0000	29.5000	29.5333	0.5508
Sample 4A	10 percentile, D(v,0.1)	0.0228	0.0232	0.0236	0.0232	0.0004
	50 percentile, D(v,0.5)	3.5700	3.9700	4.3200	3.9533	0.3753
	90 percentile, D(v,0.9)	76.5000	75.8000	75.5000	75.9333	0.5132
	Average D[4,3]	22.8000	22.8000	23.5000	23.0333	0.4041
Sample 5A	10 percentile, D(v,0.1)	0.0187	0.0187	0.0189	0.0188	0.0001
	50 percentile, D(v,0.5)	0.5590	0.5580	0.5750	0.5640	0.0095
	90 percentile, D(v,0.9)	25.5000	24.2000	26.3000	25.3333	1.0599
	Average D[4,3]	6.6900	6.6300	6.7300	6.6833	0.0503

(Miss Kaew Kajornchaiyakul) Analyst

(Mrs. Sunan Rangseekansong) Chief Scientist

(Assoc. Prof. Dr. Amorn Petsom) Director

Remark: The results are good only for those samples analyzed.

APPENDIX D
PUBLICATION

The 7th TSME International Conference on Mechanical Engineering
13-16 December 2016

AME0008

Impact of Biodiesel Contamination on Engine Wear using Four-ball Wear Tester and Laser Particle Size Analyzer

Warawut Amornprapa[1,*], Phiranat Khamsrisuk[1], Preechar Karin[1], Kobsak Sriprapha[2] and Katsunori Hanamura[3]

[1] International college, King Mongkut's Institute of Technology Ladkrabang,Bangkok, 10520, Thailand
[2] National Electronics and Computer Technology Center (NECTEC), Pathumthani, 12120, Thailand
[3] Departments of Mechanical Engineering, Tokyo institute of technology, Japan
[*] Corresponding Author: Warawut_Amo@hotmail.co.th, 02-329-8261.

Abstract

The diesel engine is a compression ignition engine which converts chemical energy into mechanical energy. The energy forces the piston to perform up and down movement. The sliding movement of the components surfaces produces friction and wear. The lubricant protects an engine by producing the oil film to minimize the contacting surfaces. An incomplete combustion leads to fuel contamination, the contamination effect to oil degradation and lubrication breakdown. This research is aimed to investigate the effects of biodiesel contamination on the engine oil properties and wear characteristics. The used SAE0W30 engine oils were collected from diesel engine vehicles (B5-7). The amount of fuel contamination and particle size were measured by FT-IR and laser particle size analyzer, respectively. The results showed that the average amount of fuel contamination in used oils from the diesel engine vehicles was about 2% by weight. In addition, the new SAE0W30 engine oils were blended with biodiesel fuel to simulate fuel contamination. Friction torque and wear characteristics were evaluated by Four-ball wear tester and the worn surfaces of the balls were examined by scanning electron microscope (SEM) and 3D optical microscope. The particles in the Four-ball tested oil were also measured. The biodiesel contamination shows the negative effect on lubricating oil such as wear scar diameter and friction torque increase. On the other hand, it shows the positive effect to reduce surface roughness.

Keywords: Lubricant, Friction and Wear, Engine, Biodiesel, Four-Ball wear tester

1. Introduction

Recently, diesel engine is widely used as the powertrain in many fields. The advantage of the diesel engine is high efficiency due to high compression ratio. The engine converts chemical energy into mechanical energy. The contacting of metal to metal surfaces inside the engine generate heat and friction that can resulted in increases wear. Lubricant has an advantage in reducing friction prevent wear and removing frictional heat. It has an ability to minimize metal to metal contact by generating a lubricating film between the surfaces. The lubrication regimes can be divided into a boundary lubrication, mixed film lubrication, and full film lubrication [1, 2].

Biodiesel is an alternative fuel which is produced from vegetable oil or animal fat which plays an important role in petroleum diesel replacement. Biodiesel is an oxygenated fuel that makes more completely combustion process which resulted in lower carbon monoxide and unburned hydrocarbon. Khongdet [3] investigated performance and wear of the diesel engine which used diesel, biodiesel blends as a fuel. The results showed that the engine power and torque were similar to diesel engine. However, the amount of wear from biodiesel engine was higher than the diesel engine. Fazal et al. and Haseeb et al. [4, 5] studied the tribological properties of the palm biodiesel blends by using Four-ball wear tester. The tests were tested at different rotating speeds and temperatures. The results showed that wear scar diameter (WSD) and friction torque were increased proportionally to rotational speeds and temperature. Fuel film thickness was reduce, when the heat and rotational speeds increase, resulting in larger WSD. On the other hand, the WSD was decreased when biodiesel blends was increased, because of higher viscosity.

Jame et al. [6] reviewed the types of diesel engine lubricant contaminations. The fuel contamination are driven into the crank case engine oil by the high pressure during the combustion process. The solid particle which is larger than lubricant film thickness can lead to abrasive and fatigue wear. Water and fuel contamination can corrosive the component surface and makes lubricant breakdown. Kiatkong et al. [7] investigated the effect of fuel contamination on engine oil properties by using high frequency reciprocating rig. The results showed that the increasing of fuel contamination decreases oil viscosity. However, the contamination of biodiesel fuel resulted in increased lubricity, which resulted in decreases wear.

This research is aimed to investigate the effects of biodiesel contamination on the engine oil properties and wear characteristics.

2. Experiment Setup

2.1 Physical and Chemical Properties of Used Oil

The main purpose of this part was to measure the amount of fuel contamination in used engine oils from the real situations. The oils were collected from diesel engine vehicles. The engine displacement volume and

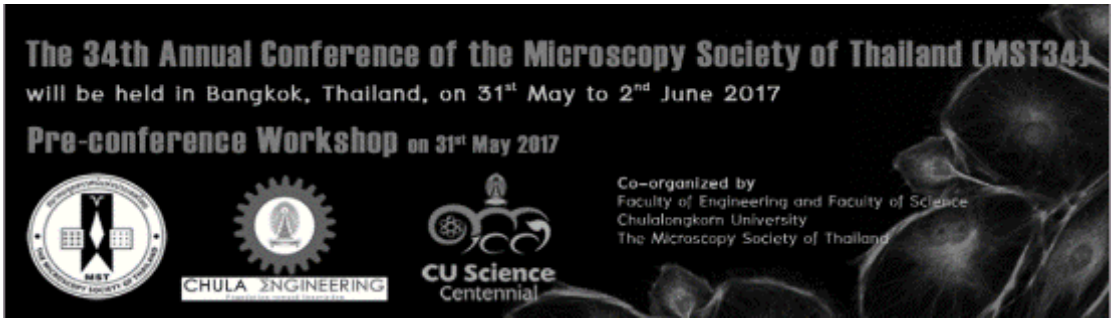

VENUE & TRAVEL INFORMATION

The 34th Annual Conference of the Microscopy Society of Thailand (MST34) is held at Grand Mercure Bangkok Fortune, Bangkok, Thailand.
The hotel located only 30 minutes from Suvarnabhumi International Airport, just a few steps from the MRT Rama 9 subway station.

The Effect of Soot Nanoparticle Size on Metal Wear Using Electron Microscopy

Warawut Amornprapa[1*], Preechar Karin[1], Kobsak Sriprapha[2] and Katsunori Hanamura[3]
[1] International college, King Mongkut's Institute of Technology Ladkrabang, Bangkok, 10520, Thailand
[2] National Electronics and Computer Technology Center (NECTEC), Pathumthani, 12120, Thailand
[3] Departments of Mechanical Engineering, Tokyo institute of technology, Japan
*Presenter e-mail address: Warawut_Amo@hotmail.co.th

Abstract

The impact of soot nanoparticles affecting metal wear was investigated. Several types of Commercial Carbon Black was used to simulate an engine soot. The wear tests were evaluated by using Four-ball wear tester. After the tests, the ball surfaces were examined by using High-Resolution Optical Microscope and Scanning Electron Microscope (SEM). The results showed that the ball wear scar diameter (WSD) increased when the primary particle size of carbon black was increased. In conclusion, it might be expected that the soot particle which was larger than the oil film thickness can increase the metal wear.

Keywords: Lubricant; Wear; Soot; Four-Ball wear tester; Electron microscopy; Laser diffraction spectroscopy

Background

Diesel engine is a compression ignition engine which converts chemical energy within the fuel into mechanical energy. Diesel fuel is injected under high pressure into the combustion chamber where the combustion process occurs. Soot is remain of incomplete combustion which consists mostly of carbon, hydrocarbon and metallic ash. The primary and agglomerated soot particles observed by Transmission Electron Microscopy (TEM) are in the range of 20 - 80 nm and 100 - 300 nm, respectively [1]. Soot can be entered into the engine oil through the piston ring clearance during the combustion process [2].

Khamsrisuk *et al.* [3] performed the used oil analysis by collecting the engine oil from the small diesel engine vehicles. The results showed that the percentage of wear metal, soot and fuel contamination increased as the engine mileage increase. The average of soot contamination was about 0.69 percent by weight. Guatam *et al.* [4] investigated the effect of soot contamination on engine oil viscosity by increasing the percentage of soot contamination. The results showed that the engine oil viscosity increased with the increase of soot contamination. The engine testing for evaluated soot tribological properties is challenging, because of the uncontrolled test parameter and the difficulty of wear measurement [5]. The specimen bench test which is easy to control test parameter and good repeatable results are used. Carbon black is a synthesis soot which has similar particle size and physical properties to engine soot. It can be used as soot representative. Ryason *et al.* [6] performed wear tests on a ball-on-flat-disk wear tester using carbon black, alumina and silica. The results showed that the balls were worn similarly in three different kinds of the samples. Karin *et al.* [7] performed wear tests on Four-Ball Wear Tester. He found that the Wear Scar Diameter (WSD) of the ball in the oil containing carbon black was higher than that of the oil alone. Hu *et al.* [8] also performed Four-Ball Wear Tester using base oil and formulated lubricant. The results showed that the WSD was high when carbon black levels increased. But, the WSD of the formulated lubricant was lower than that of the pure base oil. They suggested that the wear mechanism of soot-contaminated lubricant might be abrasion.

Biodiesel is an alternative fuel that plays an importance role in replacement using petroleum diesel. It is an oxygenated fuel that promotes more completely combustion. The soot diameter size and quantity from biodiesel engine emission is lower than that of diesel [9]. However, soot induced wear mechanisms are still not fully understood. This research aimed to investigate the effects of soot Nanoparticles on metal wear characteristics using Four-Ball Wear Tester, Laser Diffraction Spectroscopy, and Electron Microscopy.

Materials and Methods

A formulated engine oil which had the same grade as SAE0W30 was used in this research. The engine oil condition including viscosity, oxidation, nitration and total base number were measured according to ASTM standard test methods. Oil additives were measured by x-ray fluorescence.

The 23rd Small Engine Technology Conference

Call for Papers

SETC 2017 JAKARTA

Society of Automotive Engineers of Japan, Inc. SAE INTERNATIONAL IATO SAE-INDONESIA

Patronage of FISITA

VENUE : JAKARTA CONVENTION CENTER
PERIOD : November 15 to 17, 2017

DUE DATES
Abstracts due : January 31, 2017
Draft manuscripts due : April 14, 2017
Final manuscripts due : July 31, 2017

FOREWORD

JSAE, Society of Automotive Engineers of Japan, Inc., is pleased to announce that the 23rd Small Engine Technology Conference (SETC2017) will be held in Jakarta, Indonesia from November 15 to 17, 2017.

The conference is jointly organized by JSAE and SAE International with the support of Society of Automotive Engineers Indonesia (IATO) and Japan Land Engine Manufacturers Association (LEMA). We kindly ask prospective researchers and engineers in a diversified field of technologies and products with power source to submit electronic abstracts.

The conference offers up-to-date and new information in the development of technologies concerned in an exchange of participants from the globe. The events include technical visits, keynote speech, plenary session, exhibition and poster sessions besides ceremonial events of opening and awards & closing. Lunch & coffee-break for networking, welcome reception and banquet will be served as well.

Central District of Greater Jakarta City

MAIN SUBJECT AREAS

- **Product Categories** focused in this conference are:

  Vehicles with power source such as ATV, Motorcycles, Scooters, Personal Mobility, Marine, Snowmobiles, Recreational Vehicles, Utility Vehicles, Power Assist Devices, Power Assist Bicycles and Unmanned Vehicles.
  *Automobiles, Large Vessels, Large Aircraft, Locomotives and Spaceships are inapplicable.

  Machines with power source such as Snow Removal Equipment, Portable Power Generators, Agricultural Equipment, Garden Equipment, Hand Tools and Powered Exoskeleton.
  Technologies applicable for the products above are to be presented in this conference.

- **Technological Areas** focused in this conference are:

  Combustion Engines such as 4 stroke Engines, 2 stroke Engines, SI Engines, Diesel Engines, HCCI Engines, Unconventional Engines and Competition Engines.

  New Energy Sources such as Hybrid Drives, Electric Drives, Fuel Cells and Solar Cells.

  Components such as Chassis, Suspensions, Brakes, Transmissions, Drivetrains, Electrical Systems, Electronic Systems, Fuel Supply Systems and Wheels & Tires.

  Development Technologies such as Numerical Simulations, Measurements and Production Technologies.

  Fuels, Lubricants, and Tribology such as Alternative Fuels, Fuel Reformations, Additives, Friction Loss and Wear.

  Vehicle Technologies such as Dynamics, Handling, Drivability, Safety Technology & Functional Safety and Human Factors & Ergonomics.

  Environmental Impacts such as Noise, Vibration, Emissions, Aftertreatment and Life Cycle & Recyclability.

  Materials such as Composites, Metal Alloys, Heat & Surface Treatment, New Material and Material Processing.

JSAE 20179095 / SAE 2017-32-9095

Effect of Biofuel and Soot on Metal Wear Characteristic using Electron Microscopy and 3D Image Processing

Preechar Karin, Warawut Amornprapa, Phiranat Khamsrisuk, Pol-ake Budsayahem, Pattara Chammana
King Mongkut's Institute of Technology Ladkrabang

Kobsak Sriprapha
National Science and Technology Development Agency

Katsunori Hanamura
Tokyo Institute of Technology

ABSTRACT

The characteristics of soot affecting on engine oil degradation and metal wear would be studied. Soot particle contamination in engine oil was simulated using pure carbon black. Micro-nanostructure of soot particles were studied by Scanning electron microscopy (SEM), Transmission electron microscopy (TEM) and Laser diffraction spectroscopy (LDS). The metal wear behavior was studied by means of a Four-Ball tribology test with wear measured. Wear roughness in micro- scale was also investigated by high resolution Optical microscopy (OM), 3D rendering optical technique and SEM image processing method. Moreover, the impact of biofuel on engine oil degradation and metal wear was also reported.

INTRODUCTION

Diesel engine is a compression ignition engine which converts chemical energy within the fuel into mechanical energy. Diesel fuel is injected under high pressure into the combustion chamber where the combustion process occurs. Soot is remain of incomplete combustion which consists mostly of carbon, hydrocarbon and metallic ash. The primary and agglomerated soot particles observed by Transmission Electron Microscopy (TEM) are in the range of 20 - 80 nm and 100 - 300 nm, respectively [1]. Soot can be entered into the engine oil through the piston ring clearance during the combustion process [2].

Khamsrisuk *et al.* [3] performed the used oil analysis by collecting the engine oil from the small diesel engine vehicles. The results showed that the percentage of wear metal, soot and fuel contamination increased as the engine mileage increase. The average of soot contamination was about 0.69 percent by weight. Guatam *et al.* [4] investigated the effect of soot contamination on engine oil viscosity by increasing the percentage of soot contamination. The results showed that the engine oil viscosity increased with the increase of soot contamination. The engine testing for evaluated soot tribological properties is challenging, because of the uncontrolled test parameter and the difficulty of wear measurement [5]. The specimen bench test which is easy to control test parameter and good repeatable results are used. Carbon black is a synthesis soot which has similar particle size and physical properties to engine soot. It can be used as soot representative. Ryason *et al.* [6] performed wear tests on a ball-on-flat-disk wear tester using carbon black, alumina and silica. The results showed that the balls were worn similarly in three different kinds of the samples. Karin *et al.* [7] performed wear tests on Four-Ball Wear Tester. He found that the Wear Scar Diameter (WSD) of the ball in the oil containing carbon black was higher than that of the oil alone. Hu *et al.* [8] also performed Four-Ball Wear Tester using base oil and formulated lubricant. The results showed that the WSD was high when carbon black levels increased. But, the WSD of the formulated lubricant was lower than that of the pure base oil. They suggested that the wear mechanism of soot-contaminated lubricant might be abrasion.

Biodiesel is an alternative fuel that plays an importance role in replacement using petroleum diesel. It is an oxygenated fuel that promotes more completely combustion. The soot diameter size and quantity from biodiesel engine emission is lower than that of diesel [9]. However, soot induced wear mechanisms are still not fully understood. This research aimed to investigate the effects of soot Nanoparticles on metal wear characteristics using Four-Ball Wear Tester, Laser Diffraction Spectroscopy, and Electron Microscopy.

EXPERIMENTAL SETUP

A formulated engine oil which had the same grade as SAE0W30 was used in this research. The engine oil condition including viscosity, oxidation, nitration and total base number (TBN) were measured according to ASTM standard test methods. Oil additives were measured by x-ray fluorescence. The used engine oils were collected from the small diesel engine vehicles with different oil changed interval. The engine oil's mileage and oil aged were in the range 3,000-

The 14th
International Conference
on Automotive Engineering

ICAE-14

Final Program & Abstracts

Advanced Design for Future Mobility

April 2-3, 2018
Challenger, Impact, Muang Thong Thani,
Bangkok, THAILAND

The 14th International Conference on Automotive Engineering
April 2-3, 2018,
Challenger, Impact, Muang Thong Thani, Bangkok, Thailand

AEC-18IC-0702

EFFECT OF CARBON BLACK ON METALLIC WEAR USING ELECTRON MICROSCOPY

Warawut Amornprapa[1,*], Preechar Karin[1], Kobsak Sriprapha[2] and Katsunori Hanamura[3]

1King Mongkut's Institute of Technology Ladkrabang, Bangkok, 10520, Thailand

2National Science and Technology Development Agency, Pathumthani, 12120, Thailand

3Departments of Mechanical Engineering, Tokyo Institute of Technology, Japan

* Corresponding Author: Warawut_Amo@hotmail.co.th

Abstract. The impact of carbon black nanoparticles affecting metal wear is investigated. The comercial carbon black (CB) with difference primary particle sizes were mixed with the engine for simulating soot contamination. The wear test was evaluated by using Four-ball wear tester. After the tests, the ball surfaces were examined by using High-Resolution Optical Microscope and Scanning Electron Microscope (SEM). Additionally, tested oil were also measures particle size distribution using Laser diffraction spectroscopy (LDS). Base on Four-ball wear test, the 1% by weight of CB (N330, N550) contamination shows a bit higher average WSD, but the surface roughness is reduces. The ball worn surface of the engine oil with CB shows the area of grooves along with the sliding direction.

1. Introduction

Diesel engine is a compression ignition engine which converts chemical energy within the fuel into mechanical energy. Diesel fuel is injected under high pressure into the combustion chamber where the combustion process occurs. Soot is remain of incomplete combustion which consists mostly of carbon, hydrocarbon and metallic ash. The primary and agglomerated soot particles observed by Transmission Electron Microscopy (TEM) are in the range of 20 - 80 nm and 100 - 300 nm, respectively [1]. Soot can be entered into the engine oil through the piston ring clearance during the combustion process [2].

Khamsrisuk et al. [3] performed the used oil analysis by collecting the engine oil from the small diesel engine vehicles. The results showed that the percentage of wear metal, soot and fuel contamination increased as the engine mileage increase. The average of soot contamination is about 0.69 percent by weight. Guatam et al. [4] investigated the effect of soot contamination on engine oil viscosity by increasing the percentage of soot contamination. The results showed that the engine oil viscosity increases with the increase of soot contamination. The engine testing for evaluated soot tribological properties is challenging, because of the uncontrolled test parameter and the difficulty of wear measurement [2]. The specimen bench test, which is easy to control test parameter and good repeatable results, are used. Carbon black is a synthesis soot the physical properties of which is similar to the engine soot. It can be used as soot representative. Ryason et al. [5] performed wear tests on a ball-on-flat-disk wear tester using carbon black, alumina and silica. The results showed that the balls worn surfaces are similar in three different kinds of the samples. Karin et al. [6] performs wear tests on Four-Ball Wear

AUTHOR BIOGRAPHY

Author: Mr. Warawut Amornprapa

Degree: Master of Engineering

Place of Birth: Phitsanulok,Thailand

Graduate and undergraduate education:

Master of Engineering in Automotive Engineering,
King Mongkut's Institute of Technology Ladkrabang, Bangkok,

Bachelor degree in Mechanical Engineering,
King Mongkut's Institute of Technology Ladkrabang, Bangkok,

Major: Automotive Engineering

Presentations and Publications:

[1] Warawut Amornprapa1, Phiranat Khamsrisuk, Preechar Karin, Kobsak Sriprapha and Katsunori Hanamura "Impact of Biodiesel Contamination on Engine Wear using Four-ball Wear Tester and Laser Particle Size Analyzer", 2016, The 7th TSME International Conference on Mechanical Engineering, 13-16 December 2016, Ching mai, Thailand.

[2] Warawut Amornprapa1, Preechar Karin, Kobsak Sriprapha and Katsunori Hanamura "The Effect of Soot Nanoparticle Size on Metal Wear Using Electron Microscopy", 2017, Proceedings of the 34th MST Annual Conference, 31st May – 2nd June 2017, Bangkok, Thailand

[3] Preechar Karin, Warawut Amornprapa, Phiranat Khamsrisuk, Pol-ake Budsayahem, Pattara Chammana, Kobsak Sriprapha and Katsunori Hanamura. "Effect of Biofuel and Soot on Metal Wear Characteristic using Electron Microscopy and 3D Image Processing, 2017, JSAE 20179095 / SAE 2017-32-0095

[4] Warawut Amornprapa1, Preechar Karin, Kobsak Sriprapha and Katsunori Hanamura "Effect of carbon black on metallic wear using electron microscopy", 2018, The 14th International Conference on Automotive Engineering April 2-3, 2018, AEC-18IC-0702